

## ABSTRACT

### STRESS AND STRAIN DISTRIBUTION AROUND OPENINGS IN UNDERGROUND SALT FORMATIONS

by Attru M. Chowdiah

It has been observed in nature that underground rocks show a tendency to flow under triaxial state of stress. While underground formations are generally in a triaxial stress state, biaxial and uniaxial stress states exist around openings under certain conditions. This study investigates the distribution of stress and strain around various forms of openings created in underground salt formations.

The investigation includes theoretical analyses of the stress and strain distributions and experimental evaluation of the theoretical results by using the photostress technique in the following three categories:

1. The stress strain relations in uniaxial and biaxial compression,
2. stress distribution around circular and square openings under uniaxial compression,

3. stress distribution around circular and oval openings under biaxial compression.

The values of the elastic constants of the material have been determined from the stress strain relations. A study of the strain distribution on the entire surface of test specimens has led to conclusions on homogeneity and isotropy of the material. The ultimate loads and the corresponding strain distributions around the openings under uniaxial compression have been determined. In case of biaxial compression the loads and strain distributions have been obtained when the material around the opening showed large deformations.

Expressions for theoretical stress and strain around a circular opening when subjected to equal horizontal and vertical stresses have been derived assuming plane stress condition. The value of the yield stress at which the material showed a tendency to flow was determined from the biaxial test on a solid specimen. Using this value, the theoretical stresses and strains around a circular opening under equal horizontal and vertical compression have been calculated and compared with experimental results.

From a study of the ultimate loads and the corresponding strain distributions, it was observed that the failure

Attru M. Chowdiah

did not occur when the maximum stress around the opening initially reached the uniaxial strength of the material. Based on these experimental results, empirical relations on failure strength of openings have been found.

Although the behavior of all underground materials is not identical, the results of the study on rock salt may be extended to underground formations in general.

STRESS AND STRAIN DISTRIBUTION AROUND OPENINGS  
IN UNDERGROUND SALT FORMATIONS

By

Attru M. Chowdiah

A THESIS

Submitted to  
Michigan State University  
in partial fulfillment of the requirements  
for the degree of

DOCTOR OF PHILOSOPHY

Department of Civil Engineering

1963

327051  
4/24/64

## ACKNOWLEDGEMENTS

The author wishes to express his sincere thanks to his major professor, Dr. Shosei Serata for his guidance, supervision and encouragement in completing this research program.

Thanks are due to the National Science Foundation which sponsored this research project, and to the United States Agency for International Development which sponsored the author's education at Michigan State University.

The author wishes to express his sincere appreciation to Professor L. E. Malvern for his advice, and to Professor C. E. Cutts, Professor R. K. Wen and Professor D. W. Hall for acting on his guidance committee.

Special thanks are due to Mr. Shunsuke Sakurai, graduate assistant for the help in conducting the laboratory tests, and to the other members of the research group working with Professor Shosei Serata for the help at various stages of the experimental investigation.

## TABLE OF CONTENTS

Chapter	Page
I. INTRODUCTION . . . . .	1
1.1 General Remarks	1
1.2 Objective	4
1.3 Experimental Technique	4
II. PREVIOUS WORK DONE ON SALT . . . . .	6
2.1 Uniaxial Compression Test	6
2.2 Triaxial Test	8
2.3 Tests on Rocks	14
III. PRINCIPLES OF PHOTO STRESS . . . . .	16
3.1 History	16
3.2 Technique	16
3.3 Principles of Measurement of Strain	17
3.4 Determination of Principal Strain Difference	20
3.5 Determination of the Principal Strains	22
3.6 Selection of Plastic	23
3.7 Advantages	25
3.8 Limitations	27
IV. THEORETICAL STRESS AND STRAIN . . . . .	29
4.1a Strength Theories of Rock Salt	29
4.1b Stress Strain Relations in the Plastic State	32
4.2 Uniaxial Test	36
4.3 Biaxial Test	40
4.4 Circular Hole in an Infinite Medium Under Biaxial State of Stress	42
4.5 Completely Plastic Cylinder in Plane Stress Condition	43
4.6 Elastic Plastic Cylinder in Plane Stress Condition	47

Chapter		Page
4.7	Completely Elastic Cylinder in Plane Stress Condition	53
4.8	Completely Elastic Cylinder in Plane Stress Condition Assuming Incompressibility	54
4.9	Circular Hole in an Infinite Medium Under Biaxial Compression ( $\sigma_x \neq \sigma_y$ )	57
4.10	Circular Hole in an Infinite Medium Under Uniaxial Compression	61
4.11	Square Hole in an Infinite Medium Under Uniaxial Compression	62
4.12	Oval Hole in an Infinite Medium Under Biaxial Compression	64
V.	EXPERIMENTAL PROCEDURES . . . . .	70
5.1	Preparation of Specimen	70
5.2	Testing Device	72
5.3	Loading Conditions	72
5.4	Description of the Tests	73
VI.	EXPERIMENTAL RESULTS AND ANALYSIS . . . . .	81
6.1	Uniaxial Compression Test on Solid Specimens	81
6.2	Circular Hole Under Uniaxial Compression	88
6.3	Square Hole Under Uniaxial Compression	94
6.4a	Biaxial Compression on Solid Specimen-- Equal Stresses in Both Directions	96
6.4b	Biaxial Compression on a Solid Specimen	99
6.5a	Circular Hole Under Equal Horizontal and Vertical Forces	100
6.5b	Circular Hole Under Unequal Horizontal and Vertical Forces	103
6.6a	Oval Holes Under Uniform Biaxial Compression	106
6.6b	Single Oval Hole Under Uniform Biaxial Compression	108

Chapter	Page
VII. SUMMARY AND DISCUSSION . . . . .	139
7.1 The Mechanical Properties	139
7.2 Nature of Deformation and Failure	143
7.3 Theoretical Analysis	144
7.4 Evaluation of Photo Stress Method	145
7.5 Behavior of the Material	146
7.6 Relationship to the Behavior of Underground Formations in General	148
VIII. CONCLUSIONS . . . . .	149
IX. FUTURE RESEARCH . . . . .	153
BIBLIOGRAPHY . . . . .	155

LIST OF TABLES

Table	Page
4.5.5 Stresses in a completely plastic cylinder under uniform external pressure . . . . .	46
4.6.5 Stresses in an elastic plastic cylinder of external radius of 4" and internal radius of 1" . . . . .	52
6.3.11 Principal strain difference on a line through the center of the hole and normal to the direction of stress in case of a circular hole under uniaxial compression of 500 psi . . . . .	92
6.8.11 Principal strain difference in case of circular hole under uniaxial stress of 2,750 psi . . . . .	93
6.10.12 Principal strain difference and principal stress difference on lines normal and parallel to direction of load in case of a square opening under a uniaxial stress of 2,320 psi . . . . .	96
6.11.11 Relation between $\frac{\sqrt{2}}{3} \sigma_1$ and $2\sqrt{2} \epsilon_1^P$ in biaxial compression of solid specimen . . . . .	97
6.13.11 Principal stress difference and principal strain difference in a thick walled cylinder under uniform biaxial compression = 4,000 psi . . . . .	104
6.5.11 Elastic stresses around a circular hole when	
$\frac{\sigma_x}{\sigma_y} = \frac{1}{3}$ (horizontal to vertical) . . . . .	105

Table	Page
7.3.1 Experimental data on uniaxial tests . . . . .	141
7.3.2 Experimental data on biaxial tests . . . . .	143

## LIST OF FIGURES

Figure		Page
2.2.1	Mohr's envelope representing stresses in a triaxial stress state. . . . .	15
2.2.2	Relation between lateral and axial stress in a triaxial stress state when lateral strains are zero. . . . .	15
3.1	Arrangement of the components in a large field photo stress meter. . . . .	28
3.2	Rotation of the principal axes in oblique incidence measurements. . . . .	28
4.1.1 to 4.1.3	Various types of stress strain curves. . .	66
4.2.0 to 4.2.3		
4.4.1 4.9.1	Various forms of opening investigated. . .	67
4.10.1		
4.11.1		
6.15.10		
4.5.2	Stress distribution in a completely plastic cylinder in plane stress under uniform external pressure. . . . .	68
4.6.2	Stress distribution in an elastic plastic cylinder under uniform external pressure in plane stress (ratio of external to internal diameter = 4). . . . .	69
6.1.5	Axial stress strain relation in uniaxial compression (mean values of 2 tests). . .	110
6.1.6	Axial stress-Poisson's ratio relation in uniaxial compression. . . . .	111

Figure		Page
6.1.7	Stress strain relation of individual grains based on SR-4 Gages. . . . .	112
6.1.20	Failure of a solid specimen under a uniaxial stress of 3,858 psi. . . . .	137
6.3.3	Circular hole under uniaxial compressive stress of 500 psi. . . . .	113
6.4.5	Stress strain relation in uniaxial compression.	114
6.4.6	Axial stress Poisson's ratio relation in uniaxial compression. . . . .	115
6.5.2	Distribution of principal strain difference in a solid subject to a uniaxial vertical stress of 2,500 psi. . . . .	134
6.5.3	Relation between uniaxial stress and principal strain difference. . . . .	116
6.5.5	Stress strain relation in uniaxial compression.	117
6.5.6	Axial stress Poisson's ratio relation in uniaxial compression. . . . .	118
6.5.7	Principal stress difference along $x_1x$ under uniaxial compression of 2,500 psi. . . . .	119
6.5.8	Principal stress difference along $y_1y$ under uniaxial compression of 2,500 psi. . . . .	119
6.5.20	Failure of a solid specimen under a uniaxial stress of 3,556 psi. . . . .	137
6.6.20	Failure of a circular opening under a uniaxial stress of 2,500 psi. . . . .	137
6.7.20	Failure of a square opening under a uniaxial stress of 2,750 psi. . . . .	137
6.8.2	Distribution of principal strain difference around a circular opening subject to a uniaxial vertical stress of 2,750 psi.	134

Figure		Page
6.8.3	Circular hole-uniaxial compression of 2,750 psi: principal strain difference on radial lines normal, parallel and at 45° to the direction of load. . . . .	120
6.8.20	Failure of a circular opening under a uniaxial stress of 3,200 psi. . . . .	137
6.10.2	Distribution of principal strain difference around a square opening subject to a uniaxial vertical stress of 2,320 psi. . .	134
6.10.3	Principal strain difference on center line normal to load in case of square hole under uniaxial compression of 2,320 psi. .	121
6.10.4	Principal strain difference on line parallel to load in case of square hole under uniaxial compression of 2,320 psi. . . . .	121
6.10.20	Failure of a square opening under a uniaxial stress of 2,850 psi. . . . .	137
6.11.3	Vertical stress $\sigma_1$ , versus vertical strain, $\epsilon_1$ in a cube under equal compression in vertical and horizontal directions. . . . .	122
6.11.4	$\tau_o$ versus $f(\tau_o)$ in case of equal horizontal and vertical stresses. . . . .	123
6.11.20	Yielding of a solid specimen after reducing vertical stress to zero from a hydro- static stress of 4,000 psi. . . . .	138
6.12.2	Distribution of principal strain difference in a solid specimen subject to a horizontal stress of 1,000 psi and a vertical stress of 4,000 psi. . . . .	134
6.12.4	Principal stress difference versus principal strain difference in biaxial compression keeping $\sigma_2 = 1,000$ psi. . . . .	124

Figure		Page
6.12.5	Vertical stress versus vertical strain in biaxial compression keeping horizontal stress = 1,000 psi. . . . .	125
6.12.20	Yielding of a solid specimen under a vertical stress of 4,000 psi and a horizontal stress of 1,333 psi. . . . .	138
6.13.2	Distribution of principal strain difference around a circular opening subject to equal horizontal and vertical stresses of 4,000 psi. . . . .	135
6.13.5	Distribution of principal strain difference along AB in case of circular hole under equal vertical and horizontal compression of 4,000 psi. . . . .	126
6.13.20	Yielding of a circular hole under hydrostatic stress of 4,000 psi. . . . .	138
6.14.2	Distribution of principal strain difference around a circular opening subject to a vertical stress of 3,750 psi and a hori- zontal stress of 1,250 psi. . . . .	135
6.14.3	Distribution of principal strain difference along AB in case of circular hole under horizontal compression of 1,250 psi and vertical compression of 3,750 psi. . . . .	127
6.14.20	Yielding of a circular hole under a vertical stress of 4,000 psi and a horizontal stress of 1,333 psi. . . . .	138
6.15.2 and 6.15.6	Distribution of principal strain difference around oval openings, subject to equal horizontal and vertical stresses of 3,000 psi. . . . .	136

Figure		Page
6.15.7	Two oval openings under equal horizontal and vertical compression of 3,000 psi-- distribution of principal strain difference along the line joining the centers of the holes. . . . .	128
6.15.8	Two oval openings under equal horizontal and vertical compression of 3,000 psi-- distribution of principal strain difference on a vertical line through the center of pillar. . . . .	129
6.15.9	Two oval openings under equal horizontal and vertical compression of 3,000 psi-- distribution of principal strain difference on a vertical line through center of right hole. . . . .	130
6.16.3 and 6.16.6	Distribution of principal strain difference around oval opening subject to equal horizontal and vertical stresses of 3,000 psi. . . . .	136
6.16.7	One oval opening under equal horizontal and vertical compression of 3,000 psi-- distribution of principal strain difference on the horizontal line through the center of hole. . . . .	131
6.16.8	One oval opening under equal horizontal and vertical compression of 3,000 psi-- distribution of principal strain difference on the vertical line through a point 1.18 inch from center of hole. . . . .	132
6.16.9	One oval opening under equal horizontal and vertical compression of 3,000 psi-- distribution of principal strain difference on the vertical line through center of hole. . . . .	133
6.17.20	Biaxial loading device and photo stress large field meter. . . . .	138

## NOTATION

$\sigma_1', \sigma_2', \sigma_3$	Principal stresses
$\sigma_r$	Radial stress
$\sigma_\theta$	Tangential stress
$\sigma_{r\theta}$	Shear stress
$\sigma_{rp}', \sigma_{\theta p}$	Radial and tangential stresses at the elastic plastic boundary
$\sigma_x', \sigma_y$	Stresses in rectangular coordinates
$\sigma_1' = \sigma_1 - \frac{\sigma_1 + \sigma_2 + \sigma_3}{3}$	
$\sigma_2' = \sigma_2 - \frac{\sigma_1 + \sigma_2 + \sigma_3}{3}$	Deviatoric stresses
$\sigma_3' = \sigma_3 - \frac{\sigma_1 + \sigma_2 + \sigma_3}{3}$	
$\sigma_0$	Yield stress in uniaxial test
$\tau_0$	Octahedral shear stress
$k_0$	Octahedral shear strength
$\epsilon_1', \epsilon_2', \epsilon_3$	Principal strains
$\epsilon_r$	Radial strain
$\epsilon_\theta$	Tangential strain
$\epsilon_1^p, \epsilon_2^p, \epsilon_3^p$	Total plastic strains in the 3 principal directions

$\epsilon_o^p$	Generalized plastic strain
$d\epsilon_1^p, d\epsilon_2^p, d\epsilon_3^p$	Increment in plastic strain in 3 principal directions
$x, y$	Rectangular coordinates.
$r, \theta$	Polar coordinates
$\rho$	Radius of the elastic plastic boundary
$E$	Modulus of elasticity
$\eta$	Poisson's ratio
$G$	Modulus of rigidity
$mii$	Micro inch per inch
$psi$	Pounds per square inch

## CHAPTER I.

### INTRODUCTION

#### 1.1 General Remarks

Natural underground formations consist of many types of rocks which vary in composition and physical properties. A rock is a heterogeneous mixture of grains of polycrystalline materials which are randomly oriented, and distributed, sometimes with their intergranular spaces filled with water or air to varying degrees, and held together by some kind of bond force. Most of these rocks deform very little under ordinary compressive loads. But a geophysical exploration has shown that rock flows in varying degrees, depending on the environmental conditions as evidenced by folds in the rock strata.

Underground structures occur in mining operations of all kinds, in tunneling, in making cavities for underground nuclear testing or for storage of materials like radioactive waste and gaseous and liquid petrochemical products. Whatever be the use of the underground structures, a study of the physical behavior of the rocks is essential

in formulating the theories of their structural stability.

The engineer who is used to working with elastic materials like structural steel, finds it difficult to explain the behavior of rocks in terms of the engineering parameters. Some of the questions that the person who is confronted with engineering problems involving rocks has to answer, are

1. How do the individual grains deform under the load and is it possible to determine such deformation at least qualitatively?
2. To what extent does the behavior of the individual grains affect the overall behavior of the mass? In other words, what assumptions on the behavior of the mass in terms of homogeneity and isotropy can be made?
3. Can the behavior of the rock mass be described in terms of the conventional constants connected with stress and strain? Alternatively, is it possible to approximate the behavior of the material under different stress states to a Hooke solid, a Newtonian liquid or a St. Venant solid?
4. Is it possible to formulate some principles on which the design of openings in the material can be based, using the information obtained from laboratory tests on the material?

5. Would it be reasonable to extend the principles governing one type of rock to other underground formations?

By the very nature of the restraint offered by the massiveness of the material, underground openings are normally in a triaxial stress state. But the possibility of other states of stress cannot be ruled out and as a matter of fact, certain regions surrounding a cavity are in biaxial and uniaxial stress states, and for a complete understanding of the problem of stress distribution, it is first necessary to study the uniaxial and biaxial stress states as well.

Rock salt has been chosen as a model rock in the present study. It is encountered in large quantities as rock salt formations in the United States and many other parts of the world. The material is granular and crystalline and exhibits characteristics of brittle, elastic and plastic behavior, which are also shown by other rocks in varying degrees. Rock salt flows more readily than other rocks and a notable example of such a flow is the salt domes found in the southwestern United States near the Gulf of Mexico. Rock salt from one of the salt domes was used for this study, since it is sufficiently homogeneous and isotropic.

## 1.2 Objective

The behavior of rock salt differs considerably from that of a metal. It changes from its brittle behavior in uniaxial stress state to plastic behavior in triaxial stress state whereas a typical metal, like steel, behaves much the same way under all stress states.

The objective of this research is to investigate the uniaxial and biaxial properties of the material and furthermore, to analyze stress distribution around some specific forms of openings in it. The investigation includes:

1. The stress strain relation in uniaxial and biaxial compression.
2. Stress distribution around circular and square openings under uniaxial compression.
3. Stress distribution around circular and oval openings under biaxial compression.

By such an investigation it is intended to formulate the basic principles governing the stress strain distribution around cavities created in underground salt formations.

## 1.3 Experimental Technique

Photo stress technique has been used in the experimental investigation exclusively. The main considerations

which led to the choice of the technique are

1. It enables us to observe the strain distribution over the entire surface.
2. The residual strains can be measured at any time and a complete history of the behavior of the material can thus be obtained.
3. Large strains can be measured by a suitable choice of plastic.

The experimental technique is limited in the following two aspects. First, the principal strains have not been separated due to the non-availability of the oblique incidence meter. However, this does not affect the analysis, as the principal strain differences are utilized in the analysis of the large plastic strains. Secondly, the technique is restricted only to one and two dimensional analysis lacking in analysis of the third principal stress effect. Nevertheless, this does not restrict the usefulness of the technique as the two dimensional analysis may provide the first approximation to the three dimensional analysis.

## CHAPTER II

### PREVIOUS WORK DONE ON SALT

#### 2.1 Uniaxial Compression Test

The mechanical behavior of salt depends very much on the method of testing, and no standard procedure has been established. The maximum uniaxial strength of salt has been reported in the range of 2000 to 5500 psi depending upon the investigator. The wide variation in the results has been attributed to the variation in the testing procedure, rather than the strength of the material itself.

Serata<sup>30</sup> has analyzed and explained the basic mechanism of the uniaxial behavior of the material. The friction developed on the loading surfaces of the salt increases the ultimate strength and modulus of elasticity, and generally changes the stress strain curve.

The stress strain curves depend on the ratio of height to cross-sectional area of the specimen. This variation is due to the formation of a triaxial zone in the central region of the specimen.

When end friction is completely eliminated, no lateral stresses are set up anywhere in the specimen and

the stresses become completely axial. Accordingly the stress strain curve so obtained becomes independent of the end effects.

The mechanical properties obtained by Serata<sup>30</sup> after eliminating the end friction are as follows:

1. Mean maximum stress was 2300 psi with a standard deviation of 200 psi.
2. The proportional limit was arbitrarily chosen at 0.5% off-set strain, and the corresponding yield stress was in the range of 1800 psi to 2200 psi.
3. Mean value of modulus of elasticity was 0.14 million psi with standard deviation of 0.03 million psi, based on dial gage strain measurements. The size of the specimens varied from 1.75" cube to 3.5" cube, the intermediate sizes varying in height to width ratio.
4. The Poisson's ratio was more than 0.5 for stresses beyond 300 psi, based on SR 4 gage strain measurements. The value was close to 1.0 in the case of aggregate and close to 0.5 in the case of a single crystal.

The Poisson's ratio<sup>18</sup> calculated on the basis of propagation velocity of seismic wave in a salt formation at

a depth of 10,000' was 0.499998.

5. Strain hardening effects were observed. The strain hardening effects did not change with the time interval between unloading and reloading.

## 2.2 Triaxial Test

Some of the earlier triaxial tests on salt and rocks were done by Bridgman.<sup>3</sup> Specimens made of rock salt crystals were pulled under hydrostatic pressure of 420,000 psi by a tensile force which amounted to a stress of 7,300 psi on the final area of the specimen and obtained a reduction of 20% in its area. The cross section at the necking part did not have any evidence of slip plane. He pulled Solenhofen limestone under hydrostatic pressure of 400,000 psi and obtained a reduction in area of 53%. The specimen showed necking first and then there was a fracture on a single shear plane.

Handin<sup>14</sup> created a triaxial stress state in one case by confining salt in a copper jacket and compressing it in the third direction, and in the other case by exposing the salt to kerosene under pressure. Serata<sup>30</sup> used the experimental results of Handin<sup>14</sup> to plot Mohr's envelopes which showed that the envelopes at smaller confining pressures

gave smaller ultimate shear strengths than the envelopes at larger confining pressures. Beyond a certain value of the mean principal stress, the Mohr's envelope became horizontal. The point of transition of the Mohr's envelope from a curve to a horizontal straight line, defines the stresses at which the material becomes plastic. The value of the mean stress obtained from the stresses at the point of transition was found to be 5,500 psi.

Serata<sup>30</sup> made tests after reducing friction at room temperatures and also at temperatures up to 770°F and demonstrated that the salt becomes plastic. The ultimate shearing strength decreased with the increase in temperature up to 500°F, and beyond 500°F the strength decreased less rapidly. On the other hand, the ductility increased with the temperature. The differential yield strength at 2% off-set strain increased by more than 100% by increasing the mean principal stress.

Serata<sup>30</sup> created large mean stress by using a high pressure cylinder in which a cylindrical salt specimen with a cylindrical hole was confined and axially compressed. The lateral restraint provided by the cylinder wall created the lateral stress. The lateral stresses were calculated on the basis of strains measured on the outer surface of the

pressure cylinder. By applying an axial stress of 16,000 psi and measuring the closure of the cylindrical hole in the salt by the volume of the displaced mercury from the cavity, he studied the creep behavior of salt. Some of his conclusions are that the yield condition based on octahedral shear strength and the Mohr's theory of failure are applicable to salt only when the mean principal stress exceeds 5,500 psi or when the temperature of salt exceeds 500°F.

A method of determining the octahedral shear strength and to demonstrate transition from elastic to plastic state in a triaxial state of stress of a material has been developed by Serata<sup>32</sup> and investigated by Serata,<sup>32</sup> Morrison<sup>22</sup> and Raman.<sup>28</sup> The theory and the results are briefly given below.

Cylindrical salt specimens were closely fitted in a thick walled steel cylinder, under frictionless conditions. An axial stress was applied on the salt, and the lateral stress was provided by the restraint afforded by the wall of the steel cylinder. The lateral stress was calculated from the measured strains in the SR 4 gages on the outer surface of the steel cylinder.

Fig. 2.2.1 is a representation of the stresses by Mohr's envelope. The envelope A B C D E represents the

stress state for a brittle material. A B corresponds to the brittle behavior, C D E to plastic behavior and B C to the intermediate state of transition. Part A B is a representation of the Coulomb-Mohr theory of failure in the form of

$$\tau = \tau_c + \theta \sigma$$

where  $\tau$  = shear stress on the plane of failure,

$\theta$  = coefficient of internal friction in the material,

$\sigma$  = normal stress,

$\tau_c$  = the constant part of the shear strength which depends on the material.

The horizontal straight line D E represents the octahedral shear strength theory of yielding when the material is plastic. The ordinate of the line C D E is the maximum shear,  $\tau_{\max}$ , and is given by

$$\tau_{\max} = \frac{3}{2\sqrt{2}} k_o$$

When the material is confined as is the case in the material enclosed in a steel cylinder the stresses are represented by the envelope F D E. The straight line F D represents the completely elastic state and the horizontal line D E represents the plastic state. When a material is subjected to an axial stress of  $\sigma_z$ , the lateral stress in the other two principal directions are equal to  $\sigma_L$ , the

strains in the two lateral directions are zero, and the following equations hold.

In the elastic state,

$$\frac{\sigma_L}{\sigma_z} = \tan \alpha = \frac{\eta}{1-\eta}$$

$$\text{and } \sin \phi = 1-2\eta$$

where  $\phi$  is the angle made by the straight line F D of the envelope which is tangential to the Mohr's circle.

In case of rocks,  $\phi$  has values in the range of  $15^\circ$  to  $45^\circ$ , while the angle of internal friction  $\theta$  is in the range of  $50^\circ$  to  $80^\circ$ .

In the plastic state,

$$\sigma_L = \sigma_z \pm \frac{3}{\sqrt{2}} k_0$$

$$\text{and } \frac{d \sigma_L}{d \sigma_z} = \tan \beta = 1$$

resulting in  $\beta = 45^\circ$

Fig. 2.2.2 represents the relation between the stresses  $\sigma_L$  and  $\sigma_z$ . The straight lines A B and B C represent the elastic and the plastic state respectively during the loading stage. The straight line C D and D E represent the elastic and plastic state respectively during the unloading stage. E A represents the residual lateral stress in the material given by the cylinder wall due to plastic flow in

the material. The vertical distance between E D and B C gives values of  $3\sqrt{2} k_o$  for the material.

Measurements of axial and lateral strains give the equation for modulus of elasticity E of the material.

$$E = \frac{\frac{\sigma_z}{2 \sigma_L} - \frac{\sigma_L}{\sigma_L + \sigma_z}}{\frac{\epsilon_z}{2 \sigma_L} - \frac{\epsilon_L}{\sigma_L + \sigma_z}}$$

Compressibility of the material is represented by

$$\frac{\Delta v}{v} = - b \sigma_m^n,$$

where

$$\frac{\Delta v}{v} = \text{volumetric strain}$$

v = volume of material at the beginning of each cycle of loading and unloading.

b and n = constants to be determined experimentally.

Morrison<sup>22</sup> experimented on the friction reducers and found that the coefficient of static friction of a friction reducer consisting of 2 layers of plastic coated with grease-graphite mixture was the lowest and was 0.00246.

Some of his conclusions on triaxial tests on rock salt are

1.  $\beta$  was close to  $45^\circ$  with an average deviation of  $0.9^\circ$ .

2. Repeated cycles of loading increased octahedral shear strength and modulus of elasticity.

### 2.3 Tests on Rock

Tests on rocks have been done to prove that they no longer remained brittle under high confined pressures. In addition to Bridgman<sup>3</sup> whose work was briefly mentioned earlier some others have experimented with rocks.

Griggs<sup>13</sup> tested Solenhofen limestone, marble and quartz under triaxial stress state. He was unable to obtain plastic flow of the material, but obtained higher ultimate strength of marble.

Adams<sup>1</sup> demonstrated that rocks could be made to flow under high confining pressure at room temperature. The confining pressures were obtained by enclosing the specimen in a steel jacket.

Robertson<sup>45</sup> tested several varieties of rocks. He demonstrated that all rocks obeyed Hooke's law to some extent, and that marble and limestone can undergo large plastic deformations. He found that the silicate rocks and minerals did not behave plastically.

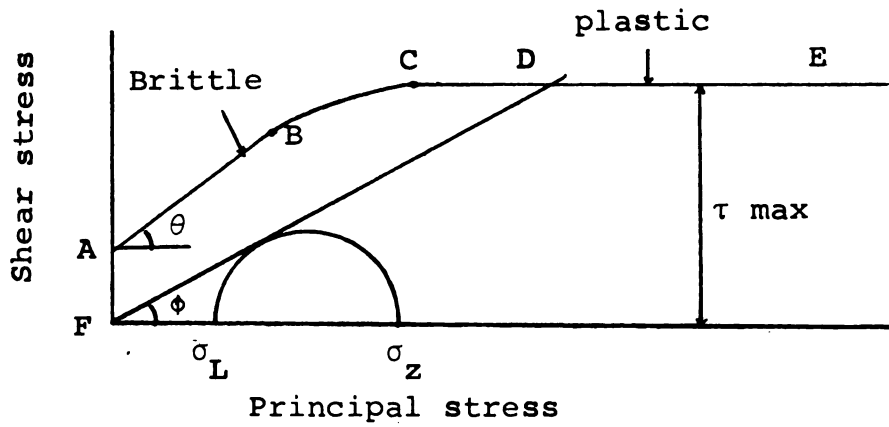


Fig. 2.2.1. Mohr's envelope representing stresses in a triaxial stress state.

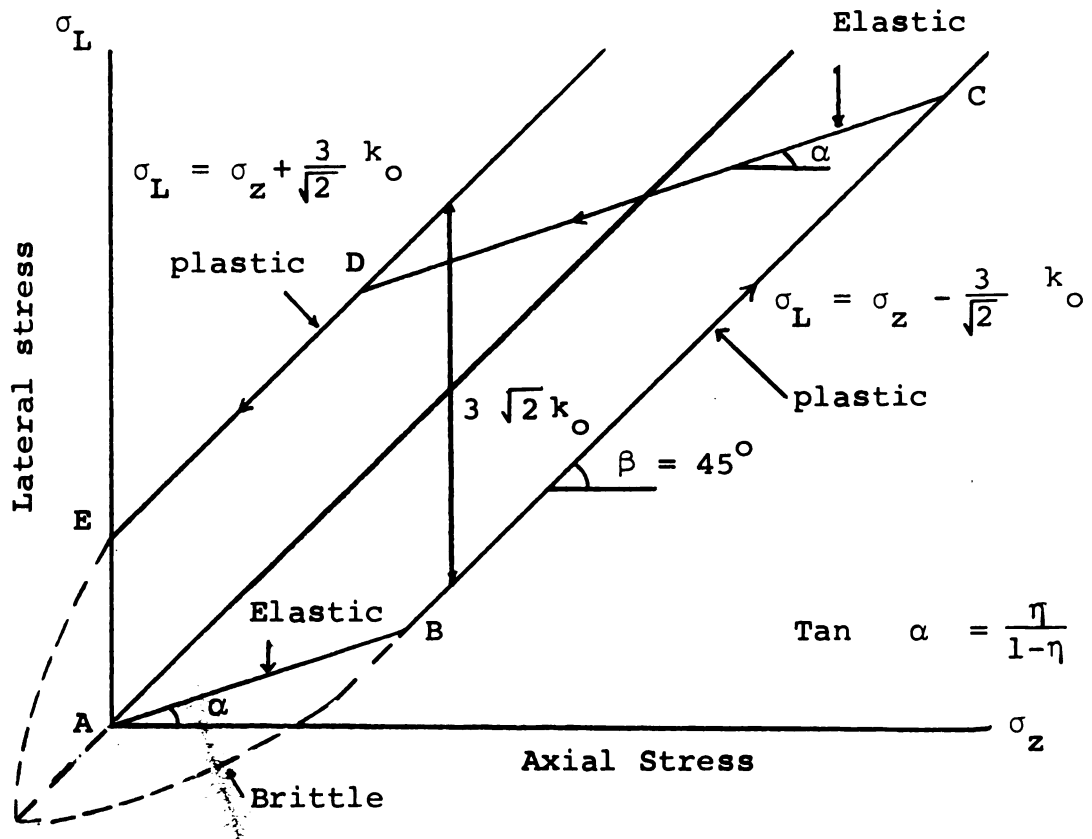


Fig. 2.2.2. Relation between lateral and axial stress in a triaxial stress state when lateral strains are zero.

## CHAPTER III

### PRINCIPLES OF PHOTOSTRESS

#### 3.1 History

The Photostress<sup>40</sup> technique was first attempted in 1930 in France using glass as a birefringent material. Subsequently plastics were developed but there were difficulties of good bond with material, sensitivity to strains and stability with regard to time. It was in 1953 that the method was successfully employed in measurement of strains in elastic and plastic ranges in France.

#### 3.2 Technique

A sheet of plastic known as photostress plastic is bonded with a special kind of cement to any part of a structure where strain distribution is to be determined. When the structure is stressed, the strains on the surface of the structure are transferred to the plastic. By the use of a reflection polariscope the strain distribution on the plastic is determined. This technique is known as photostress.

### 3.3 Principles of Measurement of Strain

The principles of photostress are essentially the same as photoelasticity. But there is an important difference. In photoelasticity, a model of the structure in which the strain distribution is required is made out of a birefringent material and the strain distribution of this model is determined. In photostress, the actual structure is coated with the photostress plastic and the strain distribution of the loaded structure is determined.

Some crystalline materials like calcite exhibit the property of double refraction or birefringence. When a ray of light passes through the crystal, it is split into two plane polarized rays which travel at different velocities and vibrate in two mutually perpendicular directions. This property is called double refraction. The photostress plastic developed by the Budd Company becomes doubly refractive or birefringent when strained and the planes of vibration of the polarized beams correspond to the directions of principal strains in the plastic.

An instrument known as a large field instrument was used in the strain measurements. It is a reflection polariscope and is schematically represented in Fig. 3.1. A ray of light originates at the light source L, passes through

the polarizer P and the quarter wave plate  $Q_1$ , passes through the photostress plastic S attached to the surface of the specimen T, is reflected from the surface of cement which bonds the plastic to the specimen, passes through quarter wave plate  $Q_2$  and the analyzer A, and is observed by the person V. The quarter wave plates can be removed from the path of the ray of light if necessary.

The plane polarized light passing through P becomes circularly polarized when it passes through  $Q_1$ . The quarter wave plate is a permanently birefringent material and when the polarized light passes through it, the light emerges with 2 components of equal amplitude vibrating at an angle of  $90^\circ$  apart. After passing through the plastic, when the circularly polarized light passes a second time through the quarter wave plate  $Q_2$ , it becomes a plane polarized light again but now the plane of polarization is at right angles to the plane of polarization of the incident ray. Thus we have a crossed-circular polariscope. In this arrangement the isoclinic lines are removed and it is easy to identify the black lines on the plastic as lines of zero maximum shear.

An isoclinic is a line connecting the points where the principal stress directions are the same. These appear

as black lines in plane polarized light. When the plane of principal stress in the plastic coincides with the plane of vibration of plane polarized light, the ray of light passes through the plastic unobstructed, but cannot pass through the analyzer if it is at right angles to the polarizer. Accordingly the directions of principal stresses are the directions of the axes of the polarizer and analyzer which are mutually perpendicular.

The method of determining the isoclinic is as follows: The quarter wave plates are removed from the path of the light, the polarizer and analyzer are set at right angles to each other and the whole system is rotated. The black lines corresponding to the directions of the axes of the system give the isoclinics. These isoclinics can be traced on the plastic or photographed.

When the quarter wave plates are removed and plane polarized white light passes through the strained plastic, a set of black and colored lines called a fringe pattern is observed. The relative retardation in the polarized rays causes the color pattern. These colored lines are called isochromatics. An isochromatic is a locus of points at which the difference of principal strains is constant.

The principal strain difference at any point can be

represented by the relation

$$\epsilon_1 - \epsilon_2 = \frac{\delta}{2tK}$$

where  $\epsilon_1$  and  $\epsilon_2$  are the principal strains,

$t$  = thickness of the plastic,

$K$  = strain sensitivity constant which depends on the plastic being used and which can be determined experimentally,

$\delta$  = retardation =  $n\lambda$ ,

where  $\lambda$  = wave length of the ray which is extinguished,

$n = 0, 1, 2, \dots$

$n$  is called the fringe order.

Usually the dividing line between the red and blue is chosen as a characteristic color for measurement of strains and is called "tint of passage." This line is sharp because the red and blue correspond to the low frequency and high frequency. Every time  $n$  changes, the tint of passage occurs.

### 3.4 Determination of Principal Strain Difference

The quarter wave plates are moved into the path of the light. The polarizer and analyzer are set at right angles to each other. The isoclinics do not appear and only the isochromatics are observed. The procedure to determine

the order of a fringe is as follows. A black line or a black region is located on the fringe pattern. This black region is the area of zero principal strain difference and will be designated as zero order fringe. The tint of passage closest to the zero order fringe is of order 1, the next tint of passage is of order 2, and then the order increases by an integer every time a tint of passage is met with. In order to cover a large number of points on the plastic, it is necessary to obtain fractional order fringes. This is achieved by a technique called goniometric compensation. Keeping the quarter wave plates in the path, the analyzer axis is rotated with respect to the polarizer axis by an angle  $\alpha$ . As the analyzer is rotated from its crossed position the tints of passage move from their original positions. The fringe order  $n$  moves to the position where the actual fringe order is  $n \pm \frac{\alpha}{180}$ . Thus a large part of the area can be covered by obtaining sufficient number of fractional order fringes. The fringe order at points not covered can be interpolated.

However, if accurate analysis at a point is required, the following procedure is adopted. The quarter wave plates are removed out of the field. The crossed polarizer analyzer system is rotated until an isoclinic falls on the point.

The quarter wave plates are brought into the field again. The analyzer alone is now rotated so that the nearest tint of passage falls on the point. If  $\alpha$  is the angle through which the analyzer is rotated, and  $n$  is the order of the fringe brought on the point, then the actual fringe order at the point =  $n \pm \frac{\alpha}{180}$ . Once the fringe order is known, principal strain difference is obtained from equation

$$\epsilon_1 - \epsilon_2 = \frac{(n \pm \frac{\alpha}{180}) \lambda}{2tK}$$

### 3.5 Determination of the Principal Strains

One of the methods of determining the principal strains is called the oblique incidence method, and is briefly given below.

In the Figure 3.2 let  $x$ ,  $y$  represent the directions of principal strains in the plastic and  $z$  the third principal strain direction normal to the plane of the plastic. Let the axis  $z$  and  $y$  rotate about the axis  $x$  by an angle  $\alpha$ . Let the light ray strike the surface of the plastic along  $z_1$  instead of  $z$ , and corresponding to this incidence, the retardation  $\delta_\alpha$  is measured. Similarly the axis  $x$  and  $z$  can be rotated by an angle  $\beta$ . Let the light ray now pass along  $z_1$  instead of  $z$  and corresponding to this incidence, the

retardation  $\delta_\beta$  is measured. From the values  $\alpha$ ,  $\beta$ ,  $\delta_\alpha$  and  $\delta_\beta$ , the principal strains along x and y can be separately determined. For convenience if we make  $\alpha = \beta = 45^\circ$ , then

$$\epsilon_x = \frac{\sqrt{2}}{3tK} \left( \delta_\alpha + \frac{\delta_\beta}{2} \right)$$

$$\epsilon_y = \frac{\sqrt{2}}{3tK} \left( \delta_\beta + \frac{\delta_\alpha}{2} \right)$$

where  $\epsilon_x$ ,  $\epsilon_y$  are the principal strains.

This technique is done by using an oblique incidence meter.

### 3.6 Selection of Plastic

The type of plastic and its thickness depends on the strain conditions of the test piece. The Budd Company furnishes a list of plastics available, their thicknesses, the recommended maximum strains and the strain sensitivity constant K. From this information, the value of the principal strain difference to produce one fringe is calculated. A rough estimate of the expected max. strain difference determines the number of fringes that can be expected. It is very difficult to observe more than 4 fringes produced by white light, because the fringes tend to fade away at higher fringe orders. Accordingly, when white light is used, a plastic which would give 4 or less number of fringes is selected. Under monochromatic light there is no

tendency for the fringes to fade away and hence a larger number can be observed.

Photostress is a visual technique and the accuracy depends on the observation errors. The errors are larger in measuring smaller strains. The error can be as large as 25% for less than  $1/3$  fringe when the large field instrument is used. Hence it is better to have fringe order of one or more. It is necessary to obtain a plastic of uniform thickness.

Photostress plastic available from the Budd Company is in the form of sheets and viscous liquid.

There are 2 types of sheet, the type S and the type M. The type S is recommended for maximum strain of 2.5%. The type M is used for large plastic deformations and elastic deformations of materials like rubber. It is recommended for maximum strains of 30 to 50%. The sheet plastic is to be used wherever possible. The sheets have uniform thickness with a tolerance of  $\pm .003$ ". They have uniform strain-optical properties and are free from internal stresses. They can be bonded at room temperature.

Liquid plastic is available in 2 types. Type A and type G are recommended for maximum strains of 2.5% and 30 to 50% respectively. It is necessary to use this in cases where it

is impossible to attach a sheet. It is recommended in the case of structures with openings of small radii of curvature, closely riveted connections, and generally small parts. It is suitable in case of very large deformations, as in drawing of sheet metal and in problems of plastic deformations. It is especially useful in case of curved surfaces both simple and complex.

### 3.7 Advantages

The strain distribution at every point of the region coated with the plastic is available. In case of strain gages, average strain over the gage length is recorded. In the photostress the strain is not an average and can be interpreted as strain with zero gage length. The analysis can be made on any loaded structure and stresses of the actual structure are obtained. The plastic can be attached to any material (salt, concrete, wood, glass, rubber, bone, any metal). It is applicable to any type of deformation elastic, plastic and elastic-plastic. It can be used under static, dynamic, and cyclic loading.

By making a suitable choice of the plastic and the strain measuring instrument, strain measurement can be made to an accuracy of  $\pm 10^{-6}$  inch/inch. Directions of principal

strains can be measured accurate to  $\pm 2^\circ$ . The shear strain distribution is obtained directly in case of normal incidence of light. Separate values of principal strains can be obtained by an additional oblique incidence measurement.

Areas of large stress concentration are easily demarcated by simple observation. This is particularly useful in cases where the loading conditions are very complex and a theoretical stress analysis cannot be done. Large strains as high as 50% can be measured. Local yielding of material can be determined with good accuracy. Measurements on any size of surface ranging from a small crystal to a large airplane wing can be made.

Strain measurements under any atmospheric conditions, even when the structure is immersed in a liquid if the liquid is transparent like water and oil, are possible. The method can be used in a wide range of temperature, from  $-60^\circ\text{F}$  to  $+350^\circ\text{F}$ , by using certain correction factors. Temperature can go up to  $+500^\circ\text{F}$  for a period of 30 minutes. The fringe patterns can be photographed, and moving pictures can be taken if strains are rapidly changing. If for some reason it is not possible to get close to the structure, the strain measurements can be made from a distance, by direct observation, television or photo-electric devices.

The plastic behavior is independent of time. A complete record of strain distribution can be obtained from the time the plastic is bonded. This is of special significance when creep time measurements are necessary.

### 3.8 Limitations

The method cannot be used on areas which are not accessible to light.

Errors in measurements are introduced due to reinforcement of the coated part with the stress plastic if the thickness or the modulus of elasticity of the coated part is small. Errors can be introduced in case of bending of plates where the measurements are being made of the points somewhere inside the plastic instead of on the surface of the plate. In such cases corrections have to be introduced in the calculations.

The strain sensitivity constant  $K$  changes for temperatures outside the range of  $-44^{\circ}$  to  $+85^{\circ}\text{F}$ . Here again corrections have to be introduced.

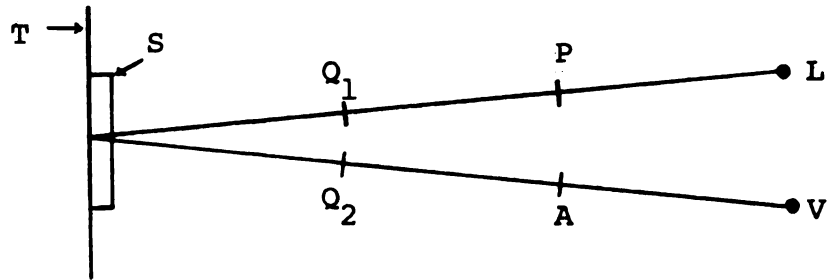


Fig. 3.1. Arrangement of the components in a large field photo stress meter.

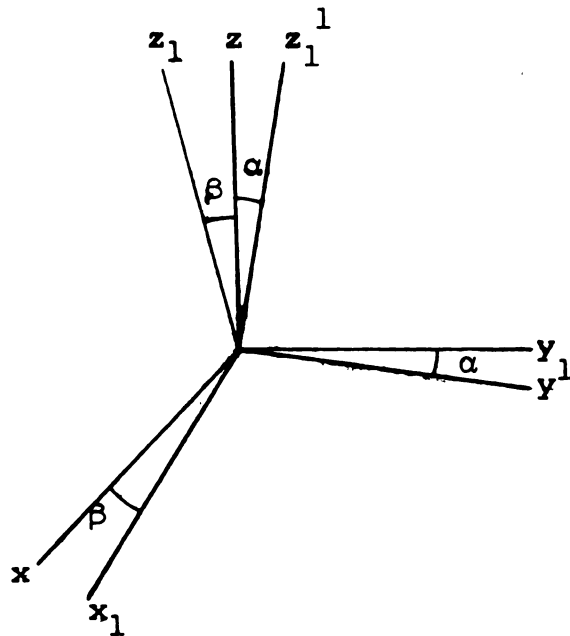


Fig. 3.2. Rotation of principal axes in oblique incidence measurements.

## CHAPTER IV

### 4.1a Strength Theories of Rock Salt

Strength theories of any solid may be described in terms of state of stress, state of strain and energy of distortion. Some of the theories which are relevant to the study of salt work are briefly examined here.

**Maximum shear stress theory:** In any state of stress, yielding will begin when the maximum shear at a point reaches a critical value. If  $\sigma_1$  and  $\sigma_3$  are the maximum and minimum principal stresses, and  $k$  is a constant for the material, then

$$\frac{\sigma_1 - \sigma_3}{2} = k$$

In case of uniaxial condition if  $\sigma_o$  is the yield stress in

the material then,  $\frac{\sigma_o}{2} = k$  and the criterion can be represented as

$$\sigma_1 - \sigma_3 = \sigma_o$$

This criterion does not make any distinction between a tensile or compressive yield strength and both are considered equal. But this is not true in case of brittle materials. The

tensile strength of salt is low compared to its compressive strength. However, the stress distribution around underground openings is predominantly compressive and hence the low tensile strength is not of any consequence. Accordingly  $\sigma_0$  has to be considered as yield strength in compression and the yield condition  $\sigma_1 - \sigma_3 = \sigma_0$  is valid in compression only.

In a triaxial stress state of salt it is found that the maximum shear stress at which failure occurs does not remain constant, but increases with the mean principal stress. Hence it is necessary to examine the material by using the Mohr's theory.

Mohr's theory: In this theory also the failure occurs when the maximum shear at a point reaches a critical value. The maximum shear stress =  $\frac{\sigma_1 - \sigma_3}{2} = k$ . The difference between this and the maximum shear stress theory is that in the Mohr's theory the critical value  $k$  is a function of  $\frac{\sigma_1 + \sigma_3}{2}$  which represents the center of the Mohr circle, whereas in the maximum stress theory  $k$  is a constant for the material. If an envelope tangent to all the circles is drawn, the point of tangency of the envelope with the largest circles is considered to represent the state of stress

on the plane of failure. This method has been extensively used to represent failure of non-metallic brittle materials.

In Mohr's theory, the envelope does not depend on the intermediate principal stress. The analysis<sup>30</sup> of triaxial tests on salt have shown that the Mohr's envelope is modified by the intermediate principal stress. Accordingly the triaxial test results can be represented by Mohr's theory, only when the mean principal stress exceeds a certain value.

Energy of distortion theory: While the maximum shear stress theory as well as the Mohr's theory do not recognize the influence of the intermediate principal stress, the energy of distortion theory takes into account, the intermediate principal stress. Hence it is necessary to consider this theory in the study of yielding in salt. According to the energy of distortion theory, yielding begins when the strain energy of distortion  $U$  reaches a critical value where,

$$U = \frac{1}{12G} \left[ (\sigma_1 - \sigma_2)^2 + (\sigma_2 - \sigma_3)^2 + (\sigma_3 - \sigma_1)^2 \right]$$

Another way of stating the same condition is that yielding begins when the octahedral shear stress  $\tau_o$  reaches a critical value where,

$$\tau_o = \frac{1}{3} \sqrt{(\sigma_1 - \sigma_2)^2 + (\sigma_2 - \sigma_3)^2 + (\sigma_3 - \sigma_1)^2}$$

In case of uniaxial condition if  $\sigma_o$  is the yield stress then the yield condition can be represented as

$$(\sigma_1 - \sigma_2)^2 + (\sigma_2 - \sigma_3)^2 + (\sigma_3 - \sigma_1)^2 = 2 \sigma_o^2$$

or,

$$\tau_o = \frac{\sqrt{2}}{3} \sigma_o$$

#### 4.1b Stress Strain Relations in the Plastic State

The solution of a plane stress problem in plastic state in a continuous medium consists in determining stresses which satisfy the following three conditions.

1. The equilibrium equations in polar coordinates,

$$\frac{\partial \sigma_r}{\partial r} + \frac{1}{r} \frac{\partial \sigma_{r\theta}}{\partial \theta} + \frac{\sigma_r - \sigma_\theta}{r} = 0 \quad (4.1.1)$$

$$\frac{1}{r} \frac{\partial \sigma_\theta}{\partial \theta} + \frac{\partial \sigma_{r\theta}}{\partial r} + 2 \frac{\sigma_{r\theta}}{r} = 0 \quad (4.1.2)$$

2. The yield condition,

$$\sigma_1 - \sigma_3 = \sigma_o, \quad (4.1.3)$$

or

$$(\sigma_1 - \sigma_2)^2 + (\sigma_2 - \sigma_3)^2 + (\sigma_3 - \sigma_1)^2 = 2 \sigma_o^2 \quad (4.1.4)$$

3. The boundary conditions.

The stress strain relations: The stress strain

relations may be expressed in the following form.<sup>26</sup>

$$\begin{aligned} d\epsilon_1^P &= \frac{F(\tau_o)}{2 \tau_o} \left[ \sigma'_1 \right] d \tau_o \\ d\epsilon_2^P &= \frac{F(\tau_o)}{2 \tau_o} \left[ \sigma'_2 \right] d \tau_o \\ d\epsilon_3^P &= \frac{F(\tau_o)}{2 \tau_o} \left[ \sigma'_3 \right] d \tau_o \end{aligned} \quad (4.1.5)$$

where  $F(\tau_o)$  is a function of  $\tau_o$  and which can be determined experimentally.

The function  $F(\tau_o)$  can be determined from the results of a uniaxial test. From the results of the uniaxial test, a relation

$$\sqrt{2\epsilon_1^P} = f(\tau_o) \quad (4.1.6)$$

can be established, where  $f(\tau_o)$  is another function of  $\tau_o$ . This will result in a relation<sup>26</sup>

$$F(\tau_o) = \frac{d f(\tau_o)}{d \tau_o} \quad (4.1.7)$$

Using value of  $F(\tau_o)$ , values of  $d\epsilon_1^P$ ,  $d\epsilon_2^P$  and  $d\epsilon_3^P$  are determined.

The stress and strain distribution can thus be determined by using the equations given above.

The generalized stress strain curve:<sup>26</sup> Another method of considering the stress strain relation is as follows.

From (4.1.5) a relation,

$$d\epsilon_o^P = \frac{2}{\sqrt{3}} \sqrt{(d\epsilon_1^P)^2 + (d\epsilon_2^P)^2 + d(\epsilon_3^P)^2}$$

or,

$$d\epsilon_o^P = F(\tau_o) d\tau_o \quad (4.1.8)$$

may be obtained, where  $d\epsilon_o^P$  is called the generalized plastic strain increment. Integration of this expression leads to

$$\epsilon_o^P = f(\tau_o) \quad (4.1.9)$$

The relation between  $\epsilon_o^P$  and  $\tau_o$  is called the generalized stress strain curve. The generalized stress strain curve in the case of a uniaxial compression test, is the relation between

$$\sqrt{2} \epsilon_1^P \text{ and } \frac{\sqrt{2}}{3} \sigma_1.$$

The generalized plastic strain  $\epsilon_o^P$  begins when  $\tau_o$  reaches a critical value  $k_1$  which is a characteristic of the material. Figure 4.1.1 represents the case of unlimited strain hardening where the value of  $\tau_o$  has an initial value of  $k_1$  and increases with  $\epsilon_o^P$ . Figure 4.1.2 represents a case of limited strain hardening where  $\tau_o$  increases gradually from an initial value of  $k_1$  to a maximum value of  $k_2$  and remains constant at  $k_2$  with increase in  $\epsilon_o^P$ . Figure 4.1.3 represents a case of perfect plasticity where the value of

$\tau_o$  remains constant at  $k_2$  with increase in  $\epsilon_o^p$ .  $k_2$  is a characteristic of the material.

Radial loading: When the ratios of the stresses remain constant throughout the loading, the loading is called radial. In such a case the total plastic strains obtained from (4.1.7) and (4.1.5) become

$$\begin{aligned}\epsilon_1^p &= \frac{f(\tau_o)}{2 \tau_o} \sigma_1' \\ \epsilon_2^p &= \frac{f(\tau_o)}{2 \tau_o} \sigma_2' \\ \epsilon_3^p &= \frac{f(\tau_o)}{2 \tau_o} \sigma_3'\end{aligned}\tag{4.1.10}$$

where  $f(\tau_o)$  can be obtained experimentally.

These equations are not strictly applicable when loading is not radial. But they have been used for non radial loading and the results so obtained have to be considered as approximate. The theory based on Eqs. (4.1.10) is called theory of plastic deformations or total strain theory. The theory based on Eqs. (4.1.5) is called the theory of plastic flow or incremental theory.

The stresses, the incremental values of strains and total strains may be obtained from the expressions given above.

#### 4.2 Uniaxial Compression Test.

The uniaxial test is the most extensively adopted form of describing the behavior of rocks under stress.

Non metallic brittle materials like salt have high compression strength but the tensile strength is very low. For such materials the mechanical properties in compression are of importance.

The conventional stress strain diagram in case of a strain hardening material depends on the strain rate and the temperature at which the test is conducted. However, the effect of strain rate at room temperature is small and can be neglected. Thus a typical stress strain curve is represented by the curve A C D in Fig. 4.2.0.

There are two methods of approximating the stress strain curve for purposes of analysis. In one method it is replaced by two straight lines AB and BD representing the elastic and the plastic part respectively and the point B represents the yield stress  $\sigma_0$  of the material. In the other method a combination of a straight line up to the yield point and a curve of the form  $\sigma = k\epsilon^m$  beyond the yield point is used. k and m are constants which have to be determined to correspond to the stress strain curve obtained experimentally.

If the specimen is unloaded in the elastic range, the path of the stress strain curve is almost parallel to the curve obtained during loading. But when the specimen is unloaded at the point C beyond the yield point, and reloaded, the path of the stress strain curve traces a loop close to a line CF drawn parallel to the elastic part AB and can be approximated by the straight lines CF and FC. If the re-loading is continued beyond the point C, the stress strain curve follows the path CD, which would be obtained if the test was done without unloading.

In some materials the stress strain diagram is a continuous curve right from the beginning and can be represented by a curve ABCD in Fig. 4.2.1. If the specimen is unloaded at a point C and reloaded, the path of the stress strain curve can be approximated by the straight lines CFC parallel to a line AG which is a tangent to the curve at A.

When strain hardening effect is small, the stress strain curve may be represented by an inclined straight line AB and a horizontal straight line BD in Fig. 4.2.2. B represents the yield point. A material with constant  $\sigma_0$  beyond the yield point is considered ideally plastic.

In cases where the elastic strains and the strain

hardening effect are both small, the stress strain curve can be represented by a horizontal straight line BD in Fig. 4.2.3.

The compression stress strain curve in salt has no straight line part. In case of materials whose stress strain relations do not conform to Hooke's law throughout the elastic range, the modulus of elasticity is defined in several ways. They are

- a. Initial tangent modulus.--The slope of the stress strain curve at the origin.
- b. Tangent modulus.--The slope of the stress strain curve at any specified stress.
- c. Secant modulus.--The slope of the secant drawn from the origin to any specified point on the stress strain curve.
- d. Chord modulus.--The slope of the chord drawn between any two specified points on the stress strain curve.

For example, according to A.S.T.M. in the case of concrete, the modulus of elasticity to the nearest 50,000 psi is

$$E = \frac{S_2 - S_1}{\epsilon - 0.000050}$$

where:

$E$  = Chord modulus of elasticity, in psi.

$S_2$  = stress corresponding to maximum applied load in psi.

$S_1$  = stress corresponding to a longitudinal strain of 50 micro in/in., in psi.

$\epsilon$  = longitudinal strain produced by stress  $S_2$ .

The Poisson's ratio, to the nearest 0.01 is

$$\eta = \frac{\epsilon_2 - \epsilon_1}{\epsilon - 0.000050}$$

where:

$\eta$  = Poisson's ratio,

$\epsilon_2$  = transverse strain at mid height of the specimen produced by stress  $S_2$ ,

$\epsilon_1$  = transverse strain at mid height of the specimen produced by stress  $S_1$ .

Salt does not exhibit a clearly defined yield point, contrary to metals. In such a case, the yield strength is defined as the stress at which the material experiences a specified value of permanent strain. A value of 0.5% for this permanent strain may be used in case of salt while 0.2% is widely used in metals.

When a cubical specimen of a brittle material like salt is compressed uniaxially, frictional forces are set up at the surfaces of contact of the specimen and the compression plates, due to the lateral expansion of the specimen. The material in contact with the compression plates tends to stick to the compression plates, and the material on the

sides and away from the surfaces of contact is crushed and separates itself leaving a central core. If friction at the surfaces of contact is eliminated, the failure takes place along planes parallel to the sides of the cube.

The material fails in several ways. Cleavage fracture occurs along parallel planes in small steps. Separation of the grains along the grain boundaries occurs due to breaking down of the cohesive forces. The material is considered isotropic in our analysis. But in reality the random orientation of grains may develop stress causing local failure of the material.

#### 4.3 Biaxial Test

The failure of the material in biaxial state of stress is different from that of the uniaxial state. The material in this case, is confined in two directions and the material flows. It is assumed that yielding begins when the quantity  $U$  reaches a critical value where,

$$U = (\sigma_1 - \sigma_2)^2 + (\sigma_2 - \sigma_3)^2 + (\sigma_3 - \sigma_1)^2.$$

In the plastic state of stress it is necessary to determine  $f(\tau_0)$  of (4.1.10) in order to calculate the strain distribution. The principal stresses are  $\sigma_1 = \sigma_2$  and  $\sigma_3 = 0$ .

$$\tau_o = \frac{\sqrt{2}}{3} \sigma_1 \quad (4.3.1)$$

$$\frac{d \tau_o}{d \sigma_1} = \frac{\sqrt{2}}{3} \quad (4.3.2)$$

$$d\epsilon_1^p = \frac{F(\tau_o)}{2 \tau_o} \sigma_1' d \tau_o \quad (4.3.3)$$

$$d\epsilon_1^p = \frac{F(\tau_o)}{6} d\sigma_1 \quad (4.3.3)$$

From a biaxial test a relation between

$2 \sqrt{2} \epsilon_1^p$  and  $\tau_o$  can be obtained.

$$\text{Let } 2 \sqrt{2} \epsilon_1^p = f(\tau_o) \quad (4.3.4)$$

Differentiating Eq. (4.3.4) gives

$$2 \sqrt{2} d\epsilon_1^p = \frac{d f(\tau_o)}{d \tau_o} \frac{d \tau_o}{d \sigma_1} d\sigma_1$$

$$2 \sqrt{2} d\epsilon_1^p = \frac{\sqrt{2}}{3} \frac{d f(\tau_o)}{d \tau_o} d\sigma_1$$

$$d\epsilon_1^p = \frac{1}{6} \frac{d f(\tau_o)}{d \tau_o} d\sigma_1 \quad (4.3.5)$$

(4.3.3) and (4.3.5) gives,

$$F(\tau_o) = \frac{d f(\tau_o)}{d \tau_o} \quad (4.3.6)$$

Hence the function  $f(\tau_o)$  can be determined by drawing a curve showing the relation between  $2 \sqrt{2} \epsilon_1^p$  and  $\frac{\sqrt{2}}{3} \sigma_1$ .

Both  $\sigma_1$  and  $\epsilon_1^p$  were measured experimentally in one of the tests.

#### 4.4 Circular Hole in an Infinite Medium Under Biaxial State of Stress (Fig. 4.4.1)

This problem is considered as a plane stress problem of a thick walled cylinder subjected to a uniform external radial pressure. In Fig. 4.4.1 is shown a circular hole of radius  $a$  in a plane of infinite dimensions and subjected to equal vertical and horizontal stress  $= p$ . Considering a circle of radius  $b$ , very large compared to the radius  $a$  of the hole, the external forces on the surface of the cylinder are  $\sigma_r = -p$  and  $\sigma_{r\theta} = 0$ . The solution of the thick walled cylinder under a uniform radial compression stress  $= p$  at its outer radius and zero radial stress at its internal radius will follow.

The stresses and strains are axially symmetric. Hence the radial stress  $\sigma_r$  and the tangential stress  $\sigma_\theta$  are the principal stresses,  $\sigma_{r\theta}$  is zero, and the stresses are independent of  $\theta$ . The principal stress  $\sigma_z$  in the direction of axis of the cylinder is zero.

The treatment as a plane stress problem is to be recognized as an approximation to the actual conditions which are in between plane stress and plane strain existing underground.

The stress and strain distribution in completely

plastic, elastic-plastic and elastic stress states are now given.

#### 4.5 Completely Plastic Cylinder in Plane Stress Condition

Stresses assuming perfect plasticity: The yield condition of (4.1.4), after substituting  $\sigma_2 = \sigma_r$ ,  $\sigma_3 = \sigma_\theta$  and  $\sigma_1 = 0$  becomes

$$\sigma_r^2 - \sigma_r \sigma_\theta + \sigma_\theta^2 = \sigma_o^2 \quad (4.5.1)$$

(4.5.1) gives

$$\sigma_\theta = \frac{1}{2} \left[ \sigma_r - \sqrt{4 \sigma_o^2 - 3 \sigma_r^2} \right] \quad (4.5.2)$$

The equilibrium equation (4.1.1) becomes,

$$\frac{\partial \sigma_r}{\partial r} + \frac{\sigma_r - \sigma_\theta}{r} = 0 \quad (4.5.3)$$

(4.5.2) in (4.5.3) gives

$$\frac{d \sigma_r}{dr} + \frac{1}{2r} \left[ \sqrt{4 \sigma_o^2 - 3 \sigma_r^2} + \sigma_r \right] = 0 \quad (4.5.4)$$

The solution of (4.5.4) is

$$-\ln r = \frac{\sqrt{3}}{2} \sin^{-1} \left[ \frac{\sqrt{3}}{2} \frac{\sigma_r}{\sigma_o} \right] + \frac{1}{2} \ln \left[ \sqrt{1 - \frac{3}{4} \frac{\sigma_r^2}{\sigma_o^2}} + \frac{\sigma_r}{2 \sigma_o} \right] + C \quad (4.5.5)$$

where C is a constant.

The boundary conditions are

$$r = a, \sigma_r = 0 \quad (4.5.6)$$

$$r = b, \sigma_r = -p \quad (4.5.7)$$

(4.5.6) in (4.5.5) gives

$$c = -\ln a \quad (4.5.8)$$

(4.5.8) in (4.5.5) gives

$$\ln \frac{a}{r} = \frac{\sqrt{3}}{2} \sin^{-1} \left[ \frac{\sqrt{3}}{2} \frac{\sigma_r}{\sigma_o} \right] + \frac{1}{2} \ln \left[ \sqrt{1 - \frac{3}{4} \frac{\sigma_r^2}{\sigma_o^2}} + \frac{\sigma_r}{2 \sigma_o} \right] \quad (4.5.9)$$

or,

$$\frac{a}{r} = \left[ e^{\frac{\sqrt{3}}{2} \sin^{-1} \left( \frac{\sqrt{3}}{2} \frac{\sigma_r}{\sigma_o} \right)} \right] \left[ \sqrt{1 - \frac{3}{4} \frac{\sigma_r^2}{\sigma_o^2}} + \frac{\sigma_r}{2 \sigma_o} \right] \quad (4.5.10)$$

(4.5.2) gives

$$\frac{\sigma_\theta}{\sigma_o} = \frac{\sigma_r}{2 \sigma_o} - \sqrt{1 - \frac{3}{4} \frac{\sigma_r^2}{\sigma_o^2}} \quad (4.5.11)$$

(4.5.9) or (4.5.10) and (4.5.11) describe the stress distribution in a completely plastic state.

$\frac{\sigma_r}{\sigma_o}$  is first obtained by trial and error from

(4.5.10) and substituting values of  $\frac{\sigma_r}{\sigma_o}$  in (4.5.11) gives

$$\frac{\sigma_\theta}{\sigma_o}$$

The second boundary condition (4.5.7) gives the relationship between external pressure  $p$  and the ratio  $\frac{a}{b}$ .

(4.5.7) in (4.5.10) gives

$$\frac{a}{b} = \left[ e^{\frac{\sqrt{3}}{2} \sin^{-1} \left( \frac{\sqrt{3}}{2} \frac{-p}{\sigma_o} \right)} \right] \left[ \sqrt{1 - \frac{3}{4} \frac{p^2}{\sigma_o^2} + \frac{-p}{2 \sigma_o}} \right] \quad (4.5.12)$$

Table 4.5.5 gives values of  $\frac{\sigma_r}{\sigma_o}$  and  $\frac{\sigma_\theta}{\sigma_o}$  in terms of  $\frac{r}{a}$  obtained by trial and error from (4.5.10) and (4.5.11).

Fig. 4.5.2 shows the relationship between  $\frac{\sigma_r}{\sigma_o}$  and  $\frac{\sigma_\theta}{\sigma_o}$  and  $\frac{a}{r}$ .

Strains for hardening plastic material: Total plastic strains may be obtained from (4.1.10) as follows.

$$\begin{aligned} \epsilon_r^p &= \frac{f(\tau_o)}{2 \tau_o} \sigma_r' \\ \epsilon_\theta^p &= \frac{f(\tau_o)}{2 \tau_o} \sigma_\theta' \end{aligned} \quad (4.5.13)$$

$$\begin{aligned} \epsilon_z^p &= \frac{f(\tau_o)}{2 \tau_o} \sigma_z' \\ \epsilon_r^p - \epsilon_\theta^p &= \frac{f(\tau_o)}{2 \tau_o} (\sigma_r' - \sigma_\theta') = \frac{f(\tau_o)}{2 \tau_o} (\sigma_r - \sigma_\theta) \end{aligned} \quad (4.5.14)$$

Table 4.5.5. Stresses in the completely plastic state under uniform external pressure.

$\frac{\sigma_r}{\sigma_o}$	$\frac{\sigma_\theta}{\sigma_o}$	$\frac{a}{r}$
0	-1	1
-0.1	-1.046	0.901
-0.2	-1.0848	0.8091
-0.3	-1.1155	0.7192
-0.4	-1.138	0.6324
-0.5	-1.1512	0.5475
-0.6	-1.1544	0.4639
-0.7	-1.1453	0.3796
-0.8	-1.1211	0.2920
-0.9	-1.0765	0.1937
-1.0	-1.0	0

Substituting  $\tau_o = \frac{\sqrt{2}}{3} \sigma_o$  in (4.5.14) gives

$$\epsilon_r^p - \epsilon_\theta^p = 1.061 f(\tau_o) \left[ \frac{\sigma_r}{\sigma_o} - \frac{\sigma_\theta}{\sigma_o} \right] \quad (4.5.15)$$

The values of  $\epsilon_r^p - \epsilon_\theta^p$  may be calculated for any cylinder after determining  $f(\tau_o)$  experimentally.

#### 4.6 Elastic Plastic Cylinder in Plane Stress Condition.

Plastic region.--Let the elastic plastic boundary be at  $r = \rho$ , and the radial stress at the elastic plastic boundary be designated by  $\sigma_{r\rho}$ . The stresses  $\sigma_r$  and  $\sigma_\theta$  are given by (4.5.9) or (4.5.10) and (4.5.11).

The boundary condition is

$$r = \rho, \quad \sigma_r = \sigma_{r\rho} \quad (4.6.1)$$

(4.6.1) in (4.5.10) gives

$$\frac{a}{\rho} = e^{\left[ \frac{\sqrt{3}}{2} \sin^{-1} \left( \frac{\sqrt{3}}{2} \frac{\sigma_{r\rho}}{\sigma_o} \right) \right]} \left[ \sqrt{1 - \frac{3}{4} \frac{\sigma_{r\rho}^2}{\sigma_o^2} + \frac{\sigma_{r\rho}}{2\sigma_o}} \right] \quad (4.6.2)$$

(4.6.2) gives  $\frac{\sigma_{r\rho}}{\sigma_o}$  for any value of  $\frac{a}{\rho}$ .

Elastic region.--The stresses in this region are obtained by considering a cylinder of external radius  $b$  and internal radius  $\rho$  with the following boundary conditions.

$$\text{at } r = b, \quad \sigma_r = -p \quad (4.6.3)$$

$$\text{at } r = \rho, \quad \sigma_r = \sigma_{r\rho} \quad (4.6.4)$$

at  $r = \rho$ , the yield condition (4.5.1) is to be

$$\text{satisfied.} \quad (4.6.5)$$

The elastic solution is of the form

$$\sigma_r = \frac{A}{r^2} + 2 C_1 \quad (4.6.6)$$

$$\sigma_\theta = -\frac{A}{r^2} + 2 C_1 \quad (4.6.7)$$

Where A and  $C_1$  are constants.

(4.6.3) in (4.6.6) gives

$$-p = \frac{A}{b^2} + 2 C_1 \quad (4.6.8)$$

(4.6.4) in (4.6.6) gives

$$\sigma_{r\rho} = \frac{A}{\rho^2} + 2 C_1 \quad (4.6.9)$$

(4.6.8) and (4.6.9) give

$$A = \frac{b^2 \rho^2 (p + \sigma_{r\rho})}{b^2 - \rho^2} \quad (4.6.10)$$

$$2 C_1 = \frac{-(pb^2 + \sigma_{r\rho} \rho^2)}{b^2 - \rho^2} \quad (4.6.11)$$

(4.6.10) and (4.6.11) in (4.6.6) and (4.6.7) give

$$\frac{\sigma_r}{\sigma_o} = \frac{b^2}{r^2} \frac{\rho^2}{a^2} \frac{\left( \frac{p}{\sigma_o} + \frac{\sigma_{r\rho}}{\sigma_o} \right)}{\left( \frac{b^2}{a^2} - \frac{\rho^2}{a^2} \right)} + \frac{- \left( \frac{p}{\sigma_o} \frac{b^2}{a^2} + \frac{\sigma_{r\rho}}{\sigma_o} \frac{\rho^2}{a^2} \right)}{\left( \frac{b^2}{a^2} - \frac{\rho^2}{a^2} \right)} \quad (4.6.12)$$

$$\frac{\sigma_{\theta}}{\sigma_o} = -\frac{b^2}{r^2} \frac{\rho^2}{a^2} \frac{\left(\frac{p}{\sigma_o} + \frac{\sigma_{r\rho}}{\sigma_o}\right)}{\left(\frac{b^2}{a^2} - \frac{\rho^2}{a^2}\right)} + \frac{-\left(\frac{p}{\sigma_o} \frac{b^2}{a^2} + \frac{\sigma_{r\rho}}{\sigma_o} \frac{\rho^2}{a^2}\right)}{\left(\frac{b^2}{a^2} - \frac{\rho^2}{a^2}\right)} \quad (4.6.13)$$

(4.6.12) and (4.6.13) give the stresses in the elastic region in terms of  $\sigma_{r\rho}$ .

$\sigma_{r\rho}$  may be expressed in terms of  $p$  by making use of condition in (4.6.5) as follows. (4.6.6) and (4.6.7)

$$\text{give, when } r = \rho, \text{ the radial stress } \sigma_{r\rho} = \frac{A}{\rho^2} + 2 C_1 \quad (4.6.14)$$

$$\text{the tangential stress } \sigma_{\theta\rho} = \frac{-A}{\rho^2} + 2 C_1 \quad (4.6.15)$$

(4.6.14) and (4.6.15) in the yield condition expressed in (4.6.5) gives, when  $r = \rho$ ,

$$\frac{3 A^2}{\rho^4} + (2 C_1)^2 = \sigma_o^2 \quad (4.6.16)$$

(4.6.10) and (4.6.11) in (4.6.16) gives

$$\frac{3}{\rho^4} \left[ \frac{b^2 \rho^2 (p + \sigma_{r\rho})}{b^2 - \rho^2} \right]^2 + \left[ \frac{-(pb^2 + \sigma_{r\rho} \rho^2)}{(b^2 - \rho^2)} \right]^2 = \sigma_o^2 \quad (4.6.17)$$

(4.6.17) gives

$$\frac{-p}{\sigma_o} = \frac{1}{4} \frac{\sigma_{r\rho}}{\sigma_o} \left[ 3 + \frac{\rho^2}{b^2} \right] - \frac{1}{2} \left( 1 - \frac{\rho^2}{b^2} \right) \sqrt{1 - \frac{3}{4} \frac{\sigma_{r\rho}^2}{\sigma_o^2}} \quad (4.6.18)$$

The above derivation for stresses is summarized and given below.

In the plastic region,  $\frac{\sigma_r}{\sigma_o}$  and  $\frac{\sigma_\theta}{\sigma_o}$  are given by (4.5.9) or (4.5.10) and (4.5.11). In elastic region,  $\frac{\sigma_r}{\sigma_o}$  and  $\frac{\sigma_\theta}{\sigma_o}$  are given by (4.6.12) and (4.6.13) in terms of  $\frac{\sigma_{r\rho}}{\sigma_o}$ .

(4.6.2) gives  $\frac{\sigma_{r\rho}}{\sigma_o}$  for any given  $\frac{a}{\rho}$ .

External pressure  $\frac{p}{\sigma_o}$  for any value of  $\frac{\sigma_{r\rho}}{\sigma_o}$  is given by (4.6.18).

The case when  $b$  is very large compared to  $\rho$ :  
In such a case  $\frac{\rho}{b}$  tends to become zero. In the plastic region the stresses  $\frac{\sigma_r}{\sigma_o}$  and  $\frac{\sigma_\theta}{\sigma_o}$  will not change and are given by (4.5.9) or (4.5.10) and (4.5.11).

In the elastic region, substituting  $\frac{\rho}{b} = 0$  in

(4.6.12), (4.6.13) and (4.6.18) gives

$$\frac{\sigma_r}{\sigma_o} = \frac{-p}{\sigma_o} \left( 1 - \frac{\rho^2}{r^2} \right) - \frac{\rho^2}{r^2} \frac{\sigma_{r\rho}}{\sigma_o} \quad (4.6.19)$$

$$\frac{\sigma_{\theta}}{\sigma_o} = \frac{-p}{\sigma_o} \left(1 + \frac{\rho^2}{r^2}\right) + \frac{\rho^2}{r^2} \frac{\sigma_{r\rho}}{\sigma_o} \quad (4.6.20)$$

$$\frac{p}{\sigma_o} = -\frac{3}{4} \frac{\sigma_{r\rho}}{\sigma_o} + \frac{1}{2} \sqrt{1 - \frac{3}{4} \frac{\sigma_{r\rho}^2}{\sigma_o^2}} \quad (4.6.21)$$

The relation between  $\frac{\sigma_{r\rho}}{\sigma_o}$  and  $\frac{a}{\rho}$  is given by (4.6.2).

The stress distribution in case of a cylinder of internal diameter of 1" and external diameter of 4" is worked out for values of  $\frac{\rho}{a}$  ranging from 1 to 4. The steps involved are

1. For assumed values of  $\frac{\rho}{a}$ , values of  $\frac{\sigma_{r\rho}}{\sigma_o}$ , and the stresses in the plastic region  $\frac{\sigma_r}{\sigma_o}$  and  $\frac{\sigma_{\theta}}{\sigma_o}$  are calculated from (4.6.2), (4.5.10) and (4.5.11).
2. Using values of  $\frac{\sigma_{r\rho}}{\sigma_o}$  obtained in step 1, values of  $\frac{-p}{\sigma_o}$  are calculated from (4.6.18).
3. Substituting values of  $\frac{\sigma_{r\rho}}{\sigma_o}$  and  $\frac{p}{\sigma_o}$  obtained in steps 2 and 3, values of  $\frac{\sigma_r}{\sigma_o}$  and  $\frac{\sigma_{\theta}}{\sigma_o}$  in the elastic region are given by (4.6.12) and (4.6.13).

Table 4.6.5 and Fig. 4.6.2 give the stress distribution for all the 4 values of  $\frac{\rho}{a}$ .

Table 4.6.5. Stresses in anelastic plastic cylinder of external radius of 4" and internal radius of 1".

	$\frac{r}{a} = 1$	$\frac{r}{a} = 2$	$\frac{r}{a} = 3$	$\frac{r}{a} = 4$
$\frac{\sigma_r}{\sigma_0}$	0	-0.56	-0.755	-0.85
$\frac{\sigma_\theta}{\sigma_0}$	0.4687	0.7831	0.8377	0.85
$\frac{\sigma_r}{\sigma_0}$	0	0	0	0
$\frac{\sigma_\theta}{\sigma_0}$	-1	-1	-1	-1
1	0	-1	0	-1
1.5	-0.2778	-0.36	-0.36	-0.36
2	-0.375	-0.56	-0.56	-0.56
2.5	-0.42	-0.667	-0.68	-0.68
3	-0.4445	-0.7254	-0.755	-0.755
3.5	-0.4591	-0.7603	-0.805	-0.815
4	-0.4687	-0.7831	-0.8377	-0.85

## 4.7 Completely Elastic Cylinder in Plane Stress Condition.

The stresses are of the form

$$\sigma_r = \frac{A}{r^2} + 2C$$

$$\sigma_\theta = \frac{-A}{r^2} + 2C$$

(4.7.1)

The boundary conditions are

$$r = a, \quad \sigma_r = 0$$

$$r = b, \quad \sigma_r = -p$$

The stresses are

$$\sigma_r = \frac{-p}{1 - \frac{a^2}{b^2}} \left(1 - \frac{a^2}{r^2}\right)$$

$$\sigma_\theta = \frac{-p}{1 - \frac{a^2}{b^2}} \left(1 + \frac{a^2}{r^2}\right)$$

(4.7.2)

$$\sigma_z = 0$$

The strains are

$$\epsilon_r = \frac{1}{E} \frac{-p}{1 - \frac{a^2}{b^2}} \left[ (1 - \eta) - \frac{a^2}{r^2} (1 + \eta) \right]$$

(4.7.3)

$$\epsilon_\theta = \frac{1}{E} \frac{-p}{1 - \frac{a^2}{b^2}} \left[ (1 - \eta) + \frac{a^2}{r^2} (1 + \eta) \right]$$

$$\epsilon_z = -\frac{2\eta}{E} \frac{-p}{1 - \frac{a^2}{b^2}}$$

Radial displacement.

$$\frac{du}{dr} = \epsilon_r \quad (4.7.4)$$

$$u = \frac{1}{E} \frac{-p}{1 - \frac{a^2}{b^2}} \left[ (1 - \eta)r + (1 + \eta) \frac{a^2}{r} \right] \quad (4.7.5)$$

#### 4.8. Completely Elastic Cylinder in Plane Stress Condition Assuming Incompressibility

$$\epsilon_r = \frac{du}{dr}$$

$$\epsilon_\theta = \frac{u}{r} \quad (4.8.1)$$

$$\epsilon_z = \epsilon_z$$

Incompressibility condition is

$$\epsilon_r + \epsilon_\theta + \epsilon_z = 0$$

$$\frac{du}{dr} + \frac{u}{r} + \epsilon_z = 0 \quad (4.8.2)$$

From (4.7.3) it is seen that  $\epsilon_z$  is independent of  $r$  and  $\theta$ .

Accordingly  $\epsilon_z$  is assumed to be independent of  $r$  and  $\theta$ .

Integrating (4.8.2) gives

$$u = -\frac{\epsilon_z r}{2} + \frac{D}{r} \quad (4.8.3)$$

where D is a constant.

$$\text{Let } u = u_1 \text{ when } r = a \quad (4.8.4)$$

(4.8.4) in (4.8.3) gives

$$u = \frac{\epsilon_z}{2} \left( \frac{a^2}{r} - r \right) + u_1 \frac{a}{r} \quad (4.8.5)$$

(4.8.5) gives

$$\epsilon_r = \frac{du}{dr} = -\frac{\epsilon_z}{2} \left( \frac{a^2}{r^2} + 1 \right) - u_1 \frac{a}{r^2}$$

$$\epsilon_\theta = \frac{u}{r} = \frac{\epsilon_z}{2} \left( \frac{a^2}{r^2} - 1 \right) + u_1 \frac{a}{r^2} \quad (4.8.6)$$

$$\epsilon_r - \epsilon_\theta = -\epsilon_z \frac{a^2}{r^2} - 2 u_1 \frac{a}{r^2}$$

The elastic stress strain relation and the incompressibility condition give

$$\sigma_r' = 2 G \epsilon_r$$

$$\sigma_\theta' = 2 G \epsilon_\theta \quad (4.8.7)$$

$$\sigma_z' = 2 G \epsilon_z$$

$$\sigma_r' - \sigma_\theta' = \sigma_r' - \sigma_\theta'$$

$$= 2 G (\epsilon_r - \epsilon_\theta) \quad (4.8.8)$$

(4.8.6) in (4.8.8) gives

$$\sigma_r - \sigma_\theta = 2G \left[ -\epsilon_z \frac{a^2}{r^2} - 2u_1 \frac{a}{r^2} \right] \quad (4.8.9)$$

Equilibrium equation is

$$\frac{d\sigma_r}{dr} + \frac{\sigma_r - \sigma_\theta}{r} = 0 \quad (4.8.10)$$

(4.8.9) in (4.8.10) gives

$$\frac{d\sigma_r}{dr} + 2G \left[ -\epsilon_z \frac{a^2}{r^3} - 2u_1 \frac{a}{r^3} \right] \quad (4.8.11)$$

Integrating,

$$\sigma_r = B - 2G a \frac{u_1}{r^2} - \epsilon_z \frac{G a^2}{r^2} \quad (4.8.12)$$

Boundary conditions are

$$\begin{aligned} r = a, \quad \sigma_r &= 0 \\ r = b, \quad \sigma_r &= -p \end{aligned} \quad (4.8.13)$$

(4.8.13) in (4.8.12) gives

$$u_1 = \frac{-p}{2G} \frac{a}{1 - \frac{a^2}{b^2}} - \epsilon_z \frac{a}{2} \quad (4.8.14)$$

$$B = \frac{-p}{1 - \frac{a^2}{b^2}} \quad (4.8.15)$$

(4.8.14) and (4.8.15) in (4.8.12) give:

$$\sigma_r = \frac{-p}{1 - \frac{a^2}{b^2}} \left[ 1 - \frac{a^2}{r^2} \right] \quad (4.8.16)$$

(4.8.14) and (4.8.16) in (4.8.9) give

$$\sigma_\theta = \frac{-p}{1 - \frac{a^2}{b^2}} \left[ 1 + \frac{a^2}{r^2} \right] \quad (4.8.17)$$

(4.8.16) and (4.8.17) in (4.8.7) gives

$$\epsilon_r = \frac{1}{6G} \frac{-p}{1 - \frac{a^2}{b^2}} \left[ 1 - 3 \frac{a^2}{r^2} \right]$$

$$\epsilon_\theta = \frac{1}{6G} \frac{-p}{1 - \frac{a^2}{b^2}} \left[ 1 + 3 \frac{a^2}{r^2} \right] \quad (4.8.18)$$

$$\epsilon_z = - \frac{1}{3G} \frac{-p}{1 - \frac{a^2}{b^2}}$$

(4.8.16) and (4.8.17) give elastic stresses.

(4.8.18) gives elastic strains.

#### 4.9 Circular Hole in an Infinite Medium Under Biaxial Compression ( $\sigma_x \neq \sigma_y$ )

Savin<sup>29</sup> gives an approximate solution for the elastic-plastic problem of a thin sheet of infinite dimensions with a hole of radius = a and subjected to stresses  $\sigma_x = \lambda_1 \sigma_0$  and

$\sigma_y = \lambda_2 \sigma_o$  at infinity.  $\lambda_1, \lambda_2$  are dimensionless quantities,  
 $0 \leq \lambda_1 \leq 1, 0 \leq \lambda_2 \leq 1$ . (Fig. 4.9.1).

In the plastic zone, the condition for plasticity based on the maximum shear stress theory is given as<sup>29</sup>

$$(\sigma_r - \sigma_\theta)^2 + 4 \sigma_{r\theta}^2 = \left[ 2 \sigma_o - |\sigma_r + \sigma_\theta| \right]^2 \quad (4.9.1)$$

The stresses in the plastic region bounded by the curve L are

$$\frac{\sigma_r}{\sigma_o} = \left( 1 - \frac{a}{r} \right)$$

(4.9.1)

$$\frac{\sigma_\theta}{\sigma_o} = 1$$

(4.9.2)

$$\frac{\sigma_{r\theta}}{\sigma_o} = 0$$

The stresses in the elastic regions are obtained as

$$\frac{\sigma_r}{\sigma_o} = \left( \frac{\lambda_1 + \lambda_2}{2} \right) \left( 1 - \gamma \frac{a^2}{r^2} \right) - \lambda \left( 1 - 2\beta \frac{a^2}{r^2} + 3\delta \frac{a^4}{r^4} \right) \cos 2\theta$$

$$\frac{\sigma_\theta}{\sigma_o} = \left( \frac{\lambda_1 + \lambda_2}{2} \right) \left( 1 + \gamma \frac{a^2}{r^2} \right) + \lambda \left( 1 + 3\delta \frac{a^4}{r^4} \right) \cos 2\theta \quad (4.9.3)$$

$$\frac{\sigma_{r\theta}}{\sigma_o} = \lambda \left( 1 + \beta \frac{a^2}{r^2} - 3\delta \frac{a^4}{r^4} \right) \sin 2\theta$$

(4.9.3)

The equation for the elastic plastic boundary curve L satisfying the yield condition on the boundary and stresses on both sides of the boundary is obtained as<sup>29</sup>

$$\frac{r(\theta)}{a} = \frac{1}{2 - \lambda_1 - \lambda_2} - \frac{2(\lambda_1 - \lambda_2)}{(2 - \lambda_1 - \lambda_2)^2} \cos 2\theta \quad (4.9.4)$$

Where

$$\begin{aligned} \gamma &= \frac{1}{(\lambda_1 + \lambda_2)(2 - \lambda_1 - \lambda_2)} \\ \beta &= \frac{2}{(2 - \lambda_1 - \lambda_2)^2} \\ \delta &= \frac{1}{(2 - \lambda_1 - \lambda_2)^4} \\ \lambda &= \frac{\lambda_2 - \lambda_1}{2}. \end{aligned} \quad (4.9.5)$$

Timoshenko<sup>36</sup> gives the stresses in a completely elastic state. The stresses are

$$\sigma_r = \frac{\sigma_x + \sigma_y}{2} (1 - \alpha^2) + \frac{\sigma_x - \sigma_y}{2} (1 + 3\alpha^4 - 4\alpha^2) \cos 2\theta$$

$$\sigma_\theta = \frac{\sigma_x + \sigma_y}{2} (1 + \alpha^2) - \frac{\sigma_x - \sigma_y}{2} (1 + 3\alpha^4) \cos 2\theta$$

$$\sigma_{r\theta} = -\frac{\sigma_x - \sigma_y}{2} (1 - 3\alpha^4 + 2\alpha^2) \sin 2\theta$$

$$\text{where } \frac{a}{r} = \alpha$$

For a specific case of  $\frac{\sigma_x}{\sigma_y} = \frac{1}{3}$ , the elastic stresses become

$$\sigma_r = \frac{2}{3} \sigma_y (1 - \alpha^2) - \frac{1}{3} \sigma_y (1 + 3\alpha^4 - 4\alpha^2) \cos 2\theta$$

$$\sigma_\theta = \frac{2}{3} \sigma_y (1 + \alpha^2) + \frac{1}{3} \sigma_y (1 + 3\alpha^4) \cos 2\theta$$

$$\sigma_{r\theta} = \frac{1}{3} \sigma_y (1 - 3\alpha^4 + 2\alpha^2) \sin 2\theta$$

$$(\sigma_r - \sigma_\theta) = \frac{4}{3} \sigma_y \alpha^2 - \frac{1}{3} \sigma_y (2 - 4\alpha^2 + 6\alpha^4) \cos 2\theta$$

On the boundary when  $r = a$ ,

$$\sigma_\theta = \frac{4}{3} \sigma_y (1 + \cos 2\theta)$$

The maximum and minimum values of  $\sigma_\theta$  on the boundary occur when  $\theta = 0^\circ$  and  $\theta = 90^\circ$  respectively and the values are

$$\text{maximum } \sigma_\theta = \frac{8}{3} \sigma_y.$$

$$\text{minimum } \sigma_\theta = 0$$

Yielding begins on the hole boundary when  $\max \sigma_\theta = \sigma_o$

or when  $\sigma_y = \frac{3}{8} \sigma_o$  and  $\sigma_x = \frac{1}{8} \sigma_o$ .

On x and y axis, the  $\sigma_r$  and  $\sigma_\theta$  are principal stresses.

When  $\theta = 90^\circ$ , and  $\frac{\sigma_x}{\sigma_y} = \frac{1}{3}$ ,

$$\sigma_r = \sigma_y (1 - 2\alpha^2 + \alpha^4)$$

$$\sigma_\theta = \sigma_y \left( \frac{1}{3} + \frac{2}{3} \alpha^2 - \alpha^4 \right)$$

$$(\sigma_r - \sigma_\theta) = -\sigma_y \left( -\frac{2}{3} + \frac{8}{3} \alpha^2 - 2\alpha^4 \right).$$

When  $\theta = 0$  and  $\frac{\sigma_x}{\sigma_y} = \frac{1}{3}$ ,

$$(\sigma_r - \sigma_\theta) = -\sigma_y \left( \frac{2}{3} + 2\alpha^4 \right)$$

The principal strain difference is when  $\theta = 90^\circ$ ,  $\epsilon_r - \epsilon_\theta = -\left(\frac{1+\eta}{E}\right) \sigma_y \left(-\frac{2}{3} + \frac{8}{3}\alpha^2 - 2\alpha^4\right)$ , when  $\theta = 0^\circ$ ,  $\epsilon_r - \epsilon_\theta = -\left(\frac{1+\eta}{E}\right) \sigma_y \left(\frac{2}{3} + 2\alpha^4\right)$ .

#### 4.10 Circular Hole in an Infinite Elastic Medium Under Uniaxial Compression of $\sigma_y = S$ (Fig. 4.10.1)

The elastic stresses are given by substituting  $\sigma_x = 0$  in the equations under biaxial compression.

The stresses are,

$$\sigma_r = \frac{\sigma_y}{2} (1 - \alpha^2) - \frac{\sigma_y}{2} (1 + 3\alpha^4 - 4\alpha^2) \cos 2\theta$$

$$\sigma_\theta = \frac{\sigma_y}{2} (1 + \alpha^2) + \frac{\sigma_y}{2} (1 + 3\alpha^4) \cos 2\theta$$

$$\sigma_{r\theta} = \frac{\sigma_y}{2} (1 - 3\alpha^4 + 2\alpha^2) \sin 2\theta$$

$$\sigma_r - \sigma_\theta = -\sigma_y \alpha^2 - \sigma_y (1 - 2\alpha^2 + 3\alpha^4) \cos 2\theta$$

where  $\frac{a}{r} = \alpha$

On the horizontal and vertical axes, the principal stresses become,

when  $\theta = 0$ ,  $\sigma_r - \sigma_\theta = -\sigma_y (1 - a^2 + 3a^4)$ ,

when  $\theta = 90^\circ$ ,  $\sigma_r - \sigma_\theta = -\sigma_y (-1 + 3a^2 - 3a^4)$ .

The tangential stress along the boundary  $r = a$  becomes,

$$\sigma_\theta = \sigma_y (1 + 2 \cos 2\theta)$$

The maximum and minimum values of  $\sigma_\theta$  on the boundary occur

when  $\theta = 0^\circ$  and  $90^\circ$  respectively and the values are

$$\text{max. } \sigma_\theta = 3 \sigma_y$$

$$\text{min. } \sigma_\theta = -\sigma_y$$

Yielding of material begins on the boundary of hole

when the applied stress becomes  $\sigma_y = \frac{\sigma_0}{3}$

#### 4.11 Square Hole in an Infinite Medium Under Uniaxial Compression (Fig. 4.11.1)

Savin<sup>29</sup> gives the solution of the problem of elastic stress distribution for a square hole of side  $a = \frac{5}{3} R$  and subjected to uniform stress of  $\sigma_x = p$  at infinity from the center of the hole.  $R$  is a parameter to make an approximation to the boundary of the hole.

The boundary of the hole is represented in rectangular coordinates as

$$x = R \left( \cos \theta - \frac{1}{6} \cos 3\theta \right)$$

$$y = R \left( \sin \theta + \frac{1}{6} \sin 3\theta \right)$$

The stresses are

$$\sigma_r + \sigma_\theta = 2 \left[ \overline{\Phi}(\alpha) + \overline{\overline{\Phi}}(\alpha) \right]$$

$$\sigma_\theta - \sigma_r + 2i \sigma_{r\theta} = \frac{2 \alpha^2}{\rho^2 \omega'(\alpha)} \left[ \overline{\omega(\alpha)} \overline{\Phi}'(\alpha) + \omega'(\alpha) \Psi(\alpha) \right]$$

$$\text{where } \overline{\Phi}(\alpha) = \frac{\phi'(\alpha)}{\omega'(\alpha)}$$

$$\Psi(\alpha) = \frac{\psi'(\alpha)}{\omega'(\alpha)}, \text{ and}$$

$$\text{where } \omega(\alpha) = R \left( \frac{1}{\alpha} - \frac{1}{6} \alpha^3 \right)$$

$$\phi(\alpha) = p R \left[ \frac{1}{4\alpha} + \frac{3}{7} \alpha + \frac{1}{24} \alpha^3 \right]$$

$$\psi(\alpha) = -p R \left[ \frac{1}{2\alpha} + \frac{91 \alpha - 78 \alpha^3}{84 (\alpha^4 + 2)} \right],$$

$\alpha$  is a complex variable and  $\omega$ ,  $\phi$ ,  $\psi$ , are functions of  $\alpha$ .

The stresses in the square hole depend on the rounding-off radius of the corners of the square hole. The stress on the hole boundary for two different rounding-off radii are given below.

Values of  $\frac{\sigma_{\theta}}{p}$

$\theta^{\circ}$	Rounding off radius = .06 a	Rounding-off radius = .0245 a
0	-0.808	-0.936
35	-0.268	-0.544
40	0.980	0.605
45	3.0	4.368
50	3.86	4.46
55	3.366	2.888
90	1.472	1.760

The maximum tangential stress occurs at the corners and increases with the decrease in the rounding-off radius at corners.

#### 4.12 Oval Hole in an Infinite Medium Under Biaxial Compression

The boundary of the opening in an infinite plate is represented in rectangular coordinates by the equations

$$\begin{aligned} x &= p \cos \beta + r \cos 3 \beta \\ y &= q \sin \beta - r \sin 3 \beta, \end{aligned} \quad (4.12.1)$$

where  $p, q, r$  are parameters of the ovaloid,  $\beta$  = angle made with the  $x$  axis.

The values of the parameters for any opening may be obtained by first choosing a suitable value for  $r$ .

Greenspan<sup>12</sup> gives the following equation for the tangential stress in the elastic state on the boundary,

$$\begin{aligned} & \left[ (p^2 + 6rq) \sin^2 \beta + (q^2 + 6rp) \cos^2 \beta \right. \\ & \quad \left. - 6r(p+q) \cos^2 2\beta + 9r^2 \right] \sigma_\theta \\ & = (\sigma_x + \sigma_y) (p^2 \sin^2 \beta + q^2 \cos^2 \beta - 9r^2) \\ & \quad - \left[ \frac{(p^2 - q^2) (\sigma_x + \sigma_y) - (p+q)^2 (\sigma_x - \sigma_y)}{(p+q-2r)} \right] x \\ & \quad \left[ (p-3r) \sin^2 \beta - (q-3r) \cos^2 \beta \right] \end{aligned} \quad (4.12.2)$$

where,

$\sigma_x, \sigma_y$  are applied stresses in the  $x, y$  directions at infinity.

In the case of a biaxial stress state with  $\sigma_x = \sigma_y = S$ , the boundary stresses are given by

$$\frac{\sigma_\theta}{2S} = \frac{\left[ \begin{aligned} & (p^2 \sin^2 \beta + q^2 \cos^2 \beta - 9r^2). \\ & - \frac{(p^2 - q^2)}{(p+q-2r)} \left( (p-3r) \sin^2 \beta - (q-3r) \cos^2 \beta \right) \end{aligned} \right]}{\left[ \begin{aligned} & (p^2 + 6rq) \sin^2 \beta + (q^2 + 6rp) \cos^2 \beta \\ & - 6r(p+q) \cos^2 2\beta + 9r^2 \end{aligned} \right]} \quad (4.12.3)$$

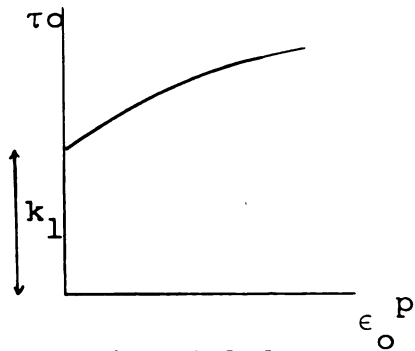


Fig. 4.1.1

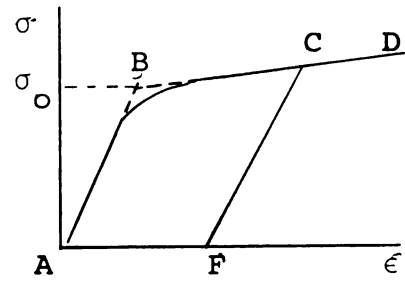


Fig. 4.2.0

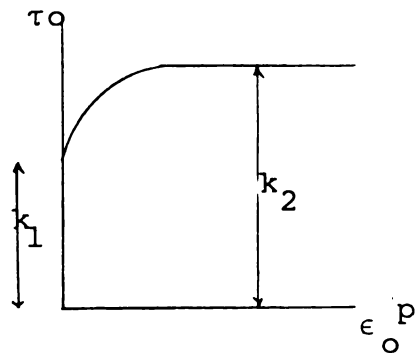


Fig. 4.1.2

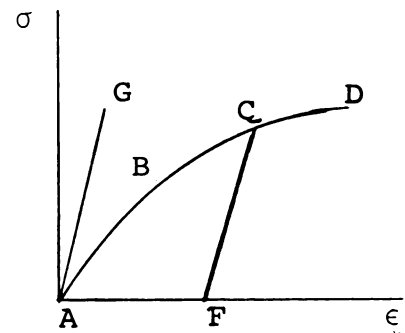


Fig. 4.2.1

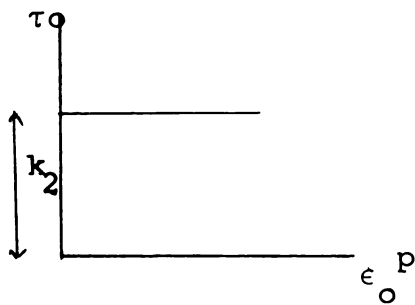


Fig. 4.1.3

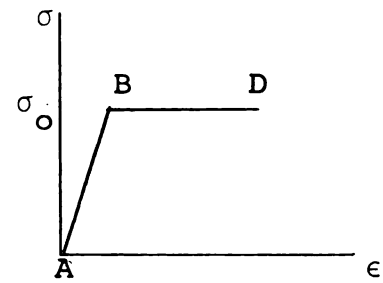


Fig. 4.2.2

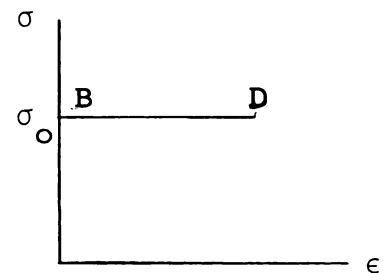


Fig. 4.2.3.

Various types of stress strain curves.

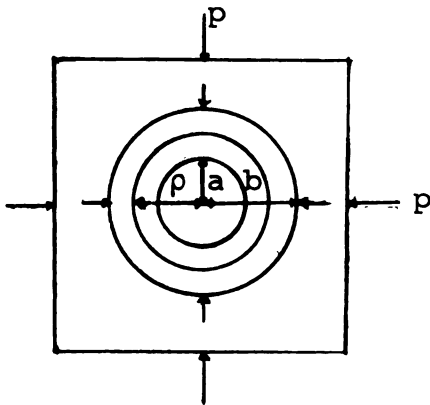


Fig. 4.4.1

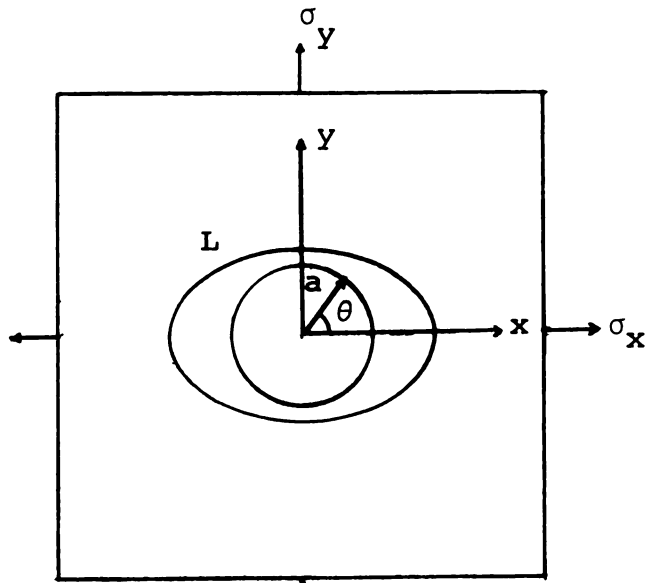


Fig. 4.9.1

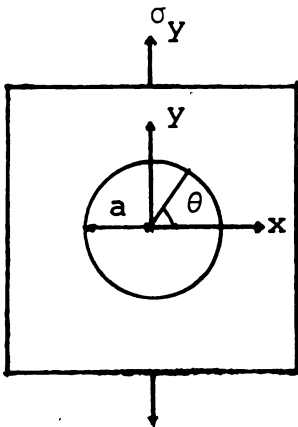


Fig. 4.10.1

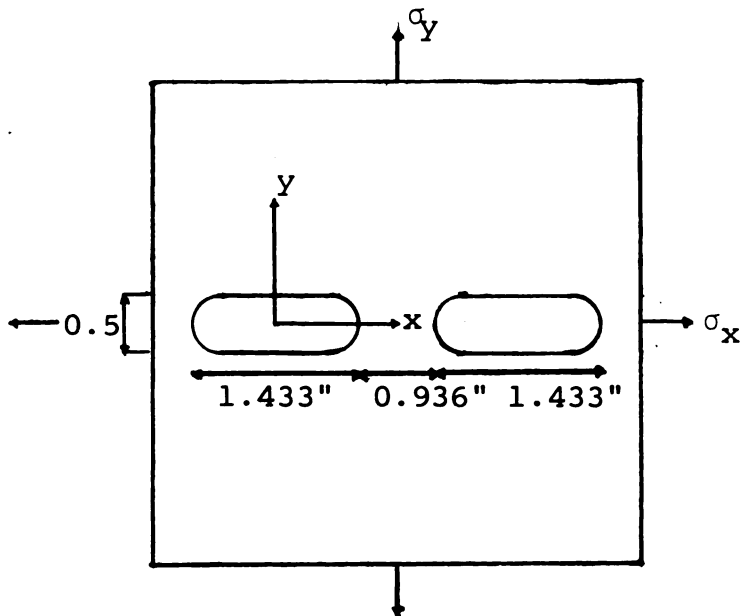


Fig. 6.15.10

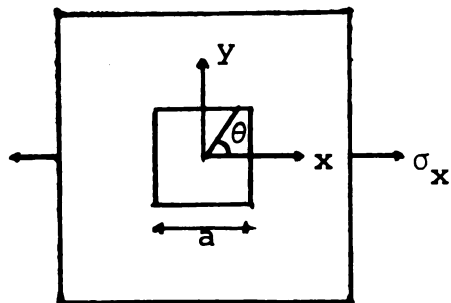


Fig. 4.11.1

a = internal radius of the circular opening, and length of side of square opening

b = external radius of thick walled cylinder

ρ = radius of elastic plastic boundary

L = elastic plastic boundary

Various forms of opening investigated.

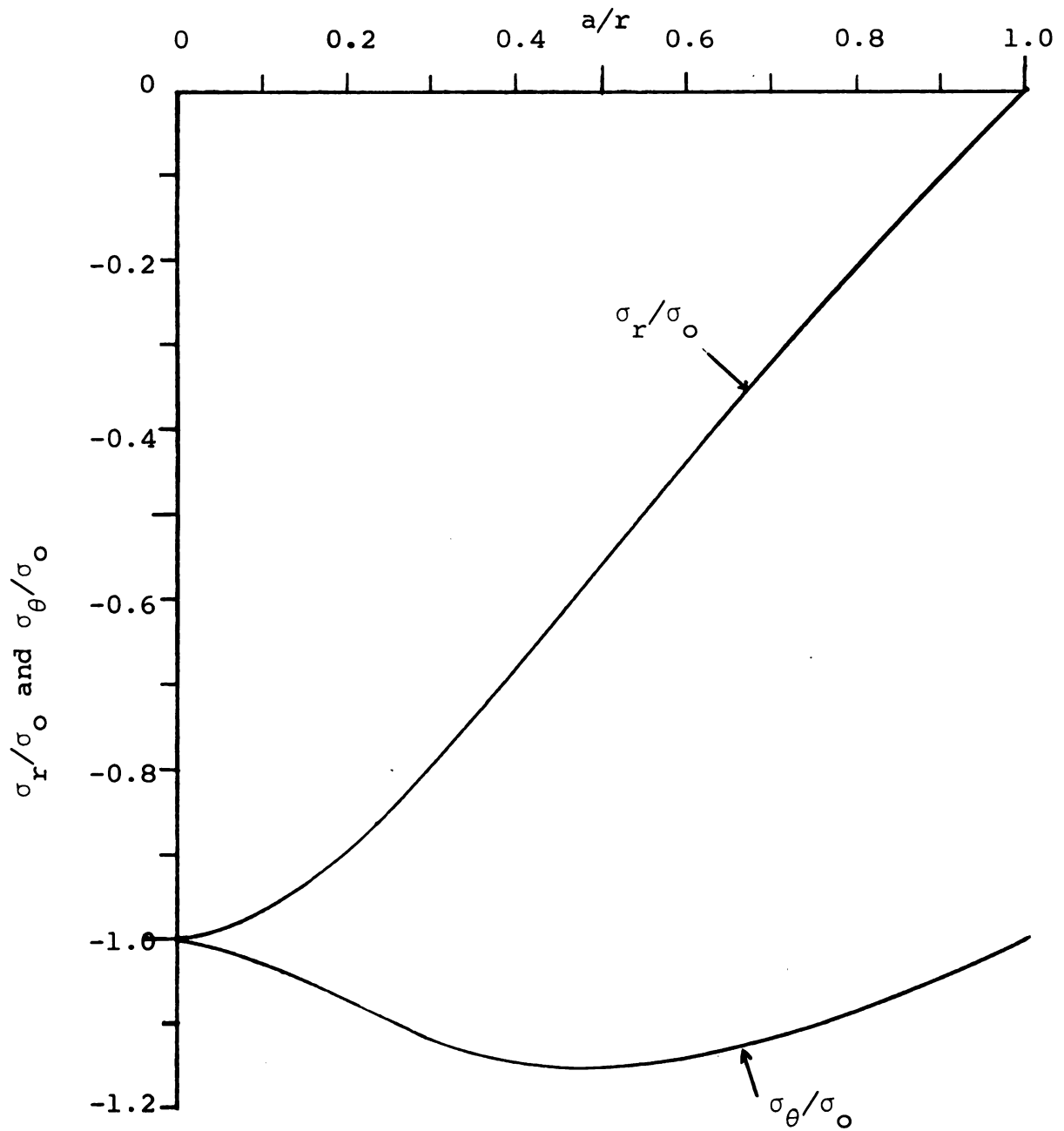


Fig. 4.5.2. Stress distribution in a completely plastic cylinder in plane stress under uniform external pressure.

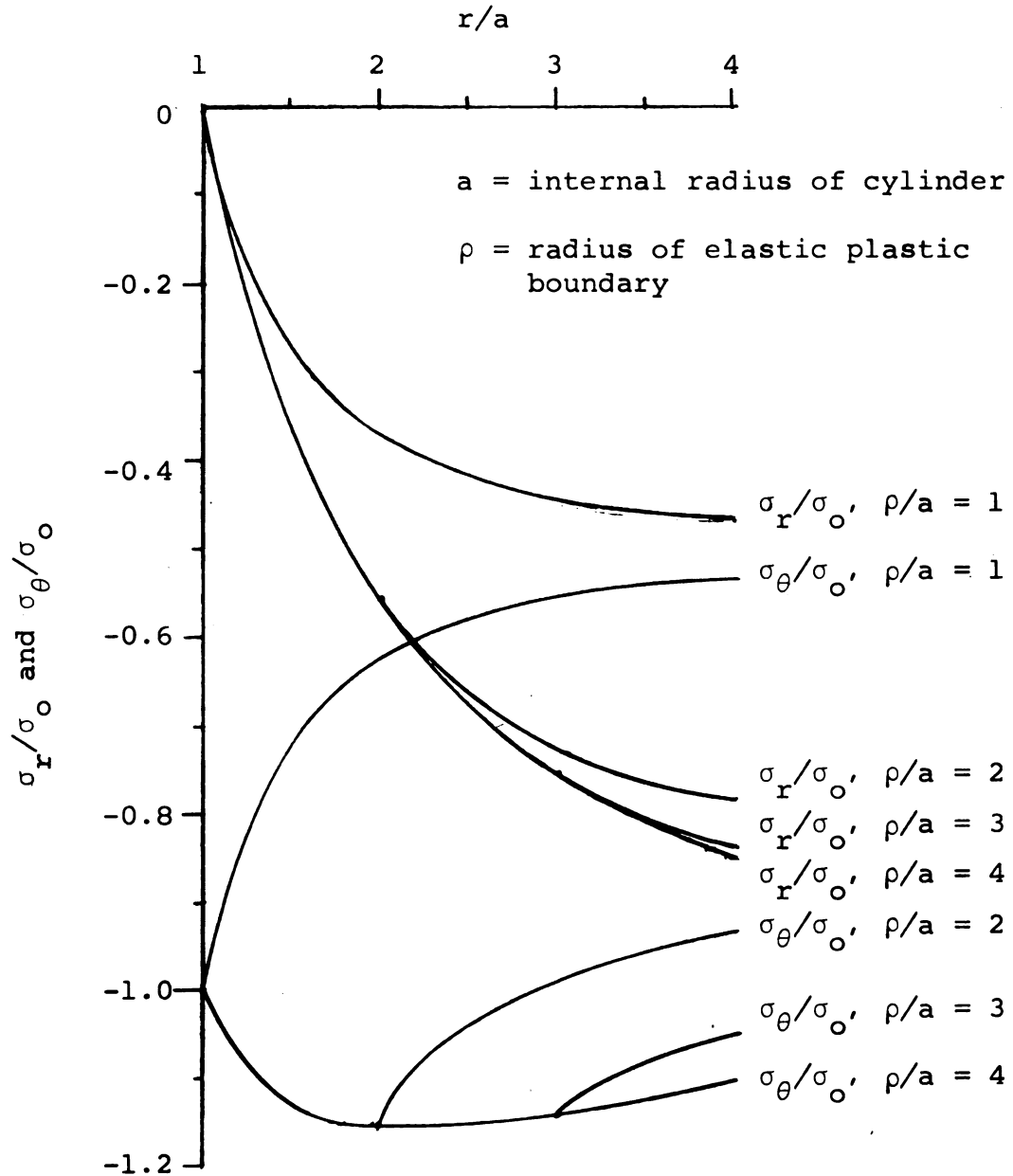


Fig. 4.6.2. Stress distribution in an elastic plastic cylinder under uniform external pressure in plane stress (ratio of external to internal diameter = 4).

## CHAPTER V

### EXPERIMENTAL PROCEDURE

#### 5.1 Preparation of Specimen

**Size:** Previous investigations by Serata<sup>30</sup> have demonstrated that the stress strain relation in case of rectangular prisms under uniaxial compression depends on the relative dimensions of the specimen, and that the variation is not great if friction at the loaded surfaces of the salt blocks is eliminated. Practical considerations of the available size of the salt block and the relative dimensions of the openings with respect to the size of the test specimen dictated the use of 5" cubes for all the tests. The salt used in the tests was obtained from a Louisiana salt dome.

**Attaching photo stress plastic:** All the photo stress plastic sheets were obtained from the Budd Company. Two types of plastic were used (1) S type of thickness 0.122" and (2) M type of thickness .072". The S type plastic was first used and it was found that the number of fringes obtained was too large. Subsequently M type plastic was used for all the tests. The first fringe occurs at a

principal strain difference of, approximately 1000 mii in case of 0.12" S type plastic and approximately 8000 mii in case of 0.072" M type plastic. The plastic was machined to the contour of the opening in the salt specimen and then was attached on to the surface of the test piece by using reflective cement. Salt has a non-reflective surface and hence reflective cement was used. The cement was allowed to dry for a period of not less than 24 hours at room temperature before any testing was done.

**Marking of lines:** A network of intersecting lines was drawn on the plastic surface by using a red grease pencil. It was possible to obtain fine lines on the surfaces of two of the plastic sheets by etching with a steel pin and filling the etchings with a grease pencil. But the other plastics were soft and lines had to be drawn with a fine grease pencil without any etching.

**SR-4 Gages:** In some of the experiments the strains were measured by SR-4 gages. It is not possible to obtain a completely uniform surface on salt specimens. Hence a thin layer of SR-4 precoat was applied on the surface. When the precoat dried, the strain gages were attached using Duco cement in the usual manner.

## 5.2 Testing Device

All the tests of the uniaxial group were done in a Universal testing machine of capacity 300,000 lb. The loading mechanism was such that the load could be maintained at any desired level with ease. The experiments of the biaxial group were done in a rectangular loading frame shown in Fig. 6.17.20. The frame consisted of WF steel sections connected together by angles and bolts. The load was applied by two 50 ton hydraulic jacks, one of them clamped to the top horizontal beam and acting vertically and the other clamped to the right vertical column and acting horizontally. The hydraulic pressure was supplied by a pump and the pressure was indicated in a pressure gage. The load applied was obtained by using a curve relating the pressure in the jack and load applied by it.

## 5.3 Loading Conditions

**Use of friction reducer:** In the compression tests on salt, frictional forces are developed at the loading surfaces of salt specimens. This force has a dominating effect upon the behavior of the specimen.

In order to eliminate the frictional forces at the loading surfaces in this investigation, friction reducers

were used. The friction reducer consisted of a sheet of aluminum foil placed in between two thin sheets of plastic laminated with a mixture of grease and graphite.

#### 5.4 Description of the Uniaxial Tests

##### Uniaxial compression tests on solid specimens:

The serial numbers of the experiments in this category are 1A, 1B, 4 and 5. In both the tests 1A and 1B, uniaxial compression was applied gradually from zero to the ultimate load in equal increments of 5000 lbs. (approximately 200 psi). Strain measurements were made using SR-4 gages and mechanical dial gages. Two AR-1 Rosette gages, one at the center of each of two opposing vertical faces, measured the strain on a nominal gage length of  $\frac{13}{16}$ ". Three A-18 gages, one in the axial direction on a grain, one in the axial direction but on the boundary of a grain, and one in the lateral direction on a grain measured the strains of individual grains on a relatively small nominal gage length of  $\frac{1}{8}$ ". The grains were chosen to be as near the center of the face as possible. Three dial gages, one in the axial direction, two in the lateral directions were used to measure the total deformation. The objective of these two tests was to obtain a stress strain relation under uniaxial compression and to know

something about the behavior of the individual grains.

Tests 4 and 5: The results of tests 1A and 1B showed that the magnitudes of the modulus of elasticity  $E$  and the Poisson's ratio  $\eta$  depended on the magnitude of the stress, and that the strains at every point were not equal under uniform stress. In the photo stress method of analysis, the difference of two principal strains are measured and these strains depend on the elastic constants at any stress level. In order to eliminate the use of the elastic constants in determining the principal strain difference, it was decided to obtain a relation between stress and principal strain difference by using the photo stress method. The objectives of the tests were (1) to obtain a stress versus principal strain difference curve, (2) to obtain the stress distribution on the entire surface under uniaxial stress, and (3) to test the behavior of the photo stress plastic when subjected to large strains.

In both the tests 4 and 5 uniaxial compressive load was applied gradually increasing from zero in increments of stress of 250 psi until failure. Two photo stress plastic sheets, one S-type on the rear vertical face and one M-type on the front vertical face were attached on the cube. The M-type measured large strains and the S-type measured

the small strains. One AR-1 rosette gage was attached to the center of each of the two remaining vertical faces. Three dial gages measured the total deformations in the axial and lateral directions.

Uniaxial test with circular holes: The serial numbers of the test in this category are (2), (3), (6) and (8). The diameter of the hole in all the tests was 1 inch. S-type photo stress plastic was attached to one face in the case of tests (2) and (3). The number of fringes observed in the case of S plastic was very large and so it was found necessary to use an M-type plastic in the other tests.

In test 2, an S-type plastic was attached. The average stress in the specimen was raised from zero to 2,000 psi in steps of 200 psi and then the load was gradually reduced to zero. After several days the specimen was stressed again from zero until failure of the specimen. In test 3, an S-type plastic was used. The average stress was raised from zero to 1,400 psi in steps of 100 psi and unloaded to zero. In test 6, one S-type plastic was attached to the rear face and an M-type plastic was attached to the front face of the specimen. The strain distribution was observed on the S-type plastic for stresses from 0 to 1,000 psi and later the large field meter was

shifted to the front to observe strains on the M-type. The average stress was gradually raised from 0 to failure of the specimen in increments of 250 psi. In test 8, an M-type plastic was used. The average stress was raised from 0 to failure of the specimen in increments of 250 psi.

Uniaxial tests with square holes: The serial numbers of the tests in the category are (7), (9), and (10). M-type plastic was used in all cases. The loading was gradual from 0 to failure of the specimen in steps of average stress = 250 psi.

Biaxial tests on solid specimens: The serial numbers in the group are (11) and (12). The objective of these tests was to obtain a relation between the octahedral shear stress and the plastic strains under a biaxial stress state.

In the first cycle of test 11 the specimen was loaded with equal horizontal and vertical stresses up to 3,000 psi and unloaded to zero. In the second cycle, the equal stresses in both directions were raised to 4,000 psi and brought back to zero. In the third cycle, the horizontal stress was first raised from zero to 1,000 psi and keeping it constant at 1,000 psi, the vertical stress was raised from zero to 4,000 psi. Then the vertical stress was lowered to zero and finally the horizontal stress was

also brought back to zero. In the fifth cycle both the stresses were kept equal during the loading process from 0 to 4,000 spi and then keeping the horizontal stress constant at 4,000 psi, the vertical stress was reduced to zero, and finally the horizontal stress was also brought back to zero. One M-type plastic was attached to the front face of the specimen. Three A-8 gages were attached, one each at the top, middle and bottom of the vertical center line on the rear face measured the vertical strains. One A-8 gage attached close to the center of the rear face measured the horizontal strains. One dial gage in the vertical direction and two dial gages in the horizontal direction measured total deformations.

In test 12, the horizontal stress was raised from zero to 1,000 psi in the first cycle. Keeping it constant at 1,000 psi, the vertical stress was first raised gradually to 4,000 psi and then lowered to zero. Finally the horizontal stress was lowered to zero. In the second cycle, the ratio of vertical to horizontal stress was kept constant at 3, and both stresses were gradually raised, the vertical from zero to 4,000 psi in equal increments of 750 psi and the horizontal from zero to 1,333 psi in equal increments of 250 psi. Finally both the stresses were gradually lowered

to zero keeping the same constant ratio of the stresses.

One M-type plastic was attached to the front face. Three A-8 gages, one each at the two ends and one at the middle of the horizontal center line of the rear face, were used for measuring the horizontal strains. Two additional A-8 gages attached on the middle center line as close to the center as possible were used for measuring the vertical strains. Mechanical dial gages one in the vertical direction and two in the horizontal direction were also used for the strain measurement.

Biaxial tests with circular holes: The serial numbers in this category are (13) and (14). The diameter of the hole at the center of the specimen in both tests was 1".

In test 13, one M-type plastic was attached to the front face. On the rear face, two A-18 gages, one on a horizontal center line and the other on a vertical center line were attached close to the edge of the hole. Three dial gages were also mounted for recording total deformations.

The test specimen was subjected to equal vertical and horizontal stresses. The stresses were gradually increased from zero to 4,000 psi in equal increments of 250 psi and brought back to zero at the same rate.

After releasing the load, the specimen was left

undisturbed for three days and residual strains were recorded.

In test 14, the specimen was loaded such that the ratio of the average vertical stress to the average horizontal stress was maintained at 3.0 throughout the experiment. The stresses were gradually raised, the vertical stress from zero to 4,000 psi and the horizontal stress from zero to 1,333 psi and finally both the stresses were gradually reduced to zero. Details of photo stress plastic and strain measuring arrangements are the same as in test 13.

Biaxial test on oval holes: The serial numbers of the tests in this category are (15) and (16). In both cases the hole consisted of two semi-circles of  $1/2$ " diameter connected by a rectangle  $1/2$ " wide and 0.933" long.

In test 15, there were two holes along the horizontal center line with a distance of 2.369" between the centers of the holes. One M-type plastic was used. Total deformations were measured by 3 dial gages. The specimen was subjected to equal average stresses in the vertical and horizontal direction throughout the experiment. The stresses were gradually raised from zero to 3,000 psi and kept constant at 3,000 psi for 16 hours and then gradually brought back to zero.

In test 16, there was only one hole at the middle of the horizontal center line of the specimen. Details of plastic and dial gage mounting are the same as in test 15. The specimen was subjected to equal average stresses in both the horizontal and vertical directions. The stresses were gradually raised from zero to 3,000 psi and maintained at that level for 40 hours and then gradually lowered to zero.

## CHAPTER VI

### EXPERIMENTAL RESULTS AND ANALYSIS

#### 6.1 Uniaxial Compression Test on Solid Specimens

The stress strain curves of rock salt in uniaxial compressions are shown in Figs. 6.1.5, 6.4.5 and 6.5.5. The curves are characterized by the following features.

1. No part of the curve is a straight line.
2. The strains recorded by dial gages are higher than those recorded by SR-4 gages.

However, the slope begins to change rapidly at approximately 1,000 psi. It is not possible to locate exactly either the proportional limit or the yield point. The method that is proposed is to consider the stress strain curve as a combination of several straight lines.

Modulus of elasticity E: The value of E in any stress range will be defined by chord modulus.

$$E = \frac{\sigma_f - \sigma_b}{\epsilon_f - \epsilon_b}$$

where,  $\sigma_f$ ,  $\sigma_b$  are stresses at the ends of a specific portion of the stress strain curve, and  $\epsilon_f$ ,  $\epsilon_b$  are the corresponding

strains. The value of E thus obtained for stresses in the range 0 to 1,000, 1,000 to 2,000, 2,000 to 3,000, 3,000 to failure are given below.

Stress range in psi	Average E based on SR-4 gage ( $10^6$ psi)	Average E based on dial gage ( $10^6$ psi)
0 to 1,000	1.408	0.4559
1,000 to 2,000	0.1913	0.1757
2,000 to 3,000	0.0909	0.0803
3,000 to failure	0.0596	0.0402

The values of E based on the SR-4 gages and dial gages in the stress range of 0 to 1,000 psi are 1.408 and 0.4559 million psi respectively which are not in agreement. The large difference in the values at this range is probably due to the readjustment of the end surfaces of the specimen in the initial stage of the loading. The dial gage deformations include the initial readjustment of the ends and hence the deformations are larger than those recorded at the center by the SR-4 gages. However, the values of E at stresses above 1,000 psi based on SR-4 gages are higher than those based on dial gages.

The stress strain relation based on SR-4 gages is

used for analyzing strains around openings. The basis for such a procedure is that the holes are located in the center of the specimen where the strains were measured by SR-4 gages. It is noted here that the material is not completely elastic at any stress level in uniaxial loading condition.

Poisson's ratio: Poisson's ratio,  $\eta$ , with respect to the axial stress is shown in Figs. 6.1.6, 6.4.6 and 6.5.6. The common characteristics of these curves are:

1. The values of  $\eta$  based on SR-4 gages are very high in the initial stages and decrease in a very irregular way as the stress increases.
2. All values of  $\eta$  based on SR-4 gages are greater than 0.5 except at stresses of 500 psi and 750 psi in Fig. 6.5.6.
3. The values of  $\eta$  based on dial gages increase gradually ranging from 0 to 0.9 with increase of stress.

The values are less than 0.5 for ranges of stress, 0 to 1,680 in Fig. 6.1.6, 0 to 1,280 in Fig. 6.4.6 and 0 to 1,300 in Fig. 6.5.6. It seems to be a reasonable approximation to assume that  $\eta$  varies linearly from 0 to 0.5 as the stress increases from 0 to 1,500 psi, on the basis of dial gage measurements.

Stress and strain distribution: Fig. 6.5.2 shows the strain distribution on the surface of the specimen, when it is subjected to a uniform load of 2,500 psi in the vertical direction. Fig. 6.5.7 shows the stress distribution on a horizontal axis through the center of the specimen. Fig. 6.5.8 shows the stress distribution on the vertical axis through the center of the specimen.

The strain distribution of Fig. 6.5.2 shows that the fringe pattern is almost circular. Each of the lines represents points of equal principal stress difference. Since the vertical stress is the only stress acting, the lines also represent points of equal stress. The center of the fringe pattern does not coincide with the center of the specimen. This indicates that some eccentricity in the loading exists.

Fig. 6.5.3 shows the relation between the uniaxial stress which is the principal stress difference in this case and the principal strain difference. The curve A is based on SR-4 gages attached to the center of the specimen. The curve B is based on an average of the photo stress readings at the center, two points on the horizontal center line, one on each side  $1/4$ " from the center, and two points in the vertical center line at  $1/4$ " on either side of

the center. The difference in the two curves A and B may be explained like this. The strain measured by the SR-4 strain gage is an average of the strain on its gage length of  $13/16$ ". The photo stress measurements are made at specific points only and the average of the readings at the 5 points apparently are different from the strain gage measurements. The use of these relations in strain analysis is an approximation as the material is not completely elastic.

Fig. 6.5.7 shows that the stress is maximum at 0.75" from the center. The stresses remain uniform for a distance of  $1/2$ " on either side of the point of maximum stress and does not vary very much on the right of the center, but is reduced more rapidly on the left of the center. If the eccentricity were removed, the stress distribution would be symmetrical with the center of the specimen. The stress distribution in the Figs. 6.5.7 and 6.5.8 is based on Fig. 6.5.3 (curve B).

Behavior at failure: The failure occurred in all the cases by formation of cracks, mostly vertical followed by crushing (Figs. 6.1.20 and 6.5.20). The ultimate strength values for tests 1, 2, 3, 4 were 3,752 psi, 3,858 psi, 3,203 psi and 3,556 psi respectively. The average value of the ultimate stress was 3,722 psi neglecting the lowest value. There was evidence of eccentricity in loading in

the test 4 which gave the ultimate stress of 3,203 psi and hence this value is being ignored. The specimens for tests 1 and 2 came from the same block and the specimens for tests 3 and 4 came from another block. The average value of the ultimate strength for tests 1 and 2 was 3,800 psi. For analysis of strains in uniaxial tests it is assumed that the yielding begins when the principal stress difference is 3,800 psi.

Behavior of the individual grains: The stress strain relation for individual grains are shown in Fig. 6.1.7. The axial strains on the grain boundary were very much larger than the strains on the interior of it. The axial stress strain relation for the grain boundary is closer to that obtained for the mass by the SR-4 gage than that obtained by dial gages. But on the other hand the lateral strains on the interior of the grain are very much smaller than those obtained for the mass either by SR-4 gage or by dial gages. This has to be expected and confirms the unpredictable behavior of the individual grains.

Homogeneity: In a homogeneous mass the smallest part anywhere in the mass should have the same physical properties as the mass. The irregularities at specific points along any fringe indicate that the physical properties

vary from point to point. However, the general shape of the fringe pattern of the specimen in Fig. 6.5.2 shows that the fringes have an ordered pattern. Hence it can be concluded that the material has statistical homogeneity.

**Isotropy:** In an isotropic mass, the physical properties should be the same in all directions. Salt is made up of a number of crystals whose size and orientation vary from point to point in the mass, and therefore, ideal isotropy cannot be expected. When a load is applied, the grains may slide one on another, deform in the three principal directions and rotate, depending on the properties of the individual grains and the manner in which they are packed. Accordingly local displacements, local shear strains and local changes in volume may occur.

An examination of the isoclinics show how the principal stress directions vary from point to point. As the load varies the principal stress directions vary at the points. This indicates that the principal strain directions vary from point to point because of translation, deformation and rotation of the individual grains. But the overall distribution of the principal strains leads to the conclusion that the mass is statistically isotropic.

## 6.2 Circular Hole Under Uniaxial Compression.

Fig. 6.3.3 shows the strain distribution in the case of circular hole subjected to an applied uniaxial stress of 500 psi. The maximum stress expected is 1,500 psi and according to our assumptions, the material everywhere is in the elastic state. The analytical values of  $(\epsilon_1 - \epsilon_2)$  based on the equation in section 4.10 are compared with the experimental values in Table 6.3.11. The analytical values of  $(\epsilon_1 - \epsilon_2)_1$  are based on experimental values of strain difference measured by photo stress in a uniaxial test of a solid specimen. The analytical values of  $(\epsilon_1 - \epsilon_2)_2$  are based on values of secant modulus corresponding to the stress in each direction, obtained from SR-4 gages of a uniaxial test, and on the assumption of  $\eta = 0.5$ . The experimental values are substantially higher than the analytical values. This difference is explained by the fact that the material close to the boundary of the hole is in a biaxial state of stress and at larger distances from the boundary, the material tends to be in a uniaxial state of stress. The stress strain relations are different in the two cases. The closest approximation to the experimental values are given by  $(\epsilon_1 - \epsilon_2)_2$  and this seems to be the better method of approximating strains.

Fig. 6.8.3 shows the distribution of principal strain difference on three radial lines, around a circular hole when subjected to a uniaxial stress of 2,750 psi.

The analysis is made on the assumption that the yielding begins when  $\sigma_1 - \sigma_3$  reaches a value of 3,800 psi. In the elastic stress distribution, the tangential stress is the minimum principal stress at points on a radial line normal to the direction of the applied stress. Hence yielding begins when the tangential stress reaches a value of 3,800 psi. At a distance 0.8" from the center of the 1" hole the value of tangential stress is 3,800 psi, by assuming a completely elastic state in the specimen. The strain distribution for points beyond a radius of 0.8" on the line normal to the direction of the principal stress is calculated on the basis of the elastic theory and stress strain relation shown in the Fig. 6.5.3 (curve B). Along the radial line parallel to the direction of stress, the  $\sigma_1 - \sigma_3$  never exceeds the applied stress of 2,750 psi. On a radial line at  $45^\circ$  to the direction of the applied stress,  $\sigma_z$  stress is always intermediate stress and the maximum value of  $\sigma_1 - \sigma_3 = (1.37) (2,750) = 3,770$  psi. Hence on all the points along the radial lines making  $0^\circ$  and  $45^\circ$  to the direction of applied stress, the strain distribution is

calculated on the basis of stress strain relation in Fig. 6.5.3 (curve B). The principal strain differences calculated on the above basis and those observed by photo stress are compared in Table 6.8.11. The analytical values based on Fig. 6.5.3 curve B, for points on a line normal to the direction of the load are higher than the experimental values.

Fig. 6.12.4 gives the stress strain relation when a solid is subjected to a horizontal stress of 1,000 psi and a vertical stress varying from 0 to 4,000 psi. Since the state of stress close to the opening is in a biaxial state of stress it is of interest to calculate  $(\epsilon_1 - \epsilon_2)$  on the basis of a biaxial stress strain relationship. Accordingly the values of  $(\epsilon_1 - \epsilon_2)$  have been computed based on Fig. 6.12.4--(curve B) and shown in Table 6.8.11. Again, the analytical values are higher than the experimental values. But the values based on biaxial stress strain relation are closer to the experimental values than those based on uniaxial stress strain relation.

This discrepancy is due to several reasons. The stresses computed are not strictly correct because part of the cylinder is in a plastic state. The stress state nearer the opening is in a biaxial state and that in the

region farther away tends to be uniaxial. It seems to be more correct to compute the strains in the problem based on biaxial stress strain relation.

Nature of failure: The average maximum applied stress at the time of failure was 3,043 psi. In test 2 the specimen was damaged by an initial impact loading, the applied stress was raised to 1,990 psi, brought back to zero, and after a lapse of several days, it was again raised to the point of failure. If the result of this test were neglected, the average maximum applied stress at failure was 2,850 psi. In test 6 the failure occurred very abruptly by cracking along the planes making about  $10^{\circ}$  with direction of loading and at an applied stress of 2,500 psi (Fig. 6.6.20). In test 8, the failure took place after large deformations accompanied by cracks at an applied maximum stress of 3,200 psi (Fig. 6.8.20). The circular opening which was 1" in diameter became almost elliptical with the horizontal diameter increasing in length to 1.12" and the vertical diameter decreasing in length to 0.8". In both the tests 6 and 8, cracks originated close to ends of the horizontal diameter making an angle of  $5^{\circ}$  to  $10^{\circ}$  with the vertical.

Area of hole before loading  $= 0.785 \text{ in}^2$

Area of hole after loading  
 assuming an elliptical shape  
 with major axis = 1.12" and  
 minor axis = 0.8" =  $\frac{\pi}{4} (1.12)(0.8) \text{ in}^2$   
= 0.704 in<sup>2</sup>

Area after loading  
 initial area of the hole = 0.886

Table 6.3.11. Principal strain difference on the center line normal to the direction of stress in case of a circular hole under uniaxial compression of 500 psi.

r radial distance	$(\sigma_1 - \sigma_2)$	$(\epsilon_1 - \epsilon_2)_1$	$(\epsilon_1 - \epsilon_2)_2$	$(\epsilon_1 - \epsilon_2)$
inch	psi	Analytical mii	Analytical mii	Experimental mii
.6	925	1,160	1,870	3,000
.75	570	770	1,125	1,620
1.0	465	700	562	1,100

Table 6.8.11. Principal strain difference in case of circular hole under a uniaxial stress of 2,750 psi.

$\theta$ Angle made with direction of load	Radial distance $r$  in	Experi- mental $\epsilon_1 - \epsilon_2$  mii	Analytical $\epsilon_1 - \epsilon_2$ Fig. 6.5.3  Curve B mii	Analytical $\epsilon_1 - \epsilon_2$ Fig. 6.12.4  Curve B mii
90°	0.75	11,490	25,500	
	0.8	10,080	20,500	14,600
	1.0	7,450	14,000	11,800
	1.5	9,070	10,350	11,400
	2.0	9,570	14,500	11,800
0°	0.6	10,080	1,500	3,400
	0.75	5,040	500	1,200
	1.0	6,040	2,700	2,800
	1.5	11,840	7,000	7,400
	2.0	15,620	10,000	9,400
Note		Actual by Photo Stress	Based on Uniaxial Calibration	Based on Biaxial Calibration

### 6.3 Square Hole Under Uniaxial Compression.

Figs. 6.10.3 and 6.10.4 show the strain distribution at points on lines passing through the center of the opening and making angles of  $0^\circ$  and  $90^\circ$  with the direction of the applied stress of 2,320 psi. The tangential stress on the boundary of the hole is given below, assuming that the rounding off radius is  $.06a$  where  $a$  is the length of the side of the square hole, and the stress state is elastic.

Angle made with the direction of the applied load $\theta^\circ$	$\sigma_\theta$ on the boundary (psi)
0	-1,875
35	- 622
40	2,273
45	6,960
50	8,955
55	7,809
90	3,415

According to the assumption that yielding does not occur till  $\sigma_0$  reached 3,800 psi, the material along the two center lines is elastic. Assuming that the stress strain

relation in the uniaxial test is valid the principal stress difference corresponding to the experimental values of the principal strain differences on the two center lines are calculated on the basis of Fig. 6.5.3 curve B, and are shown in Table 6.10.12. The maximum tangential stress occurs at the corners. The experimental value of maximum principal strain difference at the corners is about 40,000 mi.

Nature of Failure: The failure occurred at an applied average stress of 2,830 psi. In two of the tests the failure occurred by formation of cracks originating at two diagonally opposite corners and running at an angle of  $8^{\circ}$  to  $13^{\circ}$  with the direction of the stress (Fig. 6.7.20). The deformation in the two tests was small. In test 9, the size of the opening at the time of failure was 0.89" along the vertical center line and 1.05" along the horizontal center line. In test 10, the failure occurred by formation of cracks at all the 4 corners at an angle of  $9^{\circ}$  to  $12^{\circ}$  with the direction of the applied stress, and at a few other places originating from the ends of the specimen and ending approximately on the center line. The deformation in this test was large, the hole measuring 1.183" on the horizontal center line and 0.835" on the vertical center line (Fig. 6.10.20). The area of the hole after failure was .9878 square inches.

Table 6.10.12. Principal strain difference and principal stress difference on lines normal and parallel to direction of load in case of a square opening under a uniaxial stress of 2,320 psi.

Distance from center	Center line parallel to loading		Center line normal to loading	
	$\epsilon_1 - \epsilon_2$ (Experimental) mii	$\sigma_1 - \sigma_2$ (Fig. 6.5.3-B) psi	$\epsilon_1 - \epsilon_2$ (Experimental) mii	$\sigma_1 - \sigma_2$ (Fig. 6.5.3-B) psi
0.6	25,000	3,125		
0.625	19,000	2,850	25,000	3,125
0.75	13,500	2,550	15,500	2,662
1	7,500	2,000	11,500	2,675
1.25	4,500	1,550	10,000	2,262
1.5	5,000	1,625	9,500	2,212
1.75	5,750	1,750	9,000	2,175

#### 6.4a Biaxial Compression on Solid Specimens--Equal Stresses in Both Directions

Fig. 6.11.3 gives the stress strain relation when the specimen was subjected to equal stresses.

The stress strain curves based on SR-4 gages and dial gages are close in the stress range of 2,000 psi to 4,000 psi while loading. The unloading was done once at 3,000 psi and once at 4,000 psi. For purposes of determining

the permanent strains at other stress levels, the slope of the unloading curve from 4,000 psi by SR-4 gage was utilized. A justification for this is that the slopes of both the unloading curves from 3,000 psi and 4,000 psi are almost parallel.

Fig. 6.11.4 shows the relation between  $2\sqrt{2} \epsilon_1^P$  and  $\frac{\sqrt{2}}{3} \sigma_1$  in order to obtain the function  $f(\tau_0)$  of Eq. (4.3.4). The value of  $2\sqrt{2} \epsilon_1^P$  and  $\frac{\sqrt{2}}{3} \sigma_1$  are given in Table 6.11.11.

Table 6.11.11. Showing values of  $\frac{\sqrt{2}}{3} \sigma_1$  against  $2\sqrt{2} \epsilon_1^P$  in biaxial compression of solid specimen.

$\sigma_1 = \sigma_2$	$\frac{\sqrt{2}}{3} \sigma_1$	$2\sqrt{2} \epsilon_1^P$
psi	psi	micro in./in.
1,250	589	282
1,500	707	1,696
1,750	824	3,393
2,000	942	5,938
2,250	1,060	8,484
2,500	1,178	11,594
2,750	1,296	15,129
3,000	1,414	18,947
3,250	1,532	24,179
3,500	1,650	27,997
3,750	1,767	31,956
4,000	1,885	41,288

The results plotted in Fig. 6.11.4 are used to determine strains for other cases.

The stress strain curve in Fig. 6.11.3 does not exhibit linearity. However, except in the stress range of 1,000 psi to 1,500 psi, the curve is close to a straight line.

Behavior of the material: The photo stress analysis did not indicate any eccentricity in loading. The material did not show any kind of fringe pattern until the stresses reached 4,000 psi when there were small regions where non-uniformity of stress was seen. The examination of the isoclinics showed that while most of the region showed that the principal strains were parallel to the direction of applied loads, there were spots which showed a maximum deviation of  $15^{\circ}$  from the principal strain direction expected. The assumption that the material is statistically homogeneous and isotropic is demonstrated to be true.

When the specimen was under equal stresses of 4,000 psi, the material seemed to flow without crushing. This conclusion is based on the examination of the material after releasing the load and also comparing its behavior to the case of uniaxial stress failure.

The specimen was subjected to 4,000 psi in both

the horizontal and vertical directions and keeping the horizontal stress at 4,000 psi, the vertical stress was released gradually. It was possible to maintain stresses at 4,000 psi in the horizontal direction and 100 psi in the vertical direction. But when the confinement afforded by the 100 psi was removed, the material started failing. But the failure was different from that of a uniaxial test (Fig. 6.11.20). The material failed by formation of a crack in a vertical plane from the edge of the end plate. This shows that the material behavior has changed under biaxial stress state.

#### 6.4b Biaxial Compression on a Solid Specimen

Unequal stresses in the vertical and the horizontal directions: Fig. 6.12.2 shows the distribution of strains when the specimen was under a stress of 4,000 psi in the vertical direction and 1,000 psi in the horizontal direction. Fig. 6.12.4 shows the relation between  $(\sigma_1 - \sigma_2)$  and  $(\epsilon_1 - \epsilon_2)$ . The remarks regarding the discrepancy in the two curves made in uniaxial testing apply in this case also.

Fig. 6.12.5 shows the stress strain relation (keeping the horizontal stress at 1,000 psi) between the vertical stress and vertical strain. The stress curve does not

exhibit linearity at any stage.

Behavior of the material: Fig. 6.12.2 shows that the strain distribution is not the same at every point, but can be considered statistically uniform.

Examination of the material after releasing the load showed no signs of cracking or failure. The material seems to be flowing (Fig. 6.12.20). That the behavior of the material in biaxial stress state is different from that of the uniaxial state is demonstrated by the fact that the material did not fail when one of the principal stresses reached 4,000 psi whereas the material failed at about 3,800 psi in uniaxial compression.

#### 6.5a Circular Hole Under Equal Horizontal and Vertical Forces

Fig. 6.13.2 shows the strain distribution in case of a circular hole subjected to uniform equal pressures of 4,000 psi in the horizontal and vertical directions at the ends of the specimen. The specimen was 4.861" wide, 4.871" high and 4.876" along the axis of the hole 1" in diameter. Assuming that yielding takes place at  $\sigma_o = 4,000$  psi,  $\tau_o = 1,885$  psi. From Fig. 6.11.4 of a biaxial test,

$$f(\tau_o) = 41,300 \text{ micro inch/inch, when } \tau_o = 1,885 \text{ psi (6.5.1)}$$

Assuming that the problem is equivalent to a thick walled cylinder of external diameter of 4.864", internal diameter of 1" subjected to an external uniform pressure of 4,000 psi and is in a completely plastic state, the value of  $\epsilon_r^P - \epsilon_\theta^P$  are calculated using (4.5.10), (4.5.11), (4.5.15) and (6.5.1). These values are compared with the experimental values in Table 6.13.11 and Fig. 6.13.5. Here, the stresses based on perfect plasticity are used in the stress strain relations for hardening plastic material and this is an approximation.

The experimental values are found to be in the range of 65 to 79% of the analytical values. The possible reasons for the differences are

1. From Figs. 6.13.2 and 6.13.5, it is seen that the strain distribution is not completely symmetrical due to possible eccentricity in loading.

2. The assumption that yielding begins when  $\sigma_0$  reaches 4,000 psi may not be exact.

3. The effects of the end steel plates may not be ignored. Furthermore the strain in the direction parallel to the axis of the hole,  $\epsilon_z^P$  may be calculated by using (4.5.13) and (6.5.1) and is given below.

$$\text{At } r = a, \epsilon_z^P = 43,800 \text{ mii.}$$

The theoretical change in length of the hole, at its boundary

$$= 4.876 \times 43,800 \text{ micro inch/inch} = 0.213".$$

The length of the hole by measurement = 5.09"

$$\begin{aligned} \text{Experimental value of change in length} &= 5.09" - 4.864" \\ &= 0.226" \end{aligned}$$

This value of change in length of the hole agrees reasonably well with theoretical value.

The higher value of  $\sigma_o = 4,000$  obtained in biaxial stress state can be explained in the following way. In the case of biaxial testing the material is free to expand in the third direction, whereas in the triaxial testing, the deformation of the material is limited due to confinement in the cylinder. For a larger deformation, the value of  $\sigma_o$  will be larger and hence there is justification in assuming  $\sigma_o = 4,000$  psi in biaxial stress state and a smaller value in triaxial stress state.

The deformations: At the applied load of 4,000 psi there were no cracks and no damage of any kind (Fig. 6.13.20). Under the load, the specimen was 4.77" wide, 4.77" high and 5.09" along the axis of the hole and the hole diameter was 0.9".

$$\frac{\text{Area of the hole after loading}}{\text{initial area of hole}} = 0.81$$

Assumption regarding the behavior as a thick walled cylinder: The fringe pattern in Fig. 6.13.2 shows that the

fringes are nearly circles. The fringes become closer to a circle, near the hole. The circular cylinder behavior is approximately up to a radius of 1.2", or  $\frac{r}{a} = 2.4$

#### 6.5b Circular Holes Under Unequal Horizontal and Vertical Forces

The experimental strain distribution in the case of a circular hole subjected to a vertical stress of 3,750 psi and a horizontal stress of 1,250 psi is given in Fig. 6.14.2 From these isochromatic lines, it is noticed that  $\sigma_r - \sigma_\theta$  lines do not cross the vertical center line. The strain distribution on a horizontal axis through the center of the hole is given in Figs. 6.14.3. For the purpose of comparison the theoretical elastic stresses for points along the vertical and horizontal center lines through the hole are tabulated in Table 6.5.11.

Savin's<sup>29</sup> equation for elastic plastic boundary curve L given in (4.9.4) cannot be applied in this case

where  $\frac{\sigma_x}{\sigma_y} = \frac{1}{3}$ , because the curve L cannot encircle the hole.

The deformations: The size of the specimen before testing was 4.87" wide 4.885" high and 4.94" along the axis of the 1" diameter hole: after loading the width increased by 0.015", the height decreased by 0.145", and

Table 6.13.11. Principal stress difference and principal strain difference in a thick walled cylinder under uniform biaxial compression = 4,000 psi.

$\frac{r}{a}$	Theoretical		Analytical		Experimental		Ratio of $\frac{\text{Experimental}}{\text{Theoretical}}$ $\epsilon_r^p - \epsilon_\theta^p$
	$\frac{\sigma_r}{\sigma_o}$	$\frac{\sigma_\theta}{\sigma_o}$	$\frac{\sigma_r}{\sigma_o} - \frac{\sigma_\theta}{\sigma_o}$	$\epsilon_r^p - \epsilon_\theta^p$ micro in./in.	$\epsilon_r^p - \epsilon_\theta^p$ micro in./in.	$\epsilon_r^p - \epsilon_\theta^p$ more than 35,000	
1	0	-1	1	43,800	more than 35,000		
1.2	-0.172	-1.072	0.9	39,420	28,500		.725
1.5	-0.36	-1.125	0.765	33,500	23,250		.695
2	-0.56	-1.15	0.59	25,840	16,650		.645
2.5	-0.68	-1.148	0.468	20,500	14,380		.701
3	-0.755	-1.138	0.383	16,780	13,250		.792
3.5	-0.815	-1.12	0.305	13,360			
4	-0.85	-1.1	0.25	10,950			
4.5	-0.88	-1.088	0.208	9,110			
4.864	-0.895	-1.08	0.185	8,103			

the length of axis of the hole increased by 0.16". The horizontal diameter of the hole decreased by .02" and the vertical diameter of the hole decreased by 0.1" (Fig. 6.14.20).

Table 6.5.11. Elastic stresses around a circular hole when

$$\frac{\sigma_x}{\sigma_y} = \frac{1}{3}$$

	Horizontal Axis			Vertical Axis		
	$\theta = 0$	$\theta = 0$	$\theta = 0$	$\theta = 90^\circ$	$\theta = 90^\circ$	$\theta = 90^\circ$
	$\frac{\sigma_r}{\sigma_y}$	$\frac{\sigma_\theta}{\sigma_y}$	$\frac{\sigma_r - \sigma_\theta}{\sigma_y}$	$\frac{\sigma_r}{\sigma_y}$	$\frac{\sigma_r}{\sigma_y}$	$\frac{\sigma_r - \sigma_\theta}{\sigma_y}$
.1	0	2.667	2.667	0	0	0
.9	0.217	2.195	1.979	0.036	0.217	0.181
.8	0.349	1.836	1.486	0.129	0.349	0.220
.7	0.426	1.561	1.147	0.26	0.419	0.160
.6	0.444	1.369	0.926	0.409	0.443	0.034
.5	0.437	1.208	0.792	0.562	0.436	0.125
.4	0.417	1.105	0.718	0.705	0.414	0.291
.3	0.435	1.039	0.683	0.828	0.385	0.443
.2	0.358	1.016	0.67	0.921	0.358	0.563
.1	0.34	1.004	0.664	0.981	0.339	0.64
0	0.333	1.00	0.667	1	0.333	0.667

Area before loading = 0.785 sq. inches.

Area after loading assuming an elliptical shape .98" major axis and .9" minor axis =  $\frac{\pi}{4} (.9)(.98)$  = .693 sq. inches.

$\frac{\text{Area after loading}}{\text{Initial area}} = 0.882$

## 6.6a Oval Holes Under Uniform Biaxial Compression

The shape of the oval hole is given in Fig. 6.15.10. For these dimensions of the hole the values of  $p, q, r$  in (4.12.1) may be assumed as

$$p = 0.75''$$

$$q = 0.28''$$

$$r = -0.03''$$

The tangential stresses on the boundary of the hole assuming elastic state is given below.

Angle made with the horizontal line through center of the hole = $\beta$	Boundary stress	
	$\frac{\sigma_{\theta}}{s}$	$\sigma_{\theta}$ psi
0	3.28	9,850
10°	3.44	9,870
15°	3.6	10,800
19°	3.62	10,880
30°	2.97	8,900
60°	0.942	2,825
90°	0.79	2,370

Two oval holes symmetrically located under uniform biaxial compression,  $s$ : The distribution of principal strain difference around the holes when the specimen was subjected to a stress of 3,000 psi in horizontal and vertical directions

is shown in Fig. 6.15.2.

The load was kept constant for a period of 16 hours to observe the behavior of the material in creep. The distribution of the principal strain difference at the stress level of 3,000 psi in the beginning and at the end of 16 hours, on the entire region, was experimentally determined and shown in Fig. 6.15.6. It is analyzed on three lines, the horizontal line through the center of the holes, the vertical line through the center of the pillar and the vertical line through the center of the hole, as given in Figs. 6.15.7, 6.15.8 and 6.15.9 respectively. The strains have increased with time everywhere. The maximum principal strain difference on the boundary at the time the applied stresses first reached 3,000 psi was more than 35,800 micro in./in. After keeping the stresses constant for 16 hours the strains became very large on and near the semicircular boundary making it impossible to make any measurements in that region. The strain distribution at the beginning and at the end of the period of 16 hours is shown in Fig. 6.15.6.

Method of failure: At the initial stage of keeping the applied stresses at 3,000 psi, the average decrease in height of the hole was 0.12" and the average decrease in the width of the hole was 0.013". The stresses were gradually

raised to 4,000 psi when the defomrations became very large, the height of the holes decreasing gradually until the collapse of the holes.

Initial hole area	= 0.662 sq. inch
Hole area after loading at 3,000 psi	= 0.508 sq. inch
<u>Area of hole after loading</u> Area of hole before loading	= 0.767

#### 6.6b Single Oval Hole Under Uniform Biaxial Compression

The principal strain difference in the specimen when subjected to equal horizontal and vertical stresses of 3,000 psi are shown in Fig. 6.16.3. The stresses of 3,000 psi were maintained for a period of 40 hours. The principal strain difference at the beginning, after 16 hours and after 40 hours of reaching 3,000 psi, on the entire region was experimentally determined and shown in Fig. 6.16.6. It is analyzed on three lines, the horizontal line through the center of the hole, the vertical line at a horizontal distance of 1.18" to the right of the center of hole and on the vertical line through the center of the hole as shown in Figs. 6.16.7, 6.16.8, and 6.16.9. Inspection of these figures show that the strains have gradually increased with time at every point. The maximum  $\epsilon_1 - \epsilon_2$  on the

boundary was more than 36,000 micro in./in. at the applied stress of 3,000 psi.

At the end of the period of maintaining constant stresses for 40 hours the decrease in the height of the hole was .07" and the decrease in the width of the hole was 0.053" (Fig. 6.16.20).

Area of hole before loading	= 0.662 sq. inches
Area of hole after loading at 3,000 psi	= 0.553 sq. inches
<u>Area of hole after loading</u> Area of hole before loading	= 0.835

In the preceding sections, the multiaxial properties of rock salt and stress strain distributions of openings created in the material have been discussed. Wherever possible the theoretical and experimental results have been compared. Some results are reasonably in good agreement, and for such results which are not, reasons explaining the discrepancies have been given. In conclusion, the photo stress method has proved to be suitable for studying stress strain distribution in underground openings in rock salt.

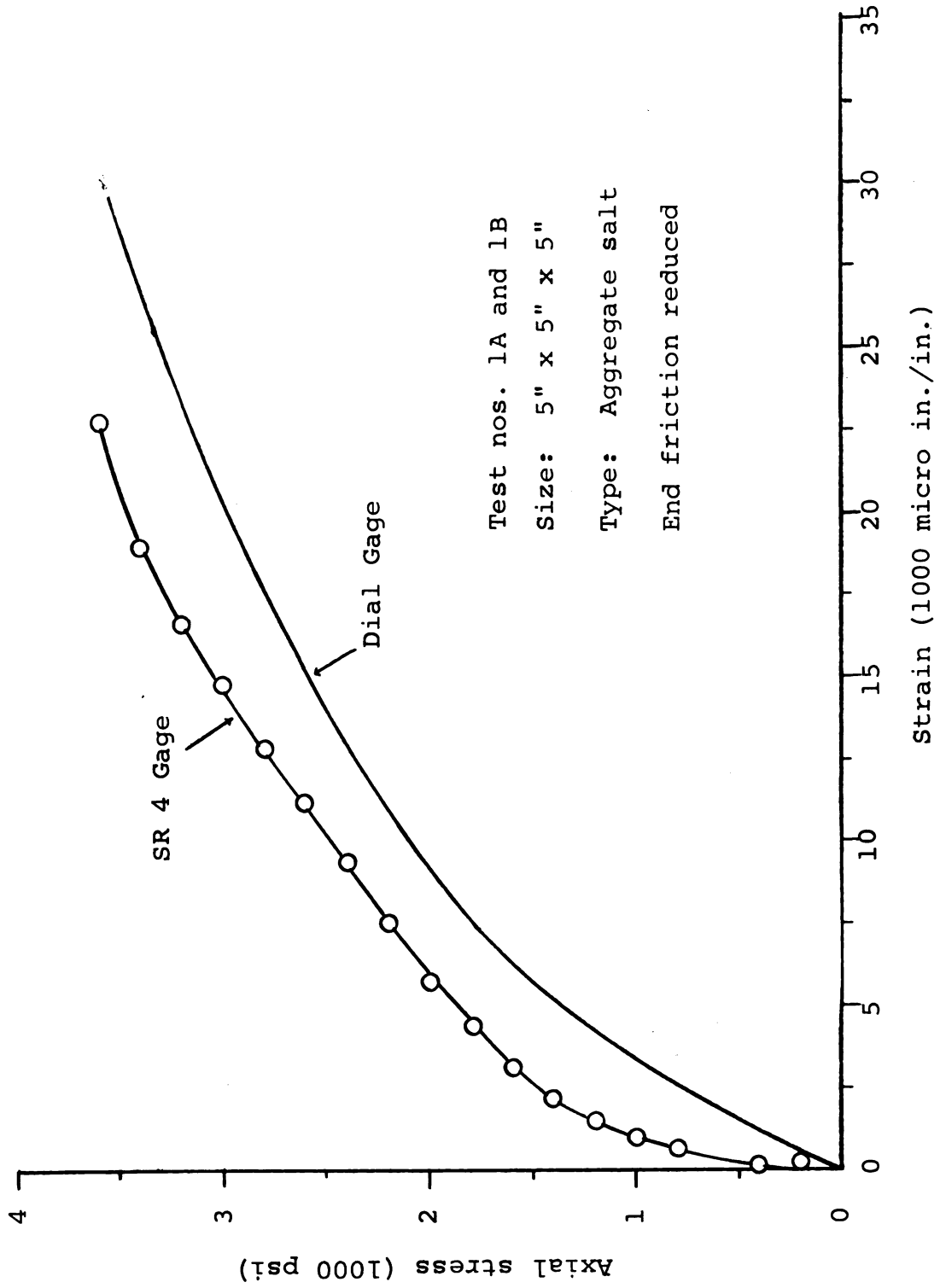


Fig. 6.1.5. Axial stress strain relation in uniaxial compression (mean values of 2 tests).

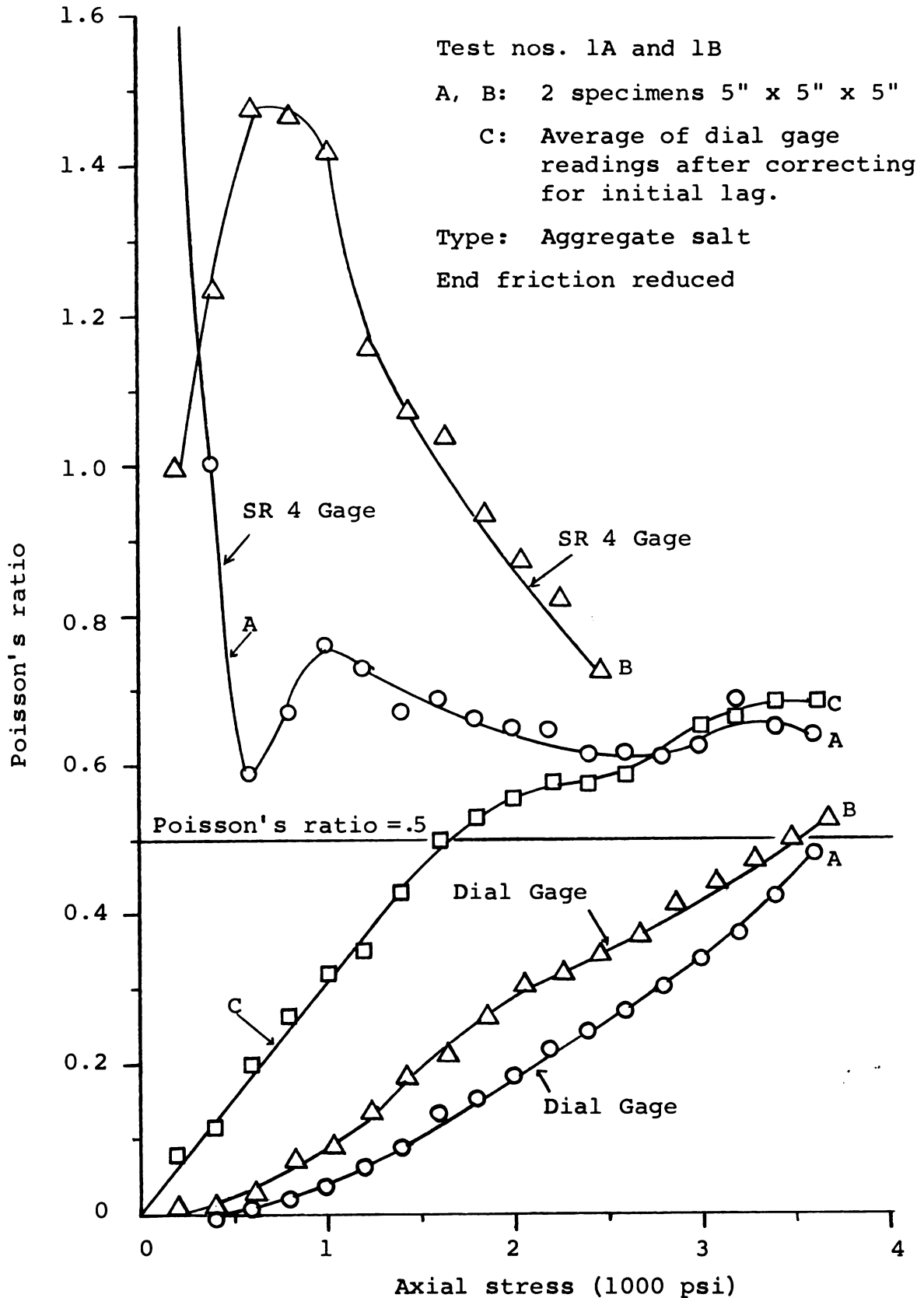


Fig. 6.1.6. Axial stress Poisson's ratio relation in uniaxial compression.

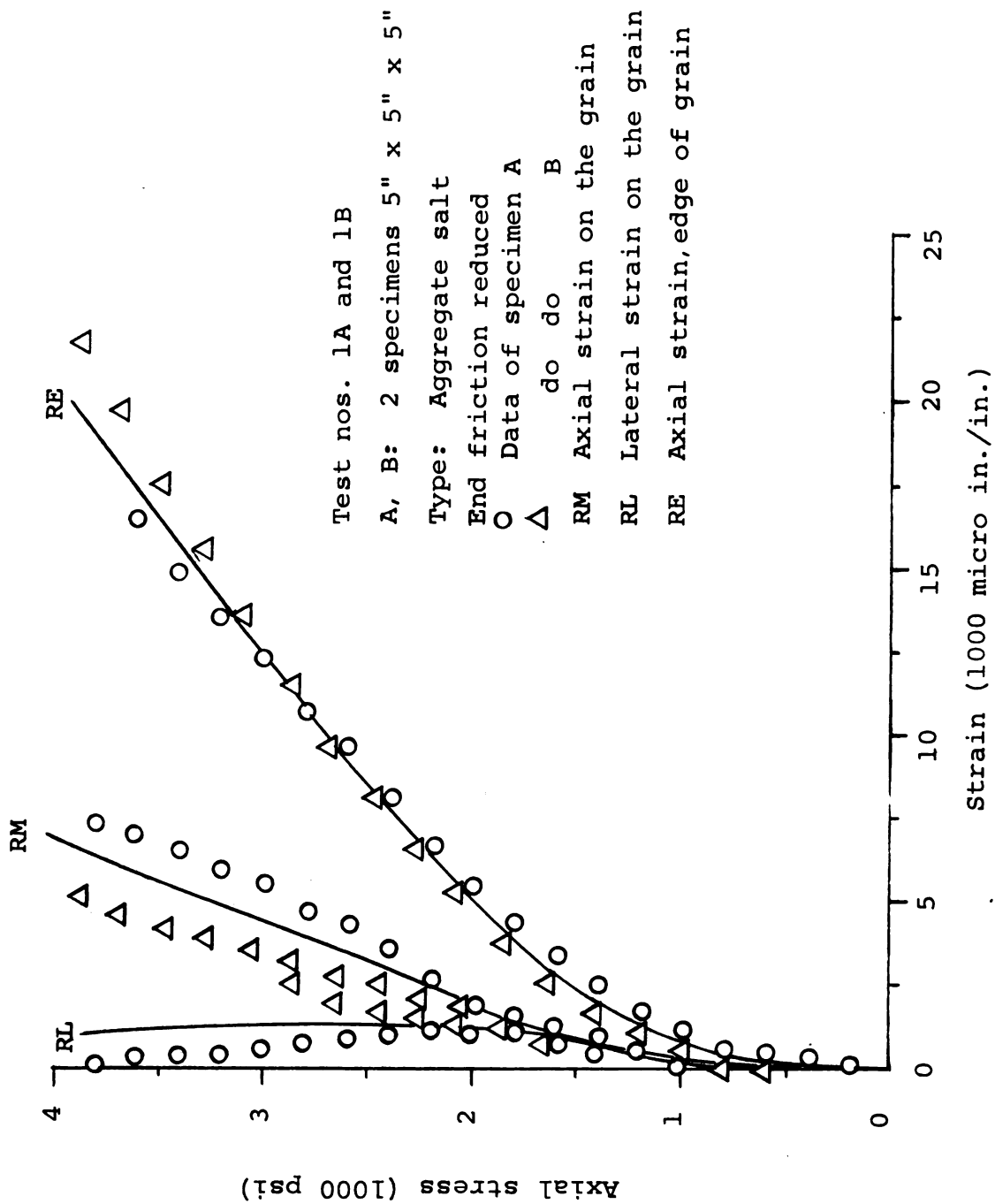


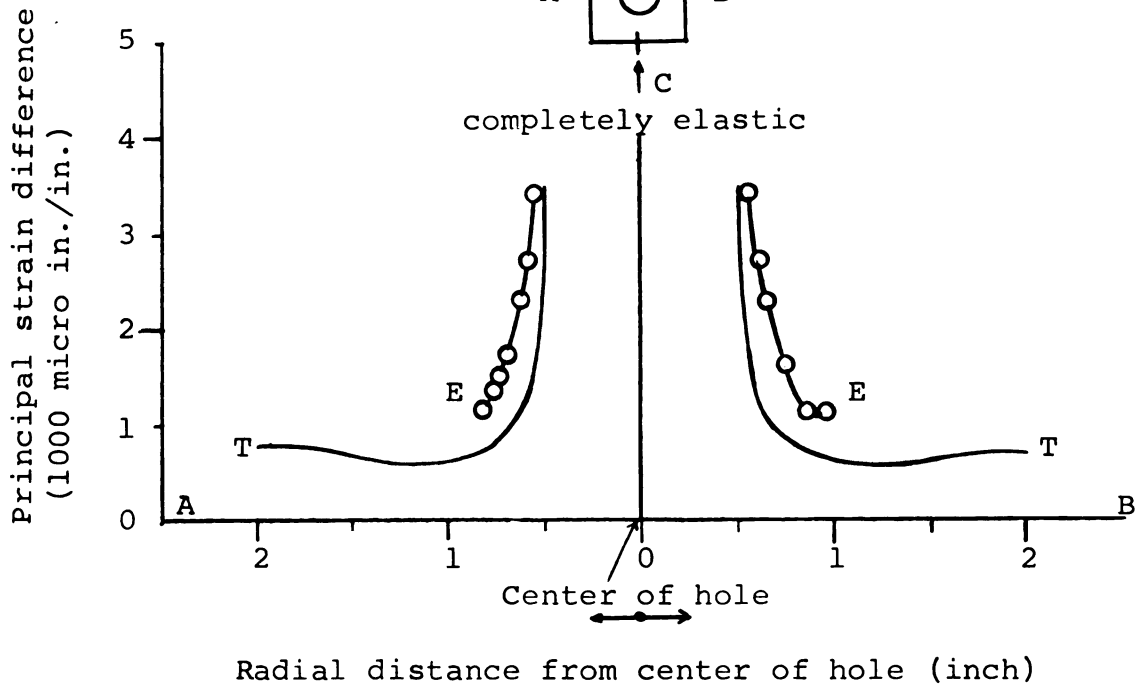
Fig. 6.1.7. Stress strain relation of individual grains based on SR 4 gages.

Principal strain difference  
at points on line AB

500 psi

Test no. 3

E: Experimental  
T: Theoretical



Principal strain difference at  
points on line CD

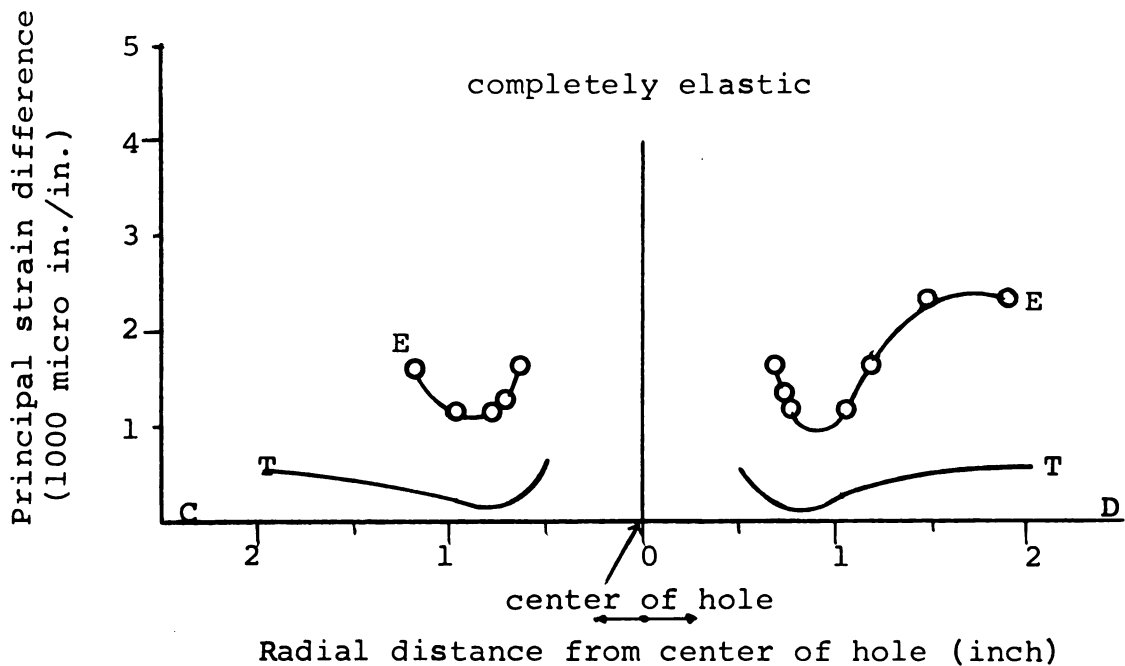


Fig. 6.3.3. Circular hole under uniaxial compressive stress of 500 psi.

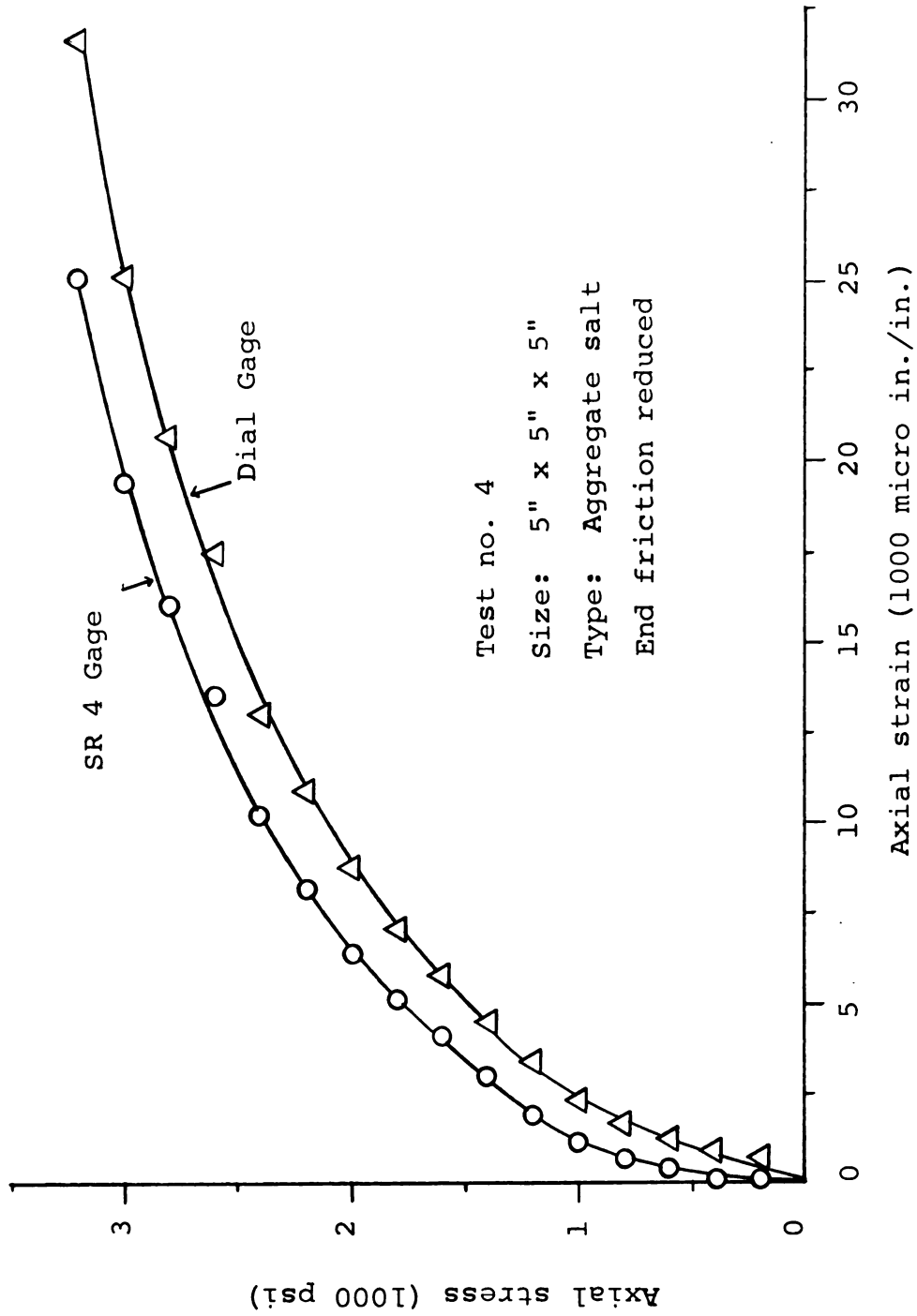


Fig. 6.4.5. Stress strain relation in uniaxial compression.

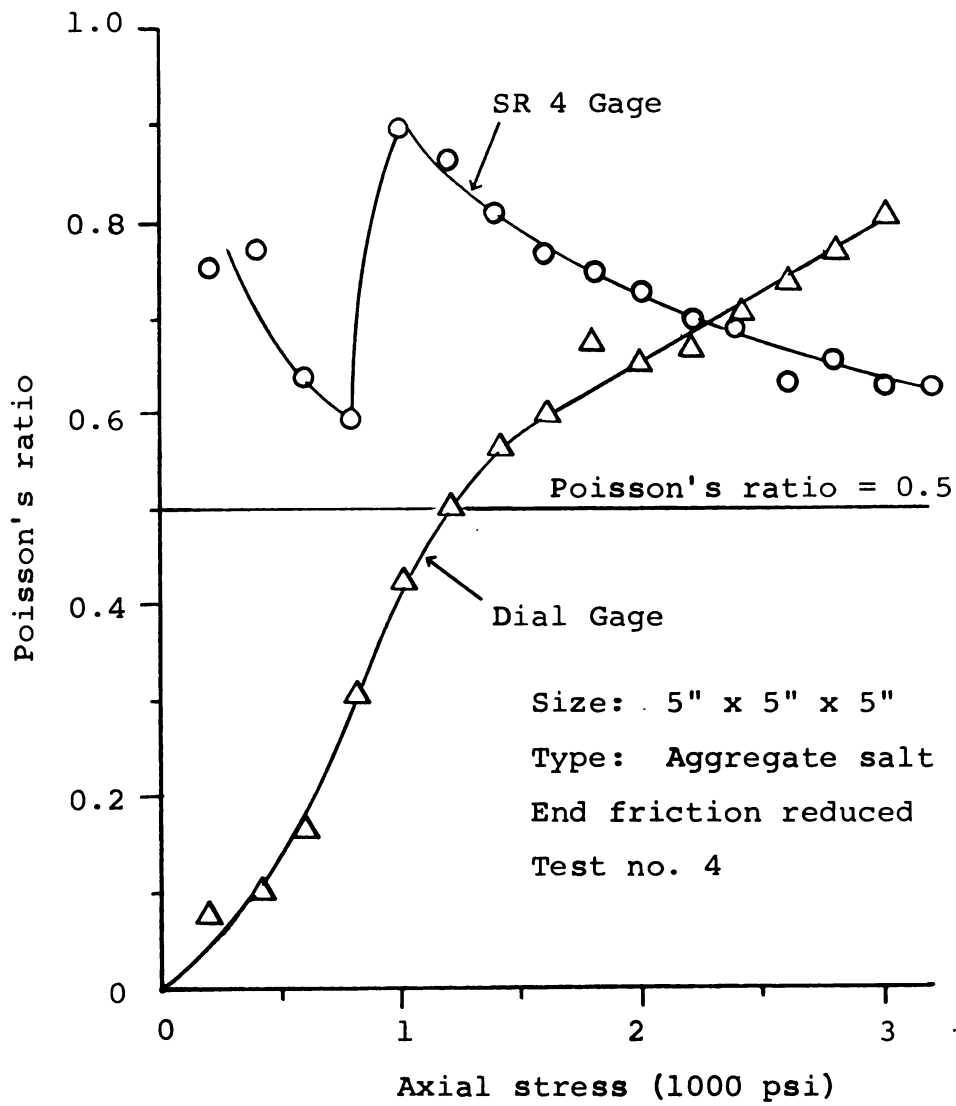


Fig. 6.4.6. Axial stress Poisson's ratio relation in uniaxial compression.

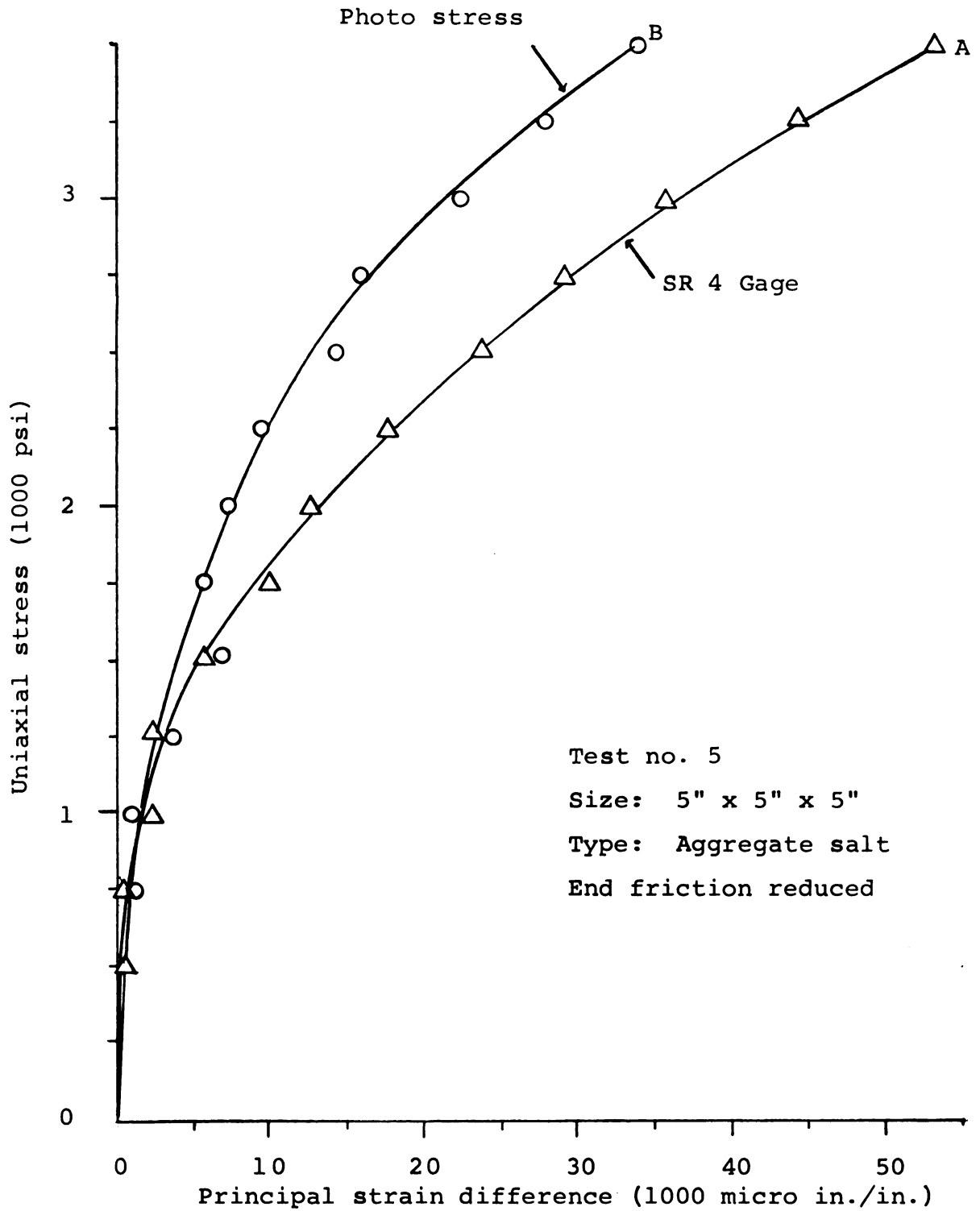


Fig. 6.5.3. Relation between uniaxial stress and principal strain difference.

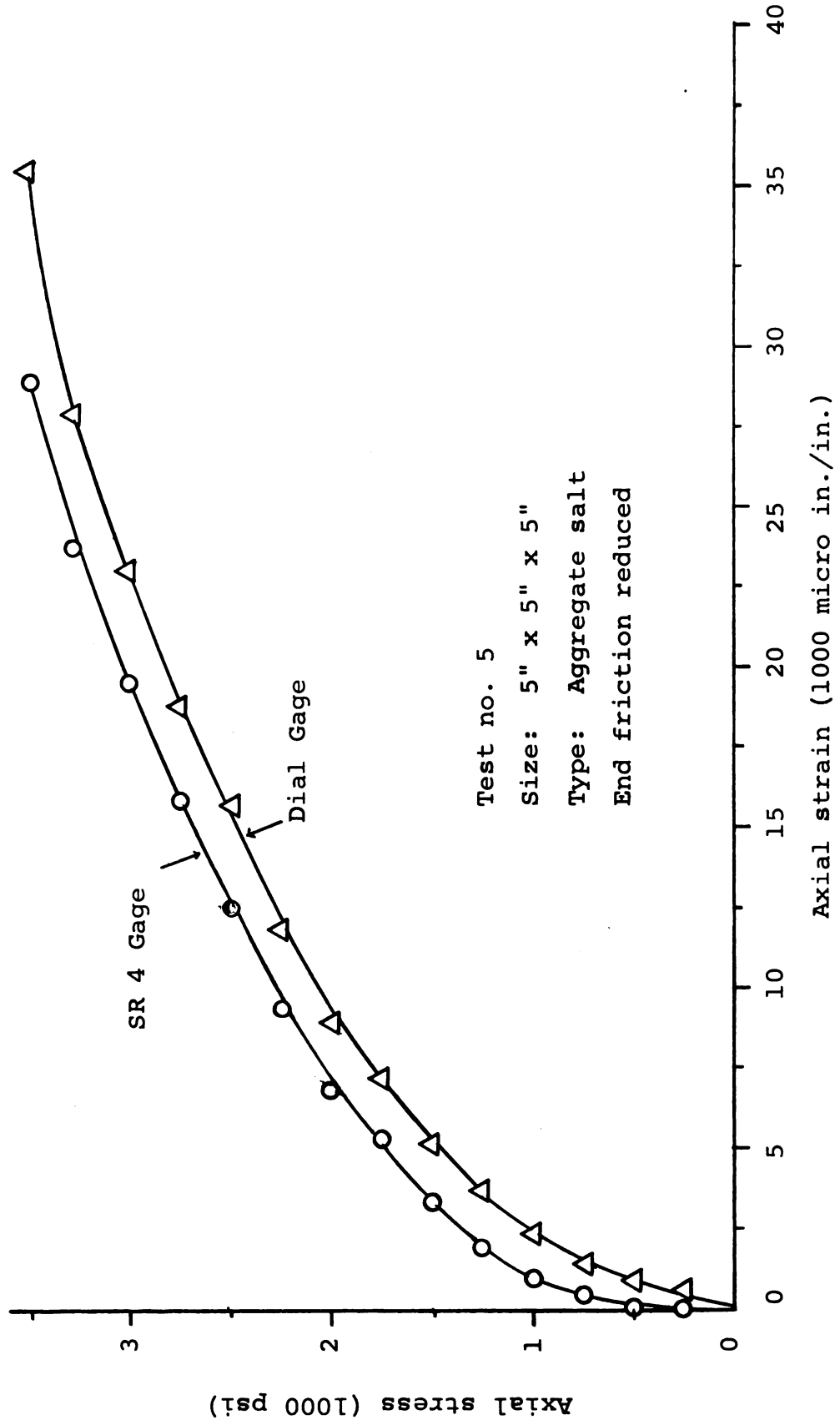


Fig. 6.5.5. Stress strain relation in uniaxial compression.

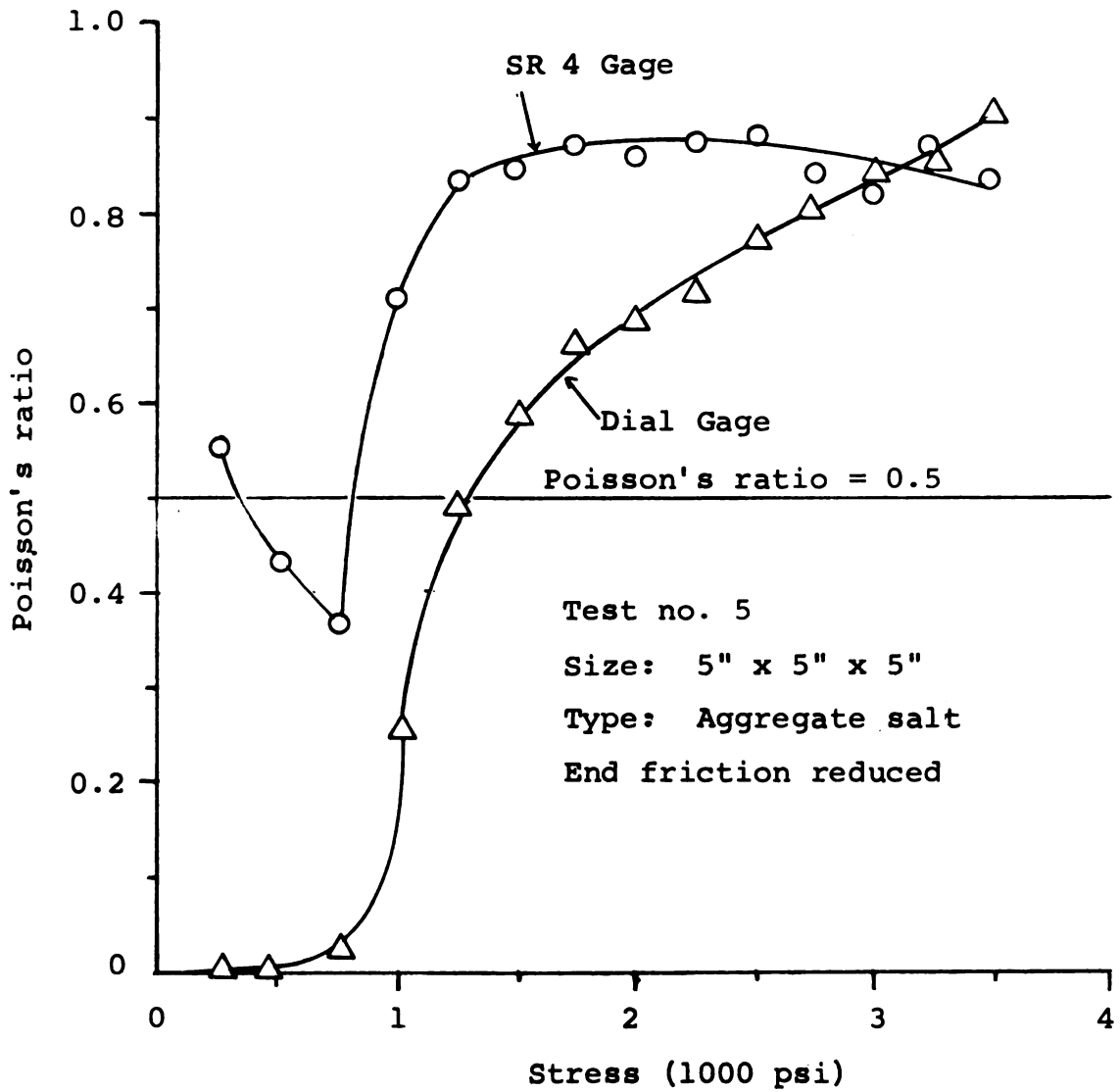


Fig. 6.5.6. Axial stress Poisson's ratio relation in uniaxial compression.

Test no. 5  
 Size: 5" x 5" x 5"  
 Type: Aggregate salt  
 End friction reduced

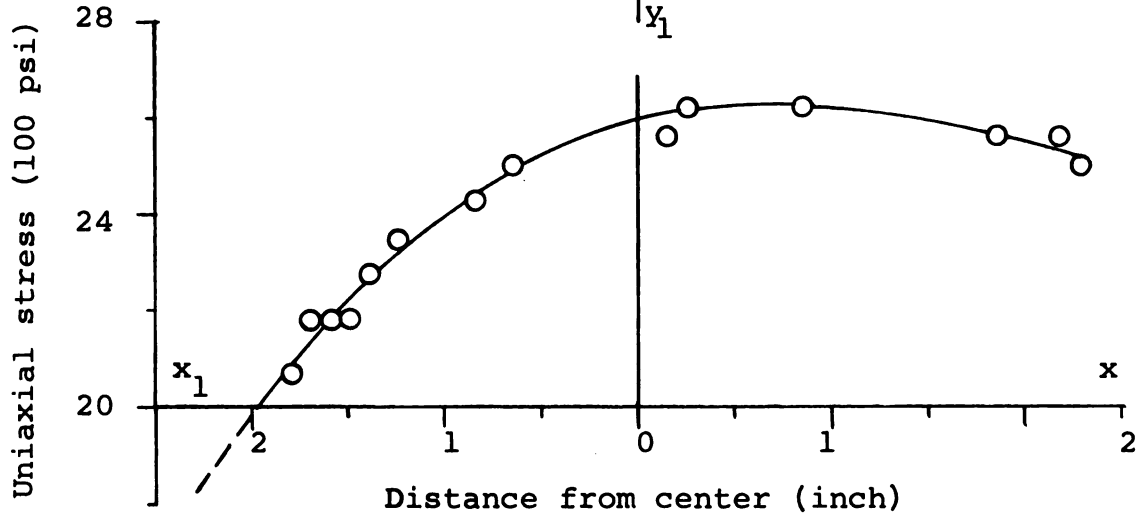
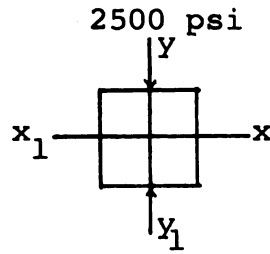


Fig. 6.5.7. Principal stress difference along  $x_1$   $x$  under uniaxial compression of 2500 psi.

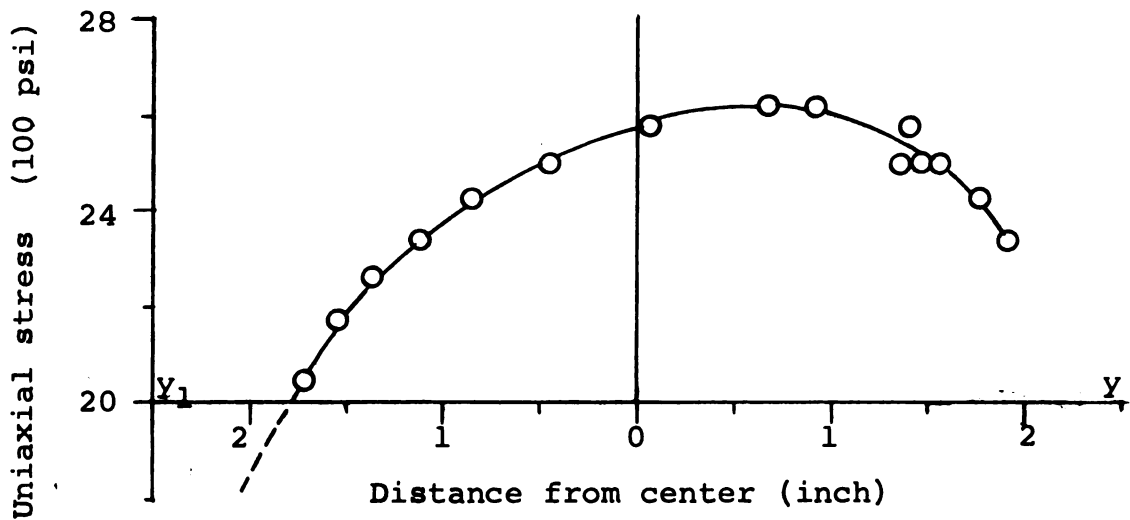
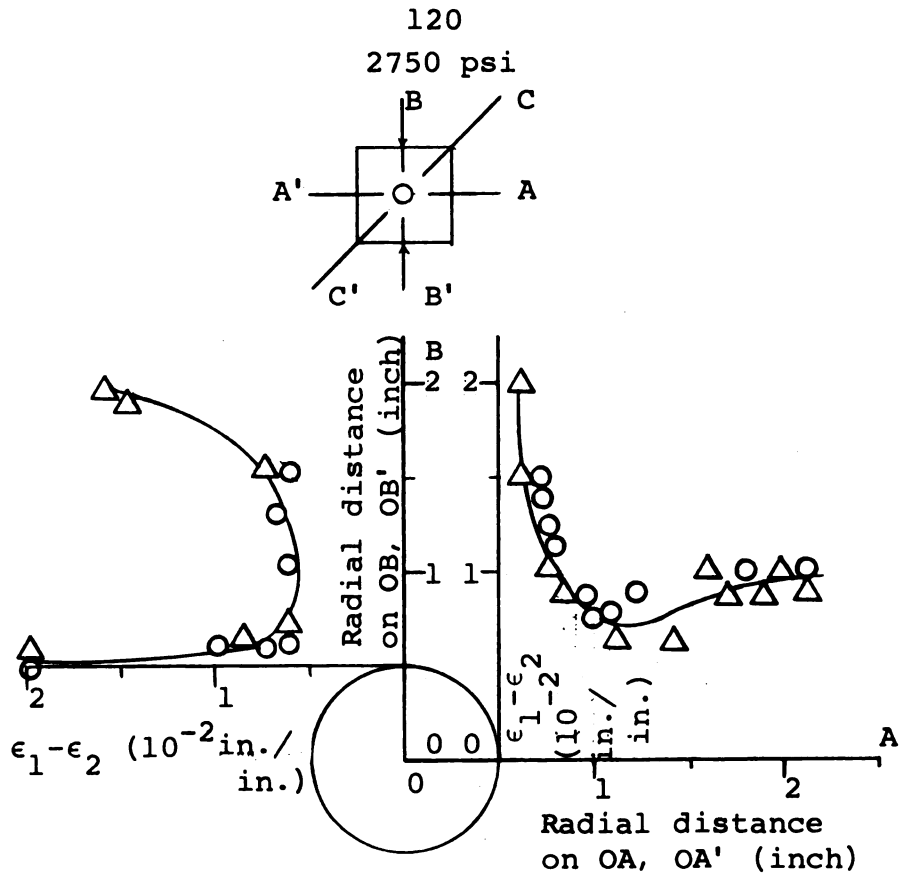


Fig. 6.5.8. Principal stress difference along  $y_1$   $y$  under uniaxial compression of 2500 psi.



Test no. 8

- On lines OA, OB, OC
- △ On lines OA', OB', OC'

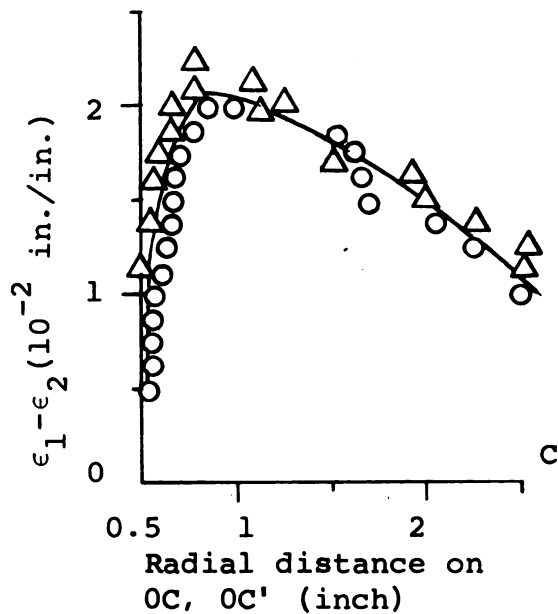


Fig. 6.8.3. Circular hole - uniaxial compression of 2750 psi. Principal strain difference on radial lines normal, parallel and at  $45^\circ$  to the direction of load.

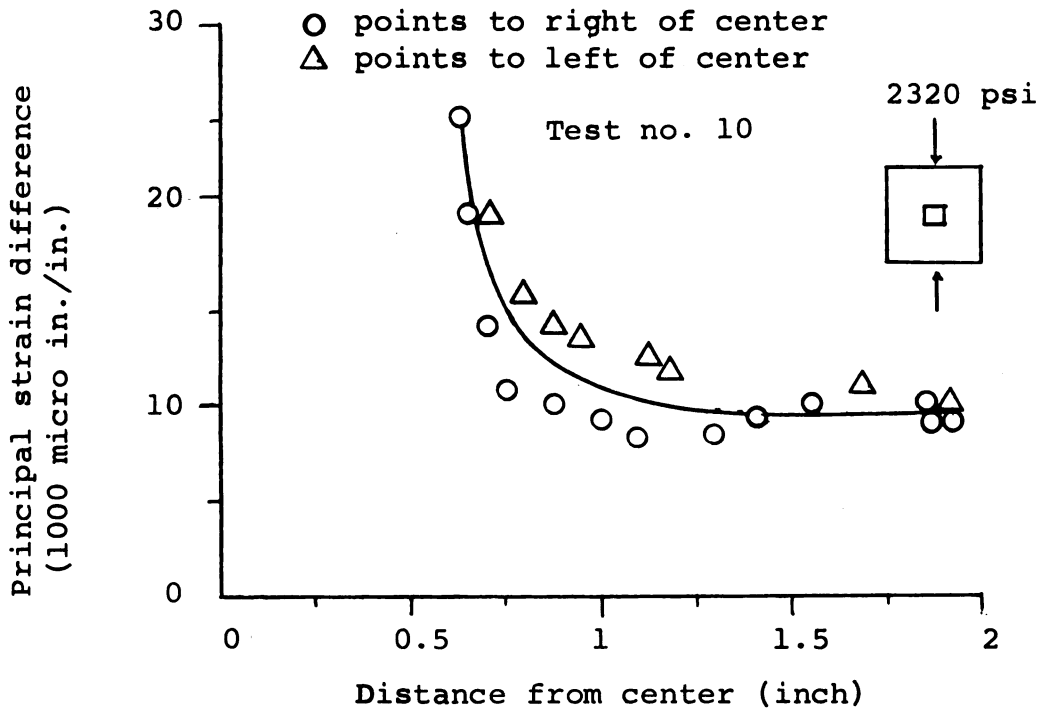


Fig. 6.10.3. Principal strain difference on center line normal to load in case of square hole under uniaxial compression of 2320 psi.

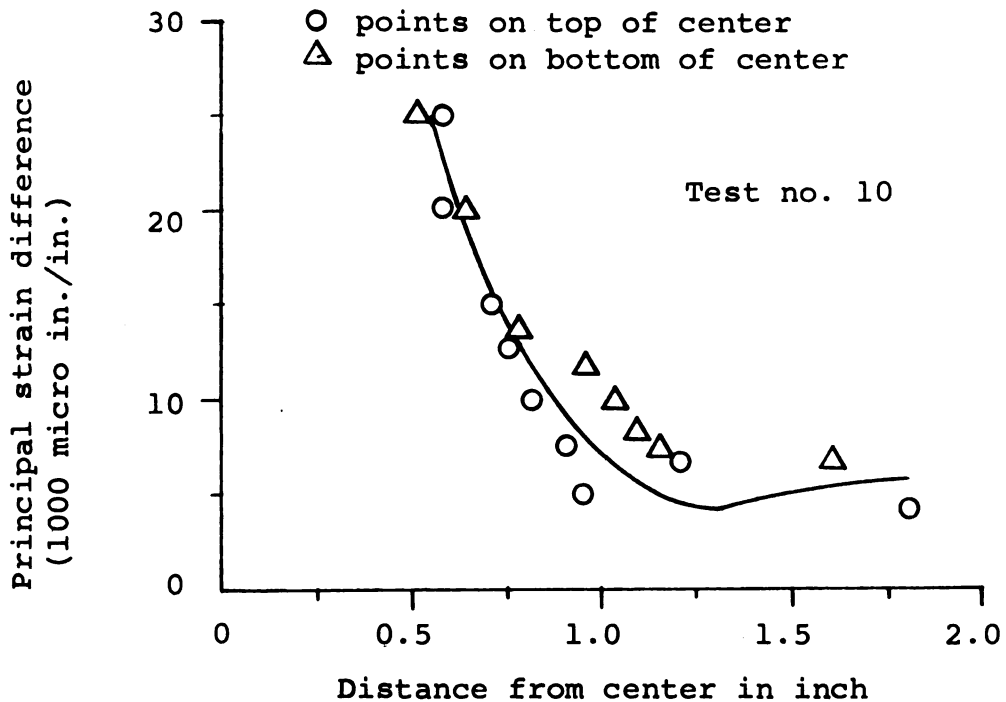


Fig. 6.10.4. Principal strain difference on line parallel to load in case of square hole under uniaxial compression of 2320 psi.

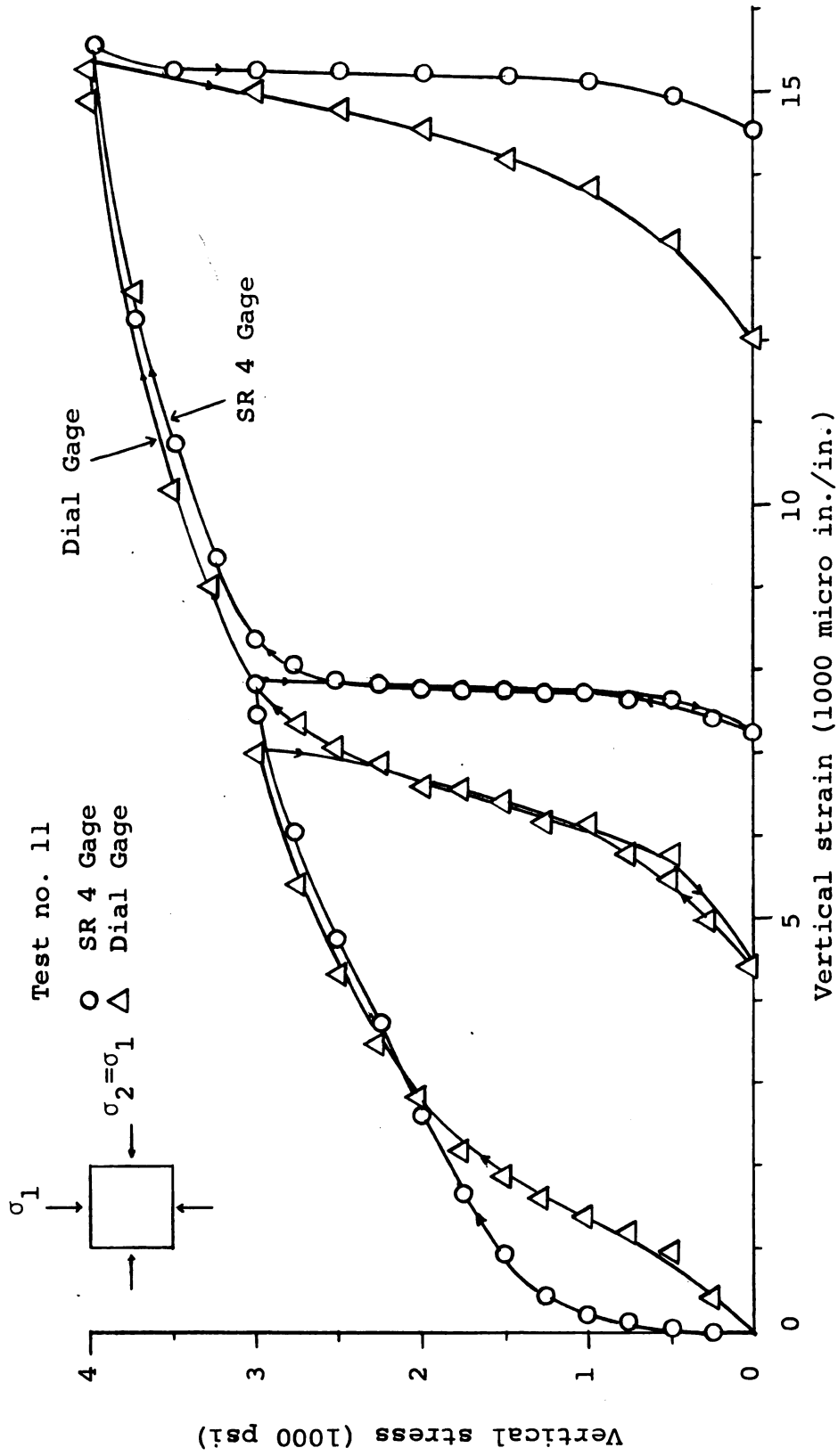


Fig. 6.11.3. Vertical stress versus vertical strain in a cube under equal compression in vertical and horizontal directions.

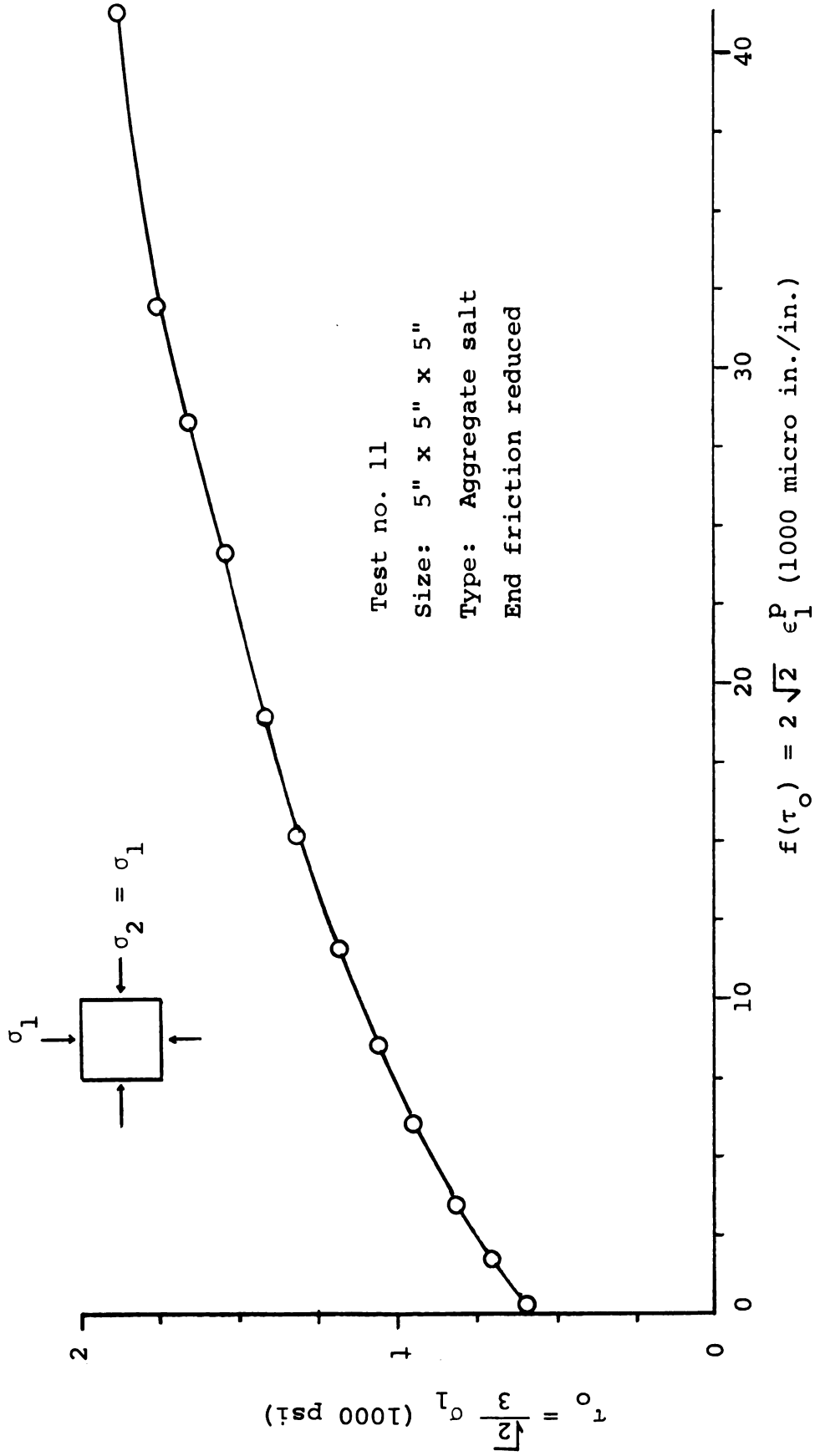


Fig. 6.11.4.  $\tau_0$  versus  $f(\tau_0)$  in case of equal horizontal and vertical stresses.

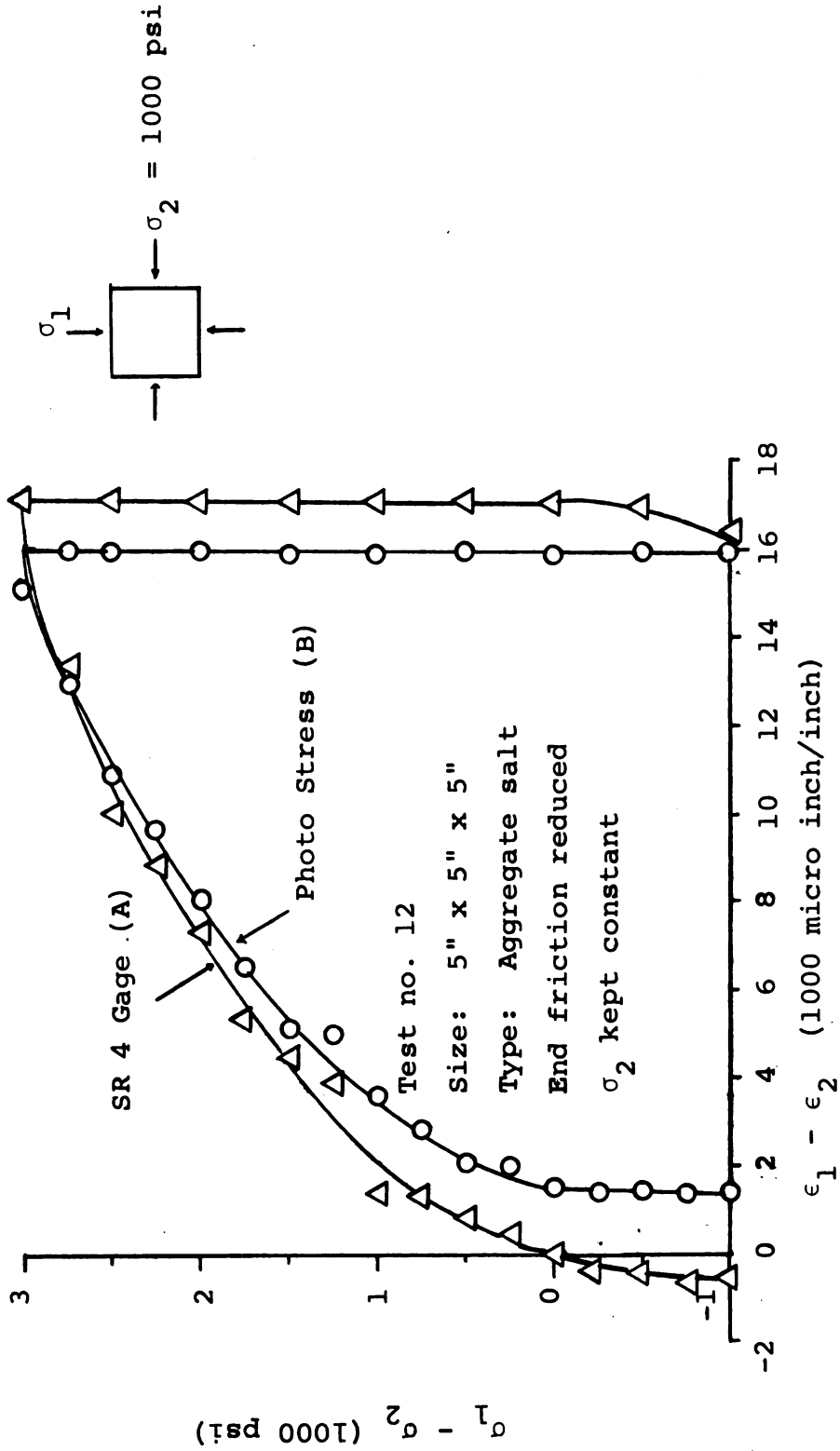


Fig. 6.12.4. Principal stress difference versus principal strain difference in biaxial compression keeping  $\sigma_2 = 1000$  psi.

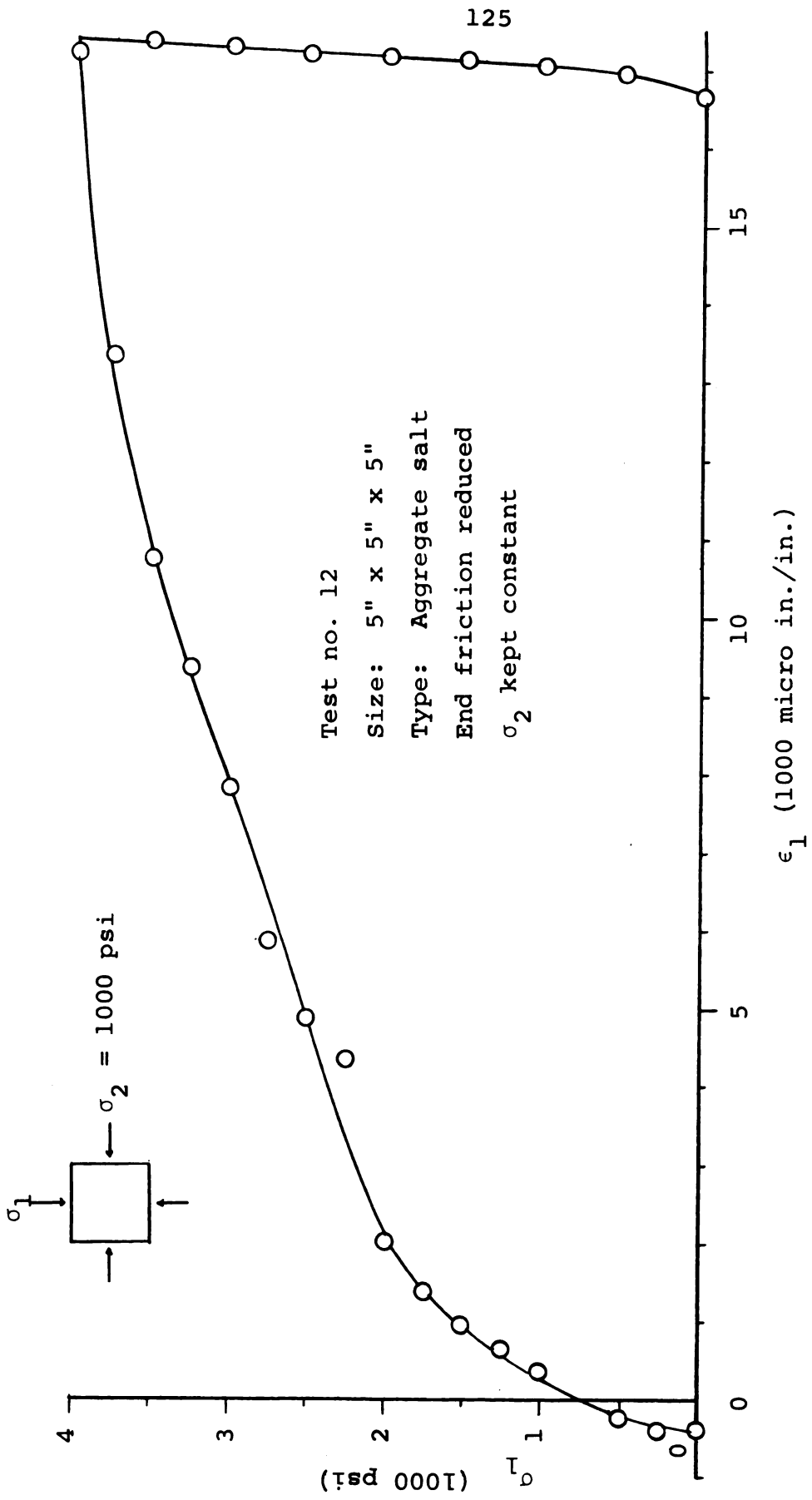


Fig. 6.12.5. Vertical stress versus vertical strain in biaxial compression keeping horizontal stress = 1000 psi.

Test no. 13

E: Experimental

F: Analytical

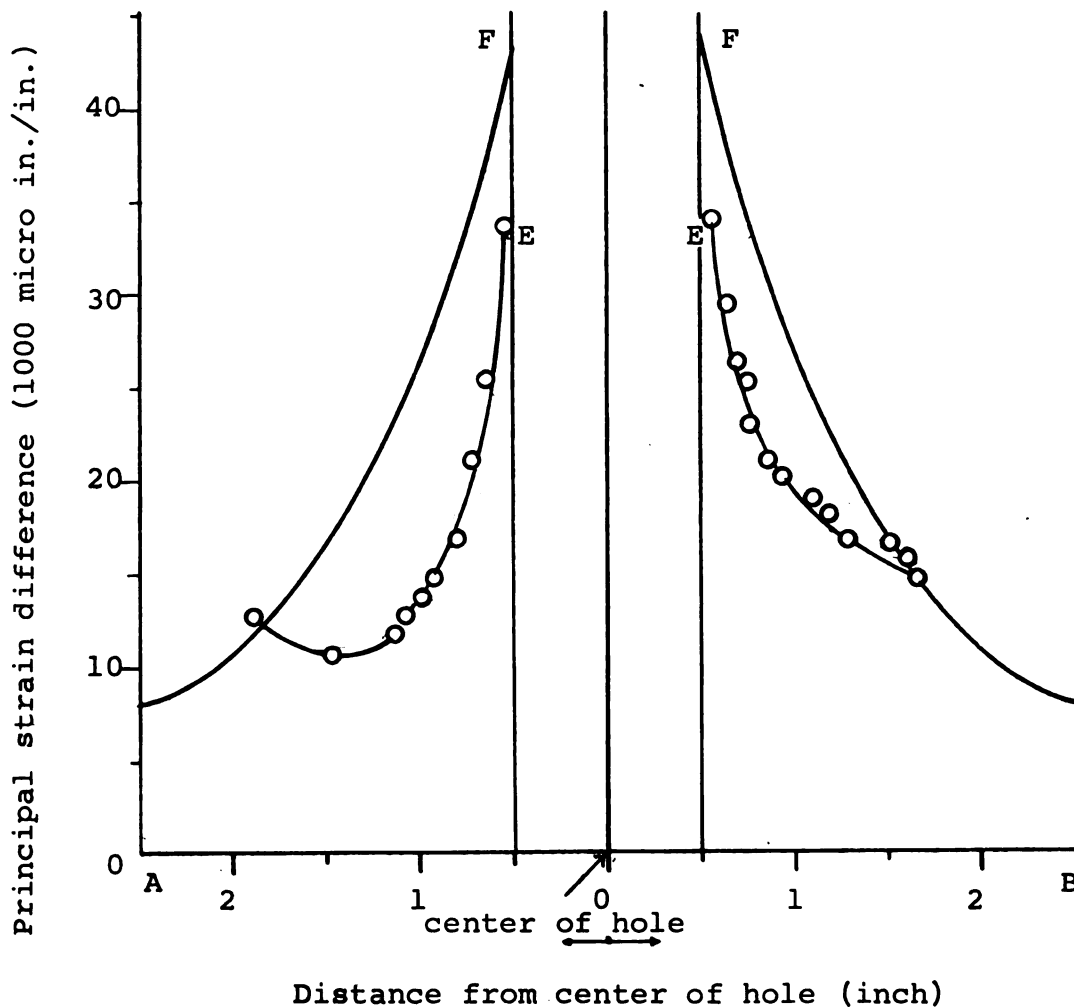
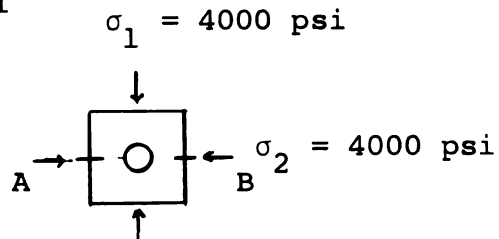


Fig. 6.13.5. Distribution of principal strain difference along AB in case of circular hole under equal vertical and horizontal compression of 4000 psi.

Test no. 14

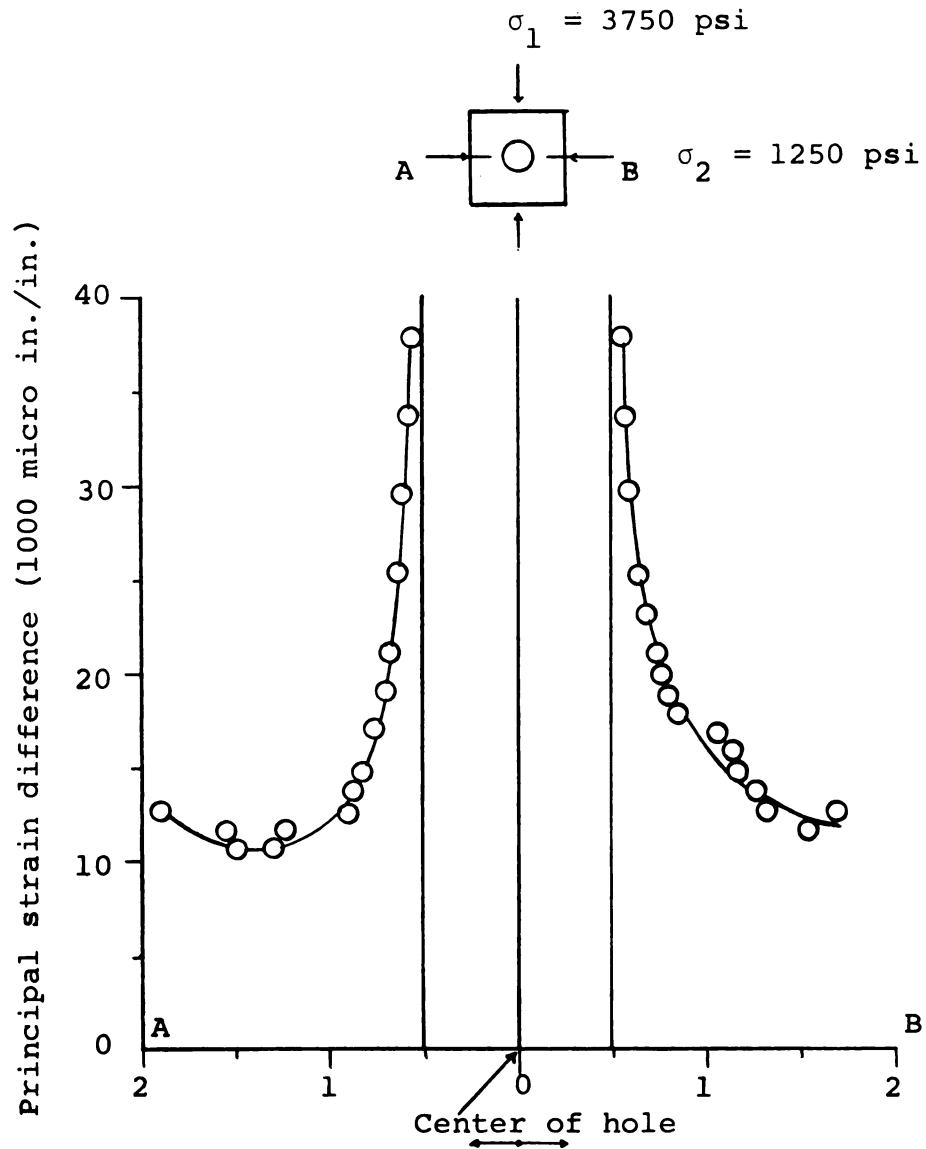


Fig. 6.14.3. Distribution of principal strain difference along AB in case of circular hole under horizontal compression of 1250 psi and vertical compression of 3750 psi.

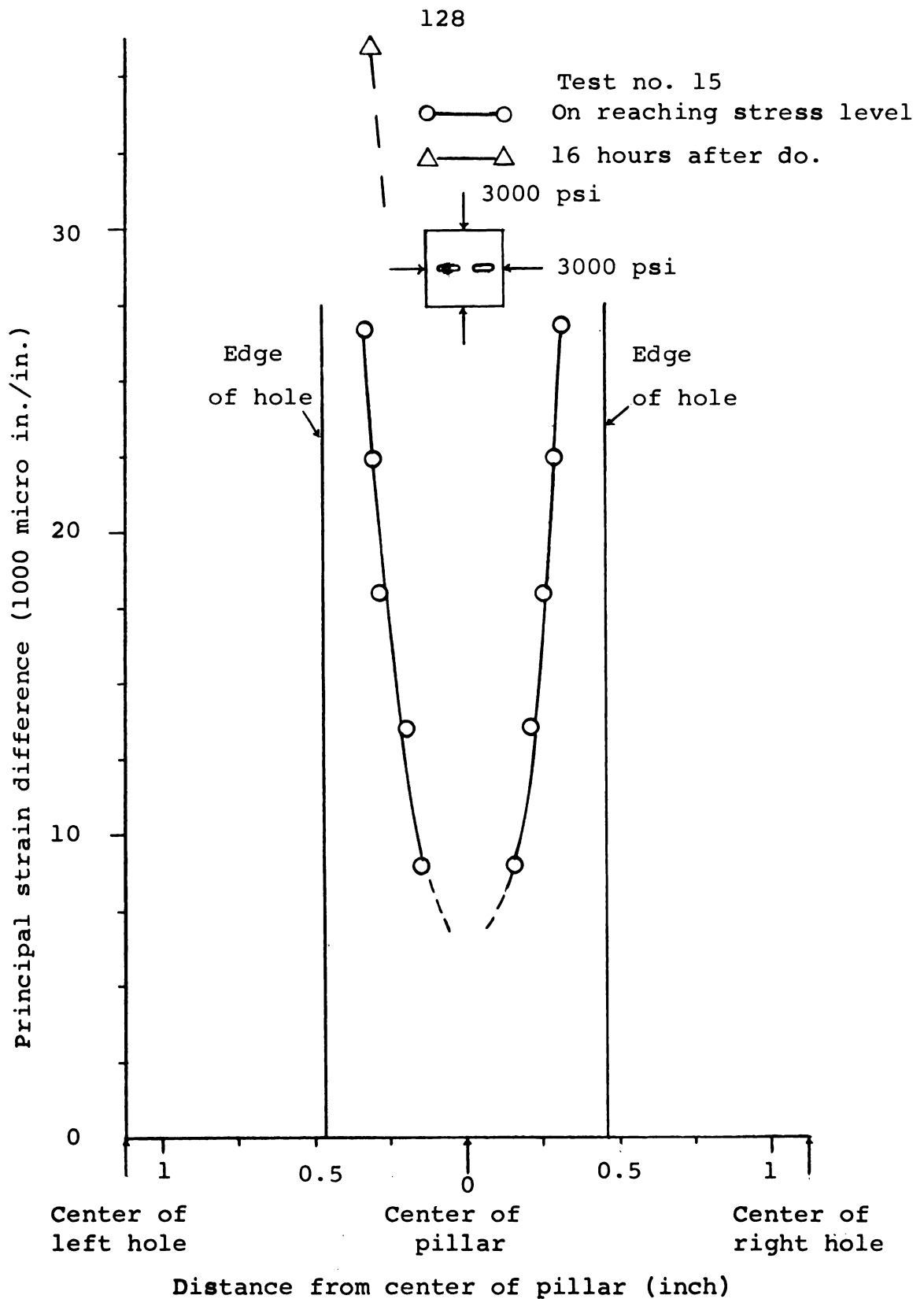


Fig. 6.15.7. Two oval openings under equal horizontal and vertical compression of 3000 psi - distribution of principal strain difference along the line joining the centers of the holes.

Test no. 15

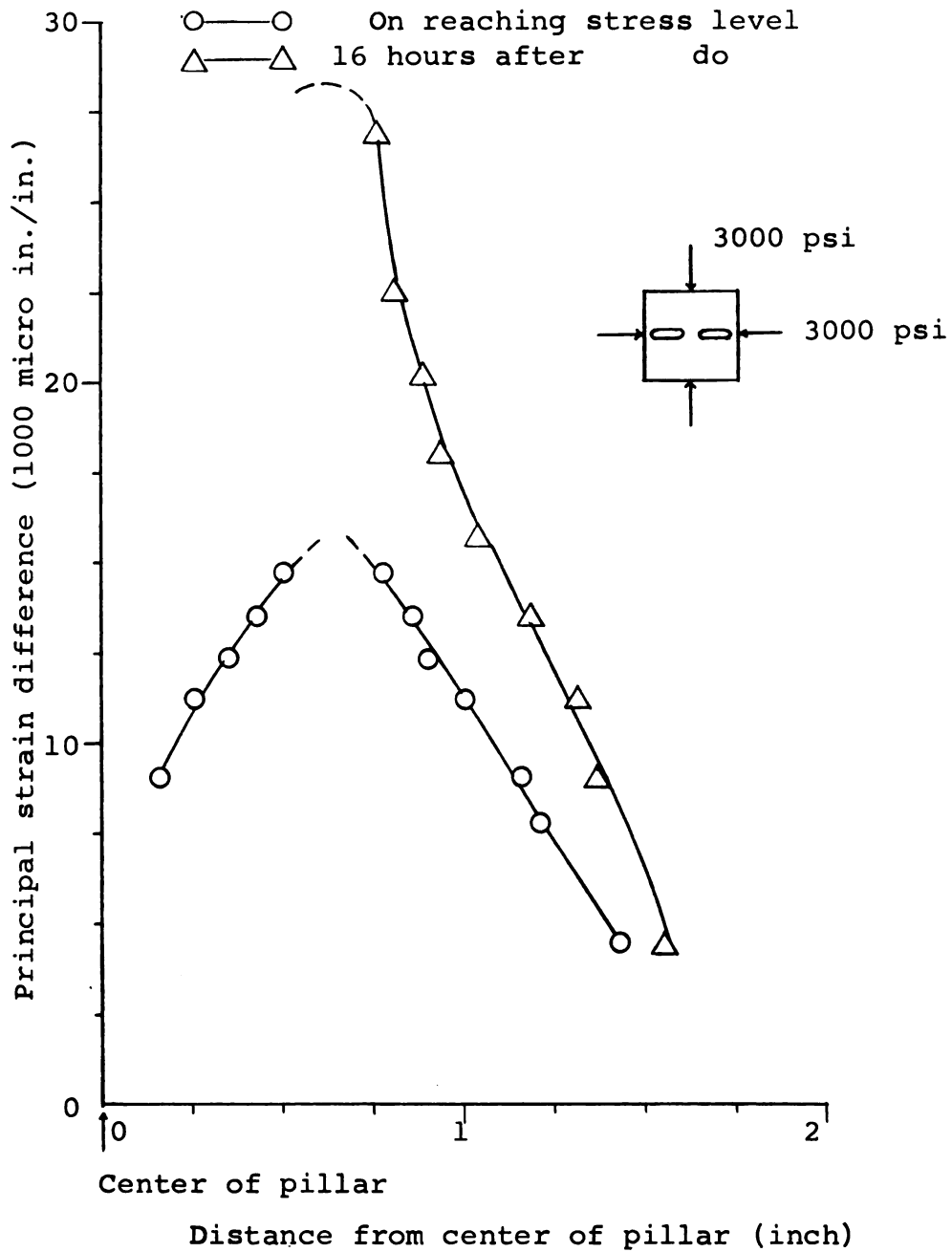


Fig. 6.15.8. Two oval openings under equal horizontal and vertical compression of 3000 psi - distribution of principal strain difference on a vertical line through center of pillar.

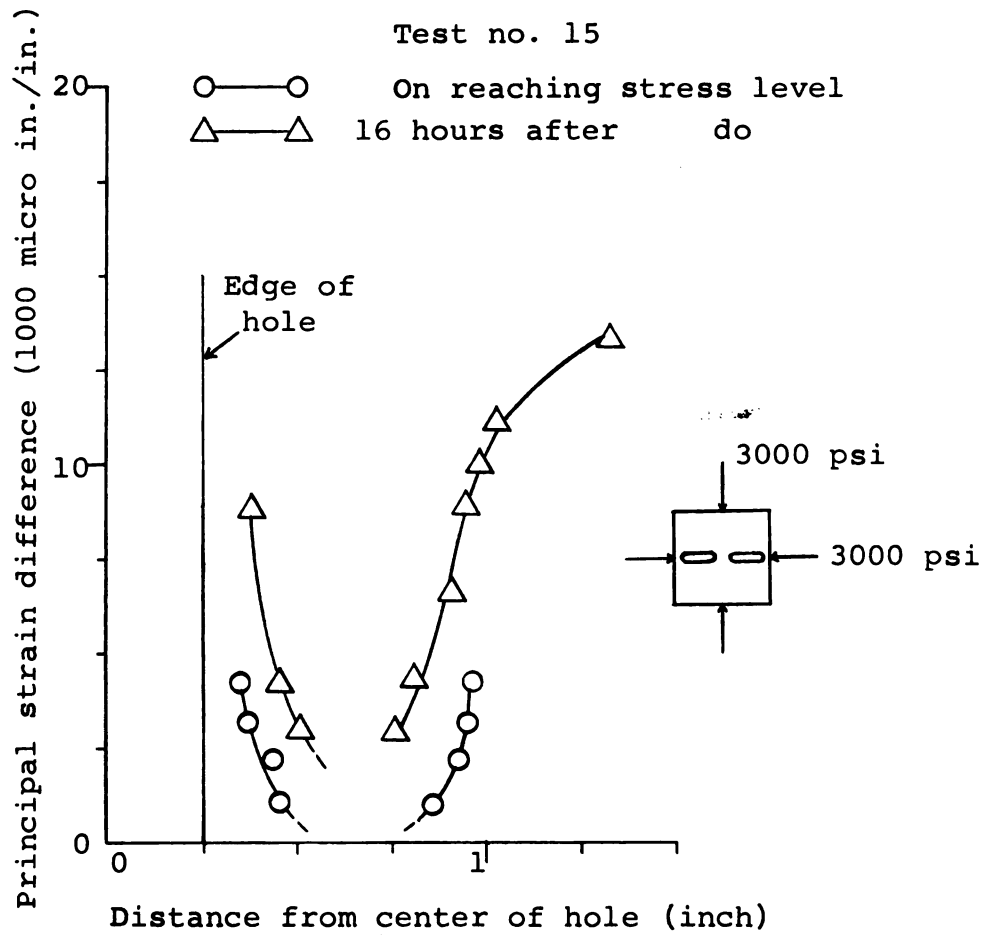


Fig. 6.15.9. Two oval openings under equal horizontal and vertical compression of 3000 psi - distribution of principal strain difference on a vertical line through center of right hole.

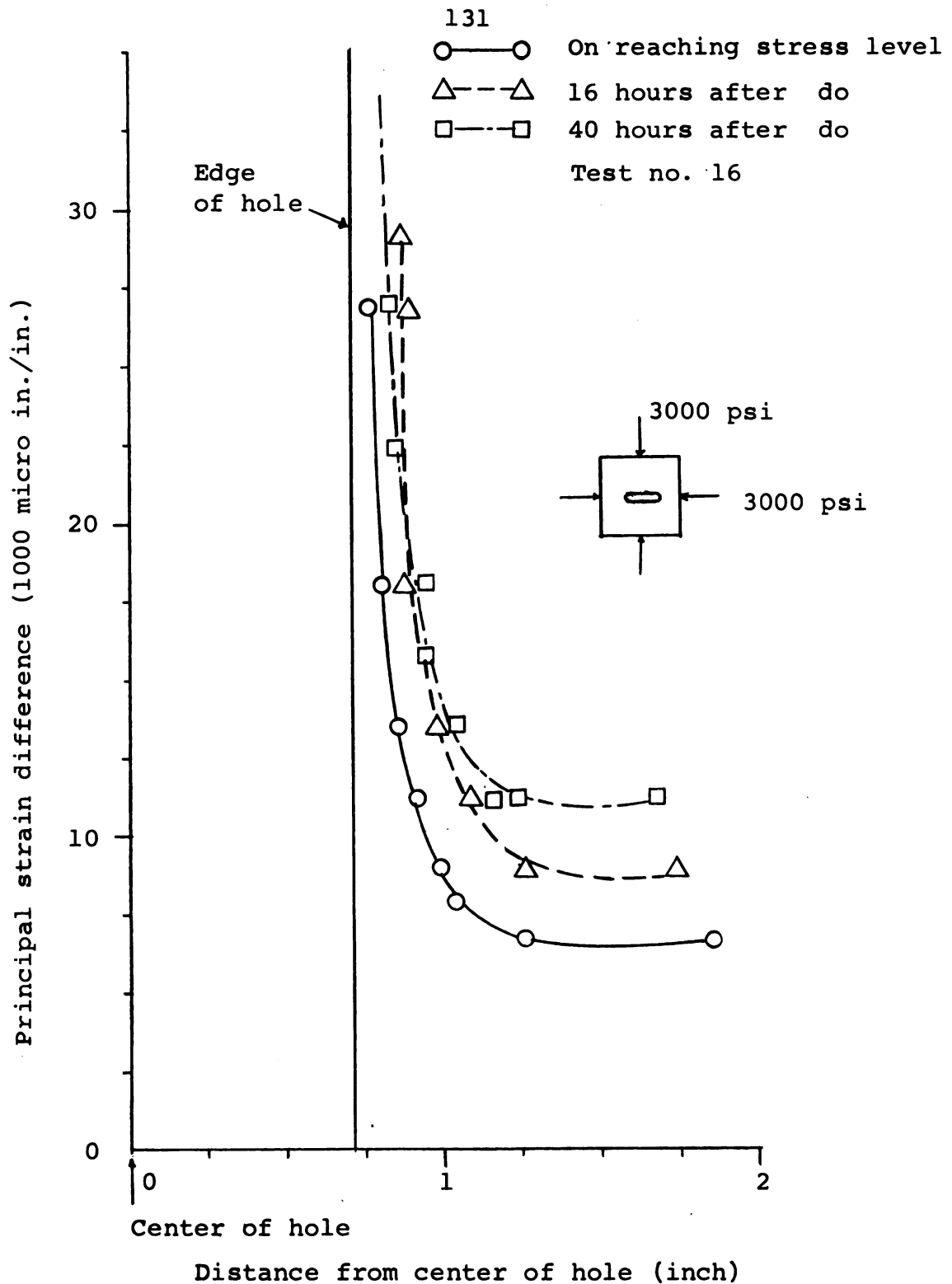


Fig. 6.16.7. One oval opening under equal horizontal and vertical compression of 3000 psi - distribution of principal strain difference on the horizontal line through center of hole.

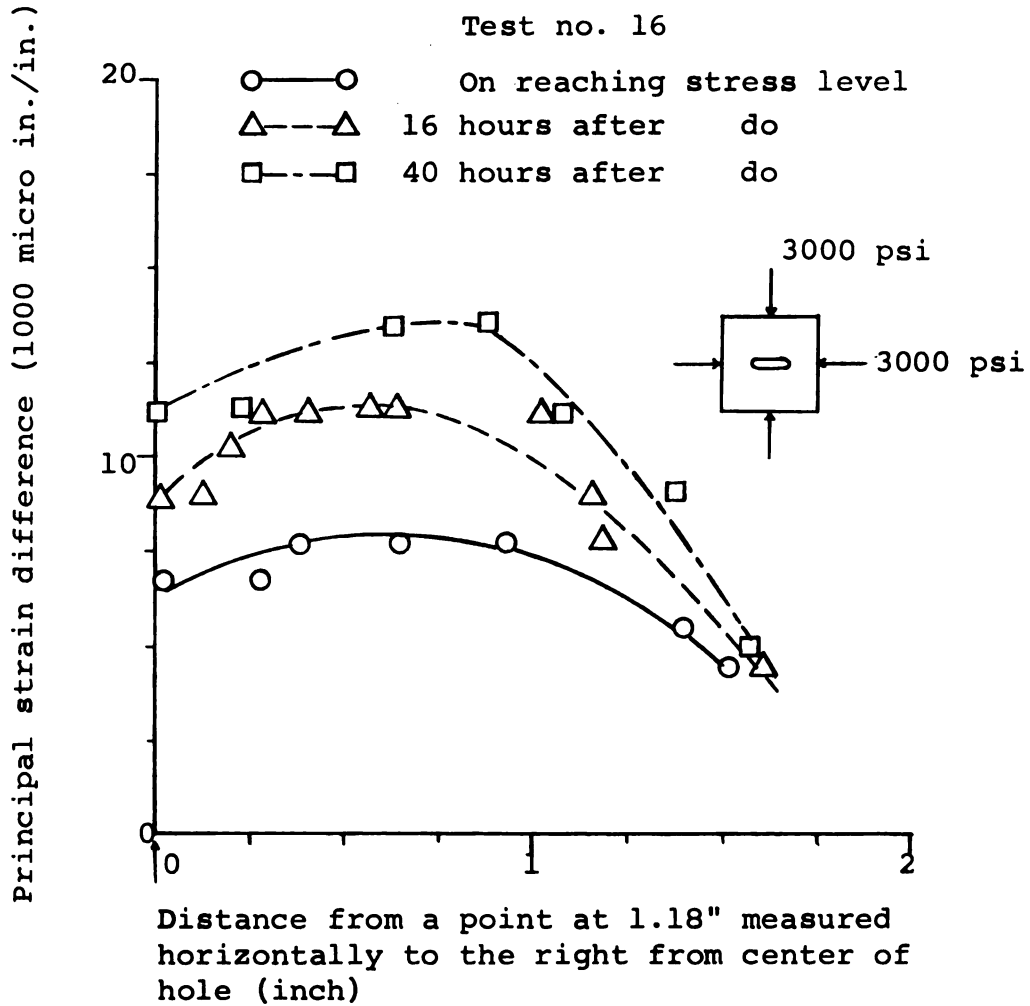


Fig. 6.16.8. One oval opening under equal horizontal and vertical compression of 3000 psi - distribution of principal strain difference on the vertical line through a point at 1.18 inch from center of hole.

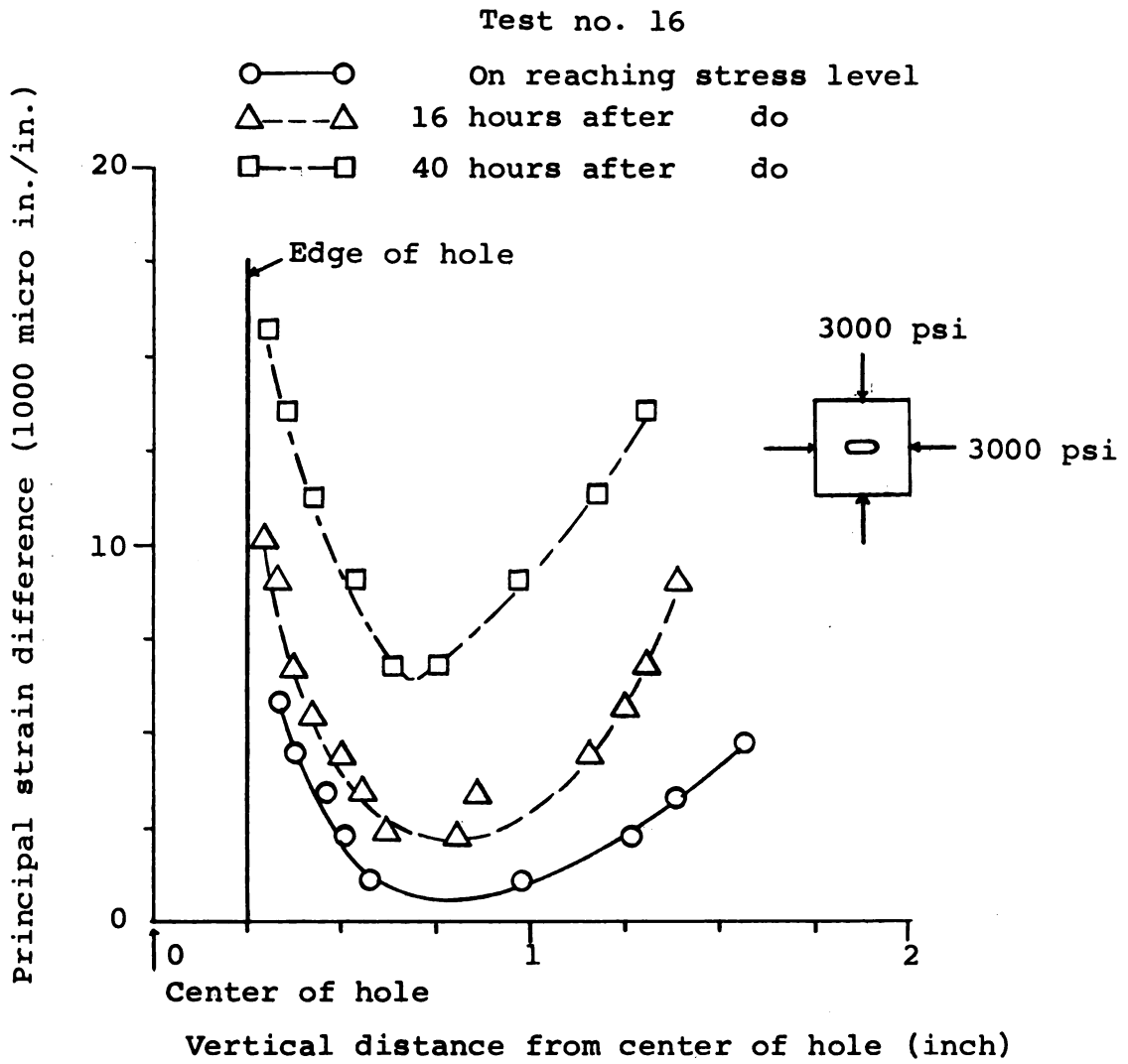
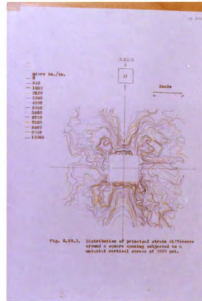
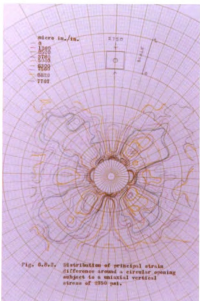
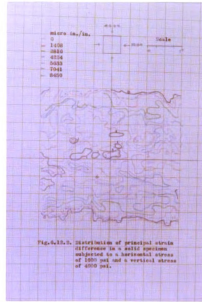
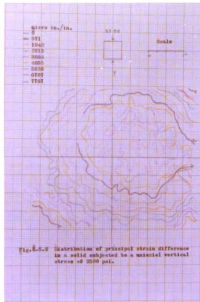
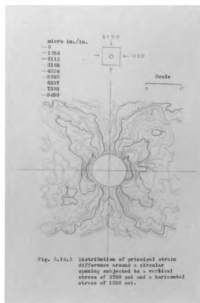
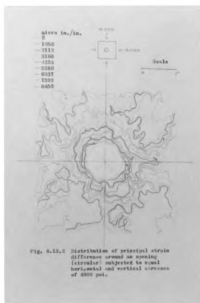
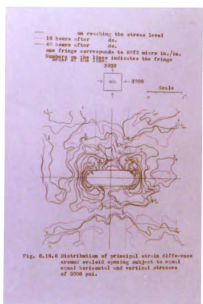
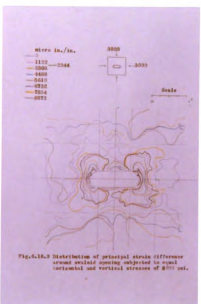
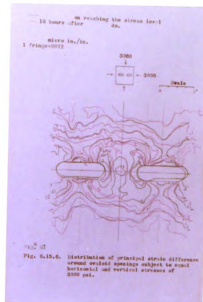
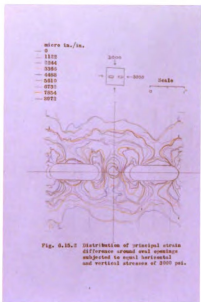


Fig. 6.16.9. One oval opening under equal horizontal and vertical compression of 3000 psi - distribution of principal strain difference on the vertical line through center of hole.







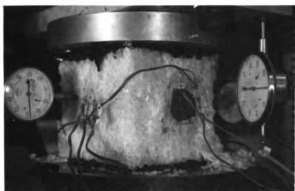


Fig. 6.1.20. Failure of a solid specimen under a uniaxial stress of 3,858 psi.

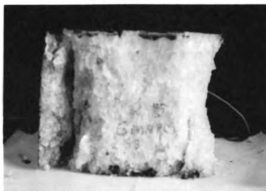


Fig. 6.5.20. Failure of a solid specimen under a uniaxial stress of 3,556 psi.

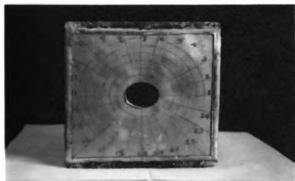


Fig. 6.8.20. Failure of a circular opening under a uniaxial stress of 3,200 psi.



Fig. 6.6.20. Failure of a circular opening under a uniaxial stress of 2,500 psi.



Fig. 6.10.20. Failure of a square opening under a uniaxial stress of 2,850 psi.



Fig. 6.7.20. Failure of a square opening under a uniaxial stress of 2,750 psi.



Fig. 6.17.20. Biaxial loading device and photo stress large field meter.

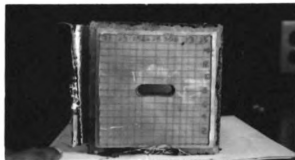


Fig. 6.16.20. Yielding of an oval hole under a hydrostatic stress of 3,000 psi.



Fig. 6.11.20. Yielding of a solid specimen after reducing vertical stress to zero from a hydrostatic stress of 4,000 psi.



Fig. 6.12.20. Yielding of a solid specimen under a vertical stress of 4,000 psi and a horizontal stress of 1,333 psi.

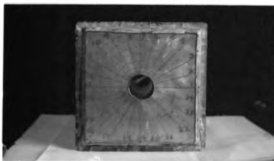


Fig. 6.13.20. Yielding of a circular hole under a hydrostatic stress of 4,000 psi.

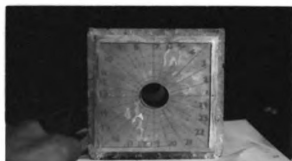


Fig. 6.14.20. Yielding of a circular hole under a vertical stress of 4,000 psi and a horizontal stress of 1,333 psi.

## CHAPTER VII

### SUMMARY AND DISCUSSION

#### 7.1 The Mechanical Properties

The stress strain relation of the salt in a uniaxial compression test is a continuous curve from the beginning to the point of failure, and as such the conventional method of calculating the values of  $E$  and  $\eta$  cannot be adopted. The curve is considered as a combination of several straight lines, and the chord modulus is defined by the slope of the straight line in any stress range. The strains obtained by dial gages are consistently higher than those obtained by SR-4 gages.

Average values of  $E$  are:

stress range psi	Average $E$ (SR-4 gages) million psi	Average $E$ (Dial gages) million psi
0 to 1,000	1.408	0.4559
1,000 to 2,000	0.1913	0.1757

The values of Poisson's ratio based on SR-4 gages are more than 0.5. This indicates that the material increased in volume under uniaxial compression, due to

separation of the grains. As an approximation based on dial gages, it may be assumed that,  $\eta$  varies linearly from 0 to 0.5 as the stress increases from 0 to 1,500 psi, and remains as 0.5 for stresses above 1,500 psi. Large values of Poisson's ratio up to even 1.0 have been observed by others.<sup>2</sup> This phenomenon has been interpreted as being caused by brittle fracture among the crystal grains resulting in volume increase of the specimen.

The average stress at failure in a uniaxial compression test was 3,800 psi, with the corresponding principal strain difference of 42,800 micro in./in. The salt used in this investigation is considerably stronger than most other salt. However, the greater strength appears to be due to its pure and homogeneous character.

In a biaxial state of stress it may be assumed that the material becomes plastic when the value of  $\sigma_o$  reaches 4,000 psi or  $\tau_o$  reaches 1,885 psi. When  $\tau_o = 1,885$ , the value of the function  $f(\tau_o)$  in (4.1.10) becomes 41,300 micro in./in. and when  $\sigma_2 = 0$ , the value of  $(\epsilon_1^P - \epsilon_2^P)$  becomes 43,800 micro in./in.

The principal strain difference at which failure takes place in a uniaxial stress state and at which plastic yielding begins in a biaxial stress state are nearly the

same. Accordingly it seems reasonable to assume that in the case of uniaxial stress states, failure occurs when the maximum principal strain difference becomes 42,800 micro inch per inch at the point of maximum stress concentration on the boundary.

Some of the experimental data are given in Tables 7.3.1 and 7.3.2.

Table 7.3.1. Experimental data on uniaxial tests.

	Solid	Circular	Square
Applied stress at failure (psi)	3,800	2,850	2,830
Relative strength	1	0.75	0.745
Max. $\epsilon_1 - \epsilon_2$ mii at applied stress	42,800 at $\sigma = 3,800$	more than 23,300 at $\sigma = 2,750$	more than 35,000 at $\sigma = 2,320$
Area of hole at failure $\div$ Initial area of hole		0.886 (of one test only)	0.987 (of one test only)
Theoretical max. stress on hole boundary (elastic)		$3\sigma$	$3.86\sigma$ (based on rounding off radius = 0.06 x length of side)

Table 7.3.2. Experimental data on biaxial test.

	Solid	Circular	Circular	Oval 2 Holes	Oval 1 Hole
Applied stress at failure	4,000	$\sigma_x = \sigma_y$	$\frac{\sigma_y}{\sigma_x} = \frac{1}{3}$	$\sigma_x = \sigma_y$ 4,000	$\sigma_x = \sigma_y$
Max. $\epsilon_1 - \epsilon_2$ mi at applied stress	17,500 at $\sigma_x = 1,000$ $\sigma_y = 4,000$	More than 35,000 at $\sigma_x = \sigma_y$ = 4,000 psi	More than 38,000 at $\sigma_y = 3,750$ $\sigma_x = 1,250$ psi	More than 36,000 at $\sigma_x = \sigma_y$ = 3,000 psi	More than 36,000 at $\sigma_x = \sigma_y$ = 3,000 psi
Hole area after loading ÷ initial hole area		0.81	0.882 at $\sigma_y = 4,000$ $\sigma_x = 1,333$	0.767	0.835
Theoretical max. stress on hole boundary (elastic)		2 $\sigma_y$	2.667 $\sigma_y$	3.62 $\sigma_y$	3.62 $\sigma_y$

## 7.2 Nature of Deformation and Failure

In uniaxial compression the material failed by formation of almost vertical cracks followed by crumbling of the sides, which indicated that the friction at the loading surfaces had been reduced to a considerable extent. In case of both circular and square openings under uniaxial compression, failure occurred along planes passing through the points of maximum stress concentration on the boundary of the opening, and making an angle of  $5^{\circ}$  to  $10^{\circ}$  with the direction of the applied load. This indicates that the behavior of the material around the openings is closer to a uniaxial stress state.

The tests on circular holes under equal biaxial stress showed sufficient justification to assume that the problem can be treated as a thick walled cylinder under uniform external pressure. The behavior as a circular cylinder was observed up to a radius of about 1.2". The ratio of experimental to theoretical values of principal strain difference is between 0.645 and 0.792. Considering the assumption of ideal behavior of the material, the results seem reasonably good.

Biaxial test on the various openings indicated that the strains are time dependent even at stress levels below

the yield point.

### 7.3 Theoretical Analysis.

The plane stress problem of a circular hole in an infinite medium subjected to equal horizontal and vertical compression has been analyzed in completely plastic, elastic-plastic and elastic states, assuming that it can be considered as a thick walled cylinder under uniform external pressure. The octahedral shear strength theory of yielding has been assumed in the analysis. The plane stress condition may be recognized as an approximation to the actual condition which is somewhere in between plane stress and plain strain. A method of calculating  $f(\tau_0)$  of (4.1.10) in case of biaxial compression has been given. As an illustration, the stresses in case of a cylinder of internal radius of 1" and external radius of 4" for various values of  $\frac{p}{a}$ , have been calculated.

The elastic stresses in case of circular and square openings under uniaxial compression, and in case of circular and oval openings under hydrostatic and non-hydrostatic compression have also been calculated.

It was found that Savin's<sup>29</sup> solution for an elastic-plastic problem of a circular opening under non-hydrostatic compression cannot be applied in a case when the elastic-

plastic boundary is not a continuous curve around the opening.

A plane stress solution for the problem in elastic-plastic stress state, of a thick walled cylinder under uniform external pressure, assuming yielding due to difference of radial and tangential stress, was worked out. This solution was found to be the same as the one for the plane strain problem under the same assumption. Since the assumed yield condition cannot be valid in the plane stress condition, because  $\sigma_z$  stress is not an intermediate stress, the solution is not incorporated in this thesis.

#### 7.4 Evaluation of the Photo Stress Method

Prior to this investigation there was no information available on the use of photo stress on brittle aggregate materials like salt. It was first tried on plaster of Paris and found unsuitable for it as the material failed without any observable magnitude of strain in the photo stress plastic. In one of the experiments the plastic became separated from the salt surface under large strains and this difficulty was overcome by making the surface more coarse but uniform. The only limitation was the impossibility of making any kind of measurements when the strains became extremely large around the openings. In fact, there is

no direct method of measuring strains at all in such a case; but it can possibly be stated in terms of volumetric strain. The method has been demonstrated to be quite successful for laboratory determination of the strain distribution on the entire region around the cavity.

It has been possible to observe the behavior of the grains in relation to the whole mass and to reach conclusions on the homogeneity and the isotropy of the material.

#### 7.5 Behavior of the Material.

The behavior of the material has been examined from the point of view of individual grains and that of the mass as a whole. An examination of the stress strain curves of the grains (Fig. 6.1.7) indicates that the stress strain relations vary for different points on the same grain. But the behavior of the grains is better understood from a study of the isochromatics and isoclinics obtained for various uniaxial and biaxial stress systems. Such a study indicates that there is neither homogeneity nor isotropy when every point on a grain and every grain in the mass is considered. The change in the direction of principal strains at a point with the change in magnitude of stress proves that the grains undergo a combination of deformations, rotation

and translation depending on the orientation of the grains, the manner in which the grains are packed and the physical properties of the grains. But the general distribution of fringe pattern and of isoclinics gives sufficient justification to assume statistical homogeneity and isotropy for the mass.

The brittle behavior of salt is dominating the behavior of the material in uniaxial stress state. Triaxial testing<sup>30</sup> has proved that the material becomes plastic in multiaxial conditions. The fact that the material in a biaxial stress state did not fail when the maximum principal stress reached 3,800 psi (which is the ultimate strength in uniaxial compression) in a solid cube as well as around the openings of different shapes, may be attributed to change of material behavior, from brittle nature to nearly becoming plastic. The same explanation may be applied to the fact that the material demonstrated a tendency towards large deformations at a higher stress level of 4,000 psi. Perhaps the behavior may be better described by a Kelvin or a Maxwell model. A precise formulation on the subject needs a more detailed investigation of biaxial as well as triaxial testing.

## 7.6 Relationship to the Behavior of Underground Formations in General

Most rocks are made up of grains of more than one polycrystalline material in varying proportions. Accordingly the degree of homogeneity and isotropy in some of the rocks would be less than that of rock salt. Field measurements<sup>38</sup> of rock in Iraq showed that in a closely jointed, finely crystalline limestone, the value of E was 1.2 million psi parallel to bedding and 1 million psi at right angles to it. The deformation characteristics of the rocks depend on the two major factors, namely, the orientation of the grains and previous stress strain history of the material. Rock bursts in deep openings have been attributed to release of conserved energy and the conserved energy depends on the history of rock formation. Accordingly it would be unreasonable to expect that all rocks would behave like salt. However, the processes of deformation and the principles of stress and strain distribution would be uniformly applicable to all materials with the same degree of homogeneity and isotropy.

## CHAPTER VIII

### CONCLUSIONS

From the theoretical and experimental analysis developed in the preceding chapters, the following conclusions may be arrived at.

1. The uniaxial compression test has indicated that the stress strain relation of rock salt does not exhibit linearity at any stage. A reasonable approximation to consider the stress strain curve as a combination of several straight lines has been made. The values of chord modulus of elasticity  $E$ , obtained by such an approximation are

Stress range	Average $E$ (SR-4 gages) million psi	Average $E$ (Dial gages) million psi
0 to 1,000	1.408	0.4559
1,000 to 2,000	0.1913	0.1757

2. The values of the Poisson's ratio obtained from SR-4 gages was greater than 0.5 throughout the test, whereas in the case of dial gages, the values increased almost linearly from 0 to 0.5 in the stress range of 0 to 1,500 psi and was larger than 0.5 beyond the stress of 1,500 psi.

Such large values indicate that the volume change occurred during the process of lateral deformation.

3. The average failure strength of the material was 3,800 psi. Both the values of modulus of elasticity and the failure strength obtained in this investigation are higher than those obtained previously.<sup>30</sup> This increase is due to the difference in the composition and the source of origin of the salt.

4. Biaxial compression showed that the material has a tendency to flow by yielding at equal horizontal and vertical stresses of 4,000 psi. The corresponding values of octahedral shear stress and the permanent strain along the direction of the stress are 1,885 psi and 14,600 micro in./in. respectively.

5. The theoretical analysis of stress and strain in case of a circular hole under hydrostatic compression, in plane stress condition, in plastic, elastic-plastic and elastic states was made. The theoretical results compared reasonably well with the experimental results. The elastic stresses were calculated in case of circular and square openings under uniaxial compression, and in case of circular and oval openings under biaxial hydrostatic and non-hydrostatic compression. The theoretical and experimental results

in elastic state did not show any agreement. This discrepancy may be attributed to the manner in which the elastic constants were calculated and partly to the low sensitivity of the photo stress plastic for small strains.

6. The theoretical analysis of stress strain distribution around the circular opening based on the assumption of thick walled cylinder under uniform external pressure, in plane stress condition has shown consistent agreement with the experimental results in completely plastic condition. The ratio of experimental to theoretical values of principal strain difference in a completely plastic state was between 0.645 and 0.792. In this case the behavior of the specimen as a cylinder was seen up to a radius of about 1.2"

$$\left(\frac{r}{a} = 2.4\right).$$

7. The circular and square openings under uniaxial compression failed by formation of well defined cracks and with little deformation at an average applied stress of 2,840 psi. The circular opening under biaxial compression of 4,000 psi tended to flow without collapsing, while the oval opening under the same biaxial compression collapsed by undergoing large deformations. This increase in the failure strength and deformation is attributed to the change in the behavior of the material from brittle to plastic.

8. The photo stress method for analyzing strain distribution surrounding the underground openings has proved to be valuable in verifying the theoretical analysis.

9. The general distribution of the fringe pattern and the isoclinics on the surface of the test specimens gave sufficient justification for the assumption of statistical homogeneity and isotropy, although the behavior of the individual grains was quite random.

## CHAPTER IX

### FUTURE RESEARCH

During the course of the present investigation, certain limitations were encountered and on that basis, the following recommendations on future research are made.

1. The analytical results in the two dimensional analysis did not show complete agreement with the experimental results. Hence it is necessary to consider the effect of the third principal stress and strain in order to analyze the stress and strain around openings. This would be possible by providing a testing device for applying stresses and measuring strains in the third principal direction.

2. An attempt at solving the problem of a circular hole under uniaxial compression in elastic-plastic state showed that it involved the solution of two non-linear partial differential equations. These could be solved by finite difference method. Hence numerical methods of analysis may be developed for determining the stress strain distribution around various forms of underground openings in uniaxial and multiaxial stress states.

3. One of the problems of practical importance is the case of multiple openings, encountered in mining operations. Analysis of stress and strain and design criteria for such openings may be developed.

4. The present investigation has shown that the strain is time-dependent to a considerable extent particularly at higher stresses. It would be more correct to consider the deformation as a combination of instantaneous strain and time dependent strain. Such a consideration would lead to a more exact analysis of stress and strain around openings. Hence Maxwell and Kelvin models may be made use of to represent the behavior of salt.

5. The present investigation has shown that the large field meter is inadequate to make point by point measurement of large strains. Furthermore, it would be desirable to separate the principal strains. Hence an oblique incidence meter and a large field meter may be acquired in order to make a more accurate analysis.

## BIBLIOGRAPHY

1. Adams, F. D., and Nicholson, J. T. "An experimental investigation into the flow of marble," Proc. Roy. Soc. (London), Series A, Vol. 195, pp. 363-401.
2. Brace, W. F. "Brittle fracture of rocks," International Conference on State of Stress in the Earth's Crust-Preprints of papers. The Rand Corporation, 1963.
3. Bridgman, P. W. "Studies in large plastic flow and fracture," McGraw-Hill Book Co., 1950.
4. D'Agostino, J., Drucker, D. C., Liu, C. K. and Mylonas, C. "An analysis of plastic behaviour of metals with bonded birefringent plastic," Proc. SESA, Vol. XII, No. 2, 1955.
5. Dahir, A. G. Unpublished paper, Michigan State University.
6. Drucker, D. C. "Stress Strain Relations in Plastic and Frictional Soils," Brown University Publication No. DA-3703/1, March, 1956.
7. Drucker, D. C. "Relation of experiments to mathematical theories of plasticity," J. Applied Mechanics 16, (4), p. 349, 1949.
8. Duffy, J., and Lee, T. C. "Measurement of surface strain by means of bonded birefringent strips," Experimental Mechanics, September, 1961.
9. Duffy, J. "Effect of thickness of birefringent coatings," Experimental Mechanics, March, 1961.
10. Emery, C. L., "Strain energy in rocks," International Conference on State of stress in the earth's crust, Preprints of papers, The Rand Corporation, 1963.
11. Frocht, M. M. "Photo elasticity," John Wiley, 1948.

12. Greenspan, M. "Effect of a small hole on the stresses in a uniformly loaded plate," *Quart. Applied Math.* Vol. II, No. 6, p. 60, 1944.
13. Griggs, David T. "Deformation of rocks under high confining pressure," *J. Geology*, Vol. XLIV, No. 5, July-August, 1936.
14. Handin, J. "An application of highpressure in geophysics," *Trans. ASME*, 75, 315-324, 1953.
15. Haythornwaite, R. M. "Range of yield condition in ideal plasticity," *Proc. ASCE* 87, EM 6, 117-133, Dec., 1961.
16. Hill, R. "The Mathematical Theory of Plasticity," Oxford at the Clarendon Press, 1950.
17. Hoffman, O. and Sachs, G. "Introduction to the theory of plasticity for engineers," McGraw-Hill Co., 1953.
18. Holyman, H. W. "Seismograph evidence on the depth of salt columns, Moss Bluff Dome, Texas," *Geophysics*, II, No. 2, 128-134, 1946.
19. Lee, E. H. "Plastic flow in a V-notched bar pulled in tension," *J. Applied Mechanics*, Vol. 74, 1952, pp. 331-336.
20. Marin, J., Ulrich, B. H., and Huges, W. P. "Plastic stress strain relations for 755-6 Aluminum Alloy subjected to biaxial tensile stresses," NACA, TN 2425, (1951).
21. Marin, J., Faupel, J. M., Dutton, V. L., and Brossman, M. W. "Biaxial plastic stress strain relations for 24 S-T Aluminum alloy," NACA, TN 1536, (1948).
22. Morrison, D. M., "The transition test as a method for determining the triaxial properties of rocks in the condition of underground formations," M.S. Thesis, Michigan State University, East Lansing, 1962.
23. Nadai, A. "Theory of flow and fracture of solids," Vol. 1, McGraw-Hill Co., 1950.

24. Obert, L., Duvall, W. I. and Merrill, R. H. "Design of underground openings in competent rock," The Bureau of Mines Bulletin 587, U. S. Government Printing Office, 1960.
25. Paul, B. "A modification of the Coulomb-Mohr theory of fracture," Paper No. 60-WA-31 Applied Mechanics Division Annual Meeting, Nov.-Dec. 1960, of ASME.
26. Phillips, A. "Introduction to plasticity," The Ronald Press Co., 1956.
27. Phillips, A., and Kaechele, L. "Combined stress tests in plasticity," J. Applied Mechanics 23(1), p. 43, 1956.
28. Raman, A. B. "Elastic plastic transition tests," M.S. Thesis, Michigan State University, 1962.
29. Savin, G. N. "Stress concentration around holes," Pergamon Press, 1961.
30. Serata, S. "Development of design principle for disposal of reactor fuel waste into underground salt cavities," Ph.D. Thesis, University of Texas, 1959.
31. Serata, S., Gloyna, E. F. "Principles of structural stability of underground salt cavities," Journal of Geophysical Research, Vol. 65, No. 9, September, 1960.
32. Serata, S. "Transition from elastic to plastic states of rocks under triaxial compression," Proceedings of the 4th Symposium of Rock Mechanics held at the Penn. State University, University Park, Pa., April, 1961.
33. Shepherd, W. M. "Plastic stress strain relations," Proc. I.M.E., Vol. 159, 1948, pp. 95-99.
- 34.1 to 5 Tatnall Measuring Systems Company.
  1. "Operating instructions for large field meter," Bulletin BN-8001, July, 1957.

2. "Photo stress sheet and liquid plastic suggestions for plastic selections," Bulletin BN-8022.
3. "Instructions for applying photo stress sheet plastic," Bulletin IB 8004.
4. "Instructions for applying photostress liquid plastic," Bulletin IB 8005.
5. "Operating instructions for small field meter," Bulletin BN-8002.
35. Theocaris, P. S., and Mylonas, C. "Visco-elastic effects in birefringent coatings," ASME. Tr. 83E (J. Applied Mechanics) 4, Dec., 1961.
36. Timoshenko, S., Goodier, J. N. "Theory of Elasticity," McGraw-Hill Co., 1951.
37. Wang, A. J. "Plastic flow in a deeply notched bar with semi-circular root," Quart. Applied Math., Vol. II, 1954, pp. 427-438.
38. Wantland, D. "Geophysical measurements of rock properties in situ," International conference on State of Stress in the earth's crust - Preprints of papers. The Rand Corporation, 1963.
39. Wuerker, R. G. "Annotated tables of strength and elastic properties of rocks," Pet. Branch, A.I.M.E. Publ. Dec., 1956.
40. Zandman, F. "Photo stress, principles and applications" Tatnall measuring systems, Phoenixville, Pa.
41. Zandman, F. "Stress analysis of guided missile tail section with the photo elastic coating technique," The Society for Experimental Stress Analysis, Paper No. 556, May, 1959.
42. Zandman, F. "The accuracy of the birefringent coating method for coatings of arbitrary thickness." The Society for Experimental Stress Analysis, Paper No. 557, 1959.

43. Zandman, F. "Photo elastic coating technique for determining stress distribution in welded structures," *Welding Journal Research Supplement*, May, 1960.
44. Zandman, F., Redner, S. S. and Riegner, E. I. "Reinforcing Effect of Birefringent Coating," Paper No. 588, *The Society for Experimental Stress Analysis*, October, 1959.
45. Robertson, E. C. "Experimental study of the strength of Rocks," *Bull. Geol. Soc. America*, Vol. 66, pp. 1275-1314, 1955.

E ONLY

USE ONLY

